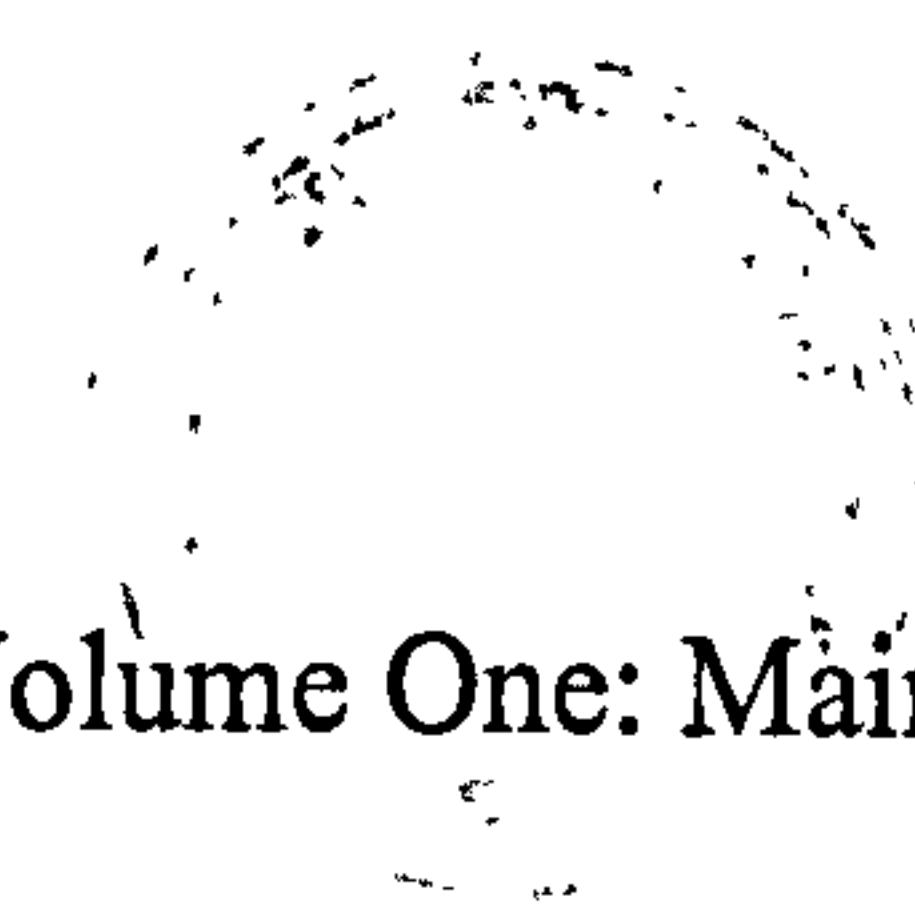


AN INVESTIGATION INTO THE EFFECTS
OF COMPLEX TOPOGRAPHY ON
PARTICLE DRY DEPOSITION

by

SIMON TOBY PARKER

A thesis submitted to
The University of Birmingham
for the degree of
DOCTOR OF PHILOSOPHY



Volume One: Main Text

Division of Environmental Health and Risk Management
School of Geography, Earth and Environmental Sciences
The University of Birmingham
February 2004

UNIVERSITY OF
BIRMINGHAM

University of Birmingham Research Archive

e-theses repository

This unpublished thesis/dissertation is copyright of the author and/or third parties. The intellectual property rights of the author or third parties in respect of this work are as defined by The Copyright Designs and Patents Act 1988 or as modified by any successor legislation.

Any use made of information contained in this thesis/dissertation must be in accordance with that legislation and must be properly acknowledged. Further distribution or reproduction in any format is prohibited without the permission of the copyright holder.

ABSTRACT

There is a requirement to predict the spatial variation of particle dry deposition following a nuclear accident. The interaction of landscape features, atmospheric flow and particle dry deposition has been investigated with this in mind. Wind tunnel studies have been used with computational fluid dynamics to predict the deposition rate relative to a flat landscape. Good quantitative agreement was seen for this relative deposition rate. Landscape shapes showed significant effects on deposition rate, increasing it by a factor of up to 2.1 in some cases. The effect of turbulence intensity in isolation was also studied, and a weak relationship to dry deposition was observed.

Computational fluid dynamics used in wind tunnel comparisons were extended to a wide range of landscape cases. Deposition rates varied spatially around the landscape features. In general, for hills and ridges, deposition was seen to increase on the windward face (a factor of 1.2 - 1.8), decrease on the leeward face and near wake, and increase in the further wake (a factor of 1.4 – 2.0), before returning to the flat value. The computational results were applied to a real landscape with the use of a customised geographical information system. Good qualitative agreement was seen when compared with a test case.

DEDICATION

To my wife and son, for their help, patience and inspiration. Without which, this thesis could never have been completed.

ACKNOWLEDGEMENTS

Thanks go to all my friends and colleagues at Birmingham. To my supervisor, Rob Kinnersley, who conceived the project, and provided advice and encouragement throughout. To Thom Huggins, for all his help with the wind tunnel experiments, many helpful conversations and for proof reading parts of this thesis. To Chris Baker, for his help, suggestions and reading material. To the wind tunnel staff, for all their help and their interest in the project. To Paul Hatton, for his help with software and hardware, over and above the call of duty. To Peter Richards, for his part in organising the CWE2000 conference competition.

Special thanks to my wife for all her support during the course of my studies and in particular for her help proof reading this thesis. Thank you.

TABLE OF CONTENTS

1.	Introduction and Literature Review.....	1
1.1.	Background.....	1
1.2.	Project scope.....	3
1.3.	Literature review.....	4
1.4.	Summary.....	30
2.	Particle Deposition to Landscapes – Wind Tunnel Experiments	33
2.1.	Introduction	33
2.2.	Methodology.....	34
2.3.	Results	51
2.4.	Discussion.....	58
2.5.	Conclusions	62
3.	Particle Deposition to Landscapes – Computational Fluid Dynamics Studies	65
3.1.	Introduction	65
3.2.	Predicting atmospheric flows	67
3.3.	Predicting particle deposition in atmospheric flows.....	79
3.4.	Conclusions	89
4.	Particle Deposition in Uniform Turbulence – Wind Tunnel Experiments.....	91
4.1.	Introduction	91
4.2.	Methodology.....	92
4.3.	Results	101
4.4.	Discussion.....	102
4.5.	Conclusions	105

5.	Particle Deposition in Uniform Turbulence – Computational Fluid Dynamics Studies	106
5.1.	Introduction	106
5.2.	Methodology.....	106
5.3.	Results	108
5.4.	Discussion.....	111
5.5.	Conclusions	114
6.	Particle Deposition to Landscapes – Further Computational Fluid Dynamics Studies..	116
6.1.	Introduction	116
6.2.	Methodology.....	116
6.3.	Results	129
6.4.	Discussion.....	140
6.5.	Conclusions	149
7.	Application of Deposition Results Within a Geographical Information System	153
7.1.	Introduction	153
7.2.	Derivation of rules governing dry deposition surrounding landscape features	156
7.3.	Identifying landscape features	158
7.4.	Applying the rules within a GIS	160
7.5.	Dispersion modelling.....	168
7.6.	Case study.....	168
7.7.	Conclusions	173
8.	Conclusions	177
8.1.	Introduction	177
8.2.	Experimental deposition measurements	178
8.3.	CFD	181
8.4.	Application	183
8.5.	Conclusions	184
	Figures	188
	Tables.....	298
	Appendices	
	References	

LIST OF FIGURES

Figure 1.1.....	189
Figure 2.1.....	190
Figure 2.2.....	191
Figure 2.3.....	192
Figure 2.4.....	192
Figure 2.5.....	193
Figure 2.6.....	194
Figure 2.7.....	195
Figure 2.8.....	196
Figure 2.9.....	197
Figure 2.10.....	197
Figure 2.11.....	198
Figure 2.12.....	198
Figure 2.13.....	199
Figure 2.14.....	200
Figure 2.15.....	201
Figure 2.16.....	201
Figure 2.17.....	202
Figure 2.18.....	202
Figure 2.19.....	203
Figure 2.20.....	203
Figure 3.1.....	204
Figure 3.2.....	205
Figure 3.3.....	205
Figure 3.4.....	206
Figure 3.5.....	206

Figure 3.6.....	207
Figure 3.7.....	207
Figure 3.8.....	208
Figure 4.1.....	209
Figure 4.2.....	210
Figure 4.3.....	211
Figure 4.4.....	212
Figure 4.5.....	213
Figure 4.6.....	214
Figure 4.7.....	215
Figure 4.8.....	216
Figure 4.9.....	217
Figure 4.10.....	218
Figure 4.11.....	219
Figure 4.12.....	220
Figure 4.13.....	221
Figure 4.14.....	222
Figure 5.1.....	223
Figure 5.2.....	224
Figure 5.3.....	225
Figure 5.4.....	226
Figure 5.5.....	227
Figure 5.6.....	228
Figure 5.7.....	229
Figure 5.8.....	230
Figure 5.9.....	231
Figure 5.10.....	232
Figure 5.11.....	233
Figure 5.12.....	234
Figure 5.13.....	235

Figure 5.14.....	236
Figure 5.15.....	237
Figure 6.1.....	238
Figure 6.2.....	239
Figure 6.3.....	240
Figure 6.4.....	241
Figure 6.5.....	242
Figure 6.6.....	243
Figure 6.7.....	244
Figure 6.8.....	245
Figure 6.9.....	246
Figure 6.10.....	247
Figure 6.11.....	248
Figure 6.12.....	249
Figure 6.13.....	250
Figure 6.14.....	251
Figure 6.15.....	252
Figure 6.16.....	253
Figure 6.17.....	254
Figure 6.18.....	255
Figure 6.19.....	256
Figure 6.20.....	257
Figure 6.21.....	258
Figure 6.22.....	259
Figure 6.23.....	260
Figure 6.24.....	261
Figure 6.25.....	262
Figure 6.26.....	263
Figure 6.27.....	264
Figure 6.28.....	265
Figure 6.29.....	266

Figure 6.30.....	267
Figure 6.31.....	268
Figure 6.32.....	269
Figure 6.33.....	270
Figure 6.34.....	271
Figure 6.35.....	272
Figure 6.36.....	273
Figure 6.37.....	274
Figure 6.38.....	275
Figure 6.39.....	276
Figure 6.40.....	277
Figure 7.1.....	278
Figure 7.2.....	279
Figure 7.3.....	280
Figure 7.4.....	281
Figure 7.5.....	282
Figure 7.6.....	283
Figure 7.7.....	284
Figure 7.8.....	285
Figure 7.9.....	286
Figure 7.10.....	287
Figure 7.11.....	288
Figure 7.12.....	289
Figure 7.13.....	290
Figure 7.14.....	291
Figure 7.15.....	292
Figure 7.16.....	294
Figure 7.17.....	296
Figure 7.18.....	297

LIST OF TABLES

Table 2.1	299
Table 2.2	299
Table 3.1	300
Table 3.2	301
Table 6.1	302
Table 6.2	303
Table 6.3	303
Table 6.4	304
Table 6.5	304
Table 7.1	305
Table 7.2	306
Table 7.3	307
Table 7.5	308

ABBREVIATIONS

CFD	-	Computational fluid dynamics
CTA	-	Constant temperature anemometer
DEM	-	Digital elevation model
DNS	-	Direct numerical simulation
FB	-	Fractional bias
GIS	-	Geographical information system
GRASS	-	Geographic Resources Analysis Support System
LES	-	Large eddy simulation
MDF	-	Medium density fibreboard
NMSE	-	Normalised mean square error
RANS	-	Reynolds averaged Navier Stokes
RNG	-	Renormalization group (k- ϵ model)
RSM	-	Reynolds stress model
TKE	-	Turbulent kinetic energy
USGS	-	United States Geological Survey

GLOSSARY

Aeolian Due to the action of the wind.

Complex topography A region of complex surface features. In this context, used to describe regions of complex variations of elevation rather than different land use. More simply, it refers to hills, ridges and valleys, etc.

Katabatic Air current moving downslope due to cooling effects, especially at night.

Laminar sublayer See viscous sublayer.

Leeward Facing away from the oncoming wind.

Loess Wind blown material, of size equivalent to silt and smaller.

Monodisperse Having a uniform size, in reference to particles.

Particle drag The force exerted on a particle by the fluid through which it moves.

Particle dry deposition The transfer of aerosol particles from suspension in the air to a surface, occurring in the absence of rainfall or fog.

Polydisperse Having a range of sizes, in reference to particles.

Raster A map in the form of a regular array of data.

Streamwise In the direction of the bulk flow.

Viscous sublayer The thin layer of a turbulent boundary layer flow, immediately adjacent to the surface, where viscous forces outweigh inertial forces, ensuring laminar flow.

Windward Facing towards the oncoming wind.

LIST OF COMMONLY USED SYMBOLS

A	coefficient for grid-generated turbulence equation
C_{air}	airborne concentration
C_c	Cunningham correction factor
C_{liquid}	concentration of fluorescein in liquid extract
C_μ	constant in k- ϵ model
d	particle diameter
g	acceleration due to gravity
H	hill height
I	turbulence intensity
k	turbulent kinetic energy
l	scale of largest turbulent eddies
L	characteristic length
M	mesh spacing
M_Ω	mass of fluorescein
n	coefficient for grid-generated turbulence equation
p	pressure
Pe	Peclet number
Re	Reynolds number
Ro	Rossby number
S	stopping distance
Sc	Schmidt number
$S_{M_{x,y,z}}$	momentum source in x,y or z direction
Stk	Stokes number
t	time (of travel from turbulence generating grid)
t_1	coefficient for grid-generated turbulence equation
u_*	friction velocity
u'	instantaneous streamwise turbulent velocity

U	mean wind speed
U_0	initial particle velocity or mean speed for same mass flow through grid, through an equivalent empty area
U_F	particle terminal velocity
v'	instantaneous lateral turbulent velocity
V	velocity
V_{air}	volume of air
V_d	deposition velocity
V_{liquid}	volume of liquid
w'	instantaneous vertical turbulent velocity
X	downwind distance, or model or experimental measurement
Y	lateral distance
y^+	dimensionless height from surface
Z	vertical height above the surface
z_0	roughness length
α	molecular mass diffusivity
ε	turbulent dissipation rate
η	scale of smallest turbulent eddies
κ	thermal diffusivity or von Karman constant
μ	dynamic (absolute) viscosity
ν	kinematic viscosity
ρ_p	particle density
ρ_f	fluid density
σ_u	streamwise turbulent velocity
Ω_R	angular velocity

1. INTRODUCTION AND LITERATURE REVIEW

1.1. Background

Accidents involving the release of radioactive material into the environment are thankfully rare. However, they do occur and as history has shown, they can have extremely serious consequences. Where there is release of material into the atmosphere its spread can be rapid. Airborne material can cause direct exposure and can also deposit onto crops, pasture and waterways. Following such an accidental release, contaminated crops and other foods need to be prevented from entering the food chain, to minimise health effects. Food producing areas need to be isolated depending on their level of contamination by atmospheric deposition. To assess the level of contamination sampling is needed. Because of the short timescale involved, the sampling regime must be limited. To make best use of the limited sampling a sampling strategy is needed based on judgement of the most likely areas of deposition.

The assessment of the area of most likely deposition is made using expert judgement, based on a range of information, including the release characteristics, meteorological conditions, landscape topography and land use. A meteorological model of dispersion will be used to predict the airborne concentrations due to the spread of the material and such models have been found to perform reasonably well. However, the amount of material deposited to the ground is less easily quantified. In the presence of rainfall, deposition is dominated by wet mechanisms and a reasonable estimate can be made, based on measured rainfall patterns. When there is no rainfall, deposition depends solely on the, generally far slower, dry deposition process. Whilst this has been well studied for uniform surfaces (Nicholson, 1988),

there is little information available on how this process varies with complex topography. In particular, how landscape features affect the spatial distribution of deposition.

It is this problem of how dry deposition varies around landscape features, which this work addresses. Because the majority of radioactive material of concern is particulate in nature this work has dealt with the deposition of aerosol material. It is intended that the results of this work could be incorporated into a partially automated expert system tool, as demonstrated by Argyraki *et al.* (1999), aimed at decreasing the probability of missing patches of ground contamination exceeding a defined threshold level.

The driving force behind this project is the specific case of the transfer of radioactive pollutants from the atmosphere to the ground. However, the results are valid for a number of other environmental transfer problems where atmospheric deposition is important, such as non-radiological chemical incidents, routine discharges and nitrate deposition to sensitive ecosystems.

1.2. Project scope

The aim of this project was to investigate the relationship between complex topography and airborne particle dry deposition, in order to predict landscape areas likely to be affected by increased or decreased dry particle deposition. Following a review of the existing literature a series of objectives were drawn up:

- To use computational techniques to model flows and dry particle deposition over complex topography
- To validate such techniques against experimental scale models
- To extend the computational techniques to a range of cases
- To derive a set of rules describing the relationship between topographic shapes and particle deposition based on the computational results
- To demonstrate an automated geographical information system (GIS) approach using these rules

In addition, a better understanding of the physical processes linking landscape topography, flow characteristics and dry deposition was sought.

The project was not intended to include other influences on particle deposition, such as wet deposition and the impact of land cover. Whilst these effects are certainly important, and may dominate the pattern of deposition under certain conditions, their impact is more easily understood. They can be incorporated into prediction models as an additional layer of information, describing how deposition will be influenced relative to that of a “baseline” case.

1.3. Literature review

1.3.1 Particle dry deposition from the atmosphere

A useful starting point when considering particle dry deposition is the examination of the physical effects that control the process. Zufall and Davidson (1998) summarised the mechanisms involved in atmospheric dry deposition as follows:

- Turbulent diffusion
- Sedimentation
- Brownian diffusion
- Interception
- Inertial forces (impaction)
- Electrical migration
- Thermophoresis
- Diffusiophoresis

Turbulent diffusion is the transport of particles along a concentration gradient due to the turbulent motions of the atmospheric flow. It is typically several orders of magnitude larger than molecular diffusion. Since there is removal of particles at the surface there is a net gradient of decreasing concentration towards the surface. Therefore, turbulent diffusion causes particles to move towards the surface. Sedimentation occurs because of gravity and its importance depends on the size of the particle (Jacobson, 1999), becoming increasingly

important for larger and more dense particles. Brownian diffusion is the motion of particles due to the thermal energy of the surrounding air, and is much weaker than turbulent diffusion in the bulk flow. It is only important where there is little turbulence. For example, within the viscous sublayer, the part of the boundary layer where viscous forces become dominant and the velocity scales linearly with height. Brownian diffusion becomes more significant for smaller particles and is most significant for particles much smaller than 100 nm, where diffusivity tends towards that of true gas molecules.

Interception is the process whereby a particle, following a fluid streamline, collides with a surface element and it can cause particles to be deposited to collecting elements. Impaction is the process whereby a particle deviates from a fluid streamline because of its inertia, and collides with a surface element. Inertial impaction can transport moderately sized particles across the viscous sublayer. Electrical migration and thermophoresis, the movement of small particles in a temperature gradient, are generally less significant than the other processes described for atmospheric flows. Diffusiophoresis, the movement of particles along a concentration gradient in two or more gases, is less significant over land, but will have a greater influence over a water surface.

The final stage of deposition is the interaction with the surface. The nature of this interaction will determine whether the particle remains attached to the surface or rebounds. Particles with large kinetic energies are more likely to rebound. The critical velocity above which bounce occurs is inversely proportional to the particle diameter (Hinds, 1999). Therefore, small particles have a higher threshold velocity and are less likely to bounce. Once a particle has attached to the surface, it can be resuspended by drag force from the air above. Particle size is again an important parameter in this respect, with smaller particles being harder to dislodge. Hinds (1999) notes that particles less than 10 μm are unlikely to be dislodged by

ordinary air forces. However, when significant amounts of deposited material form layers, large masses of particles can be dislodged. The presence of other non-contaminated particles, such as soil particles, can combine with the deposited material and may increase the likelihood of resuspension (Warner and Harrison, 1993).

There are clearly a large number of physical processes that are potentially involved in particle deposition. The relative importance of each is determined by the scenario in question. The important factors in any scenario can be broadly grouped into three sets of properties: those of the depositing contaminant, the atmospheric flow and the surface (Davidson and Wu, 1990). In the case of complex topography, the properties of the atmospheric flow and the surface are closely linked. The large-scale features of the surface influence the flow and cause changes in the amount of deposition that occurs.

The properties of the depositing particles that determine the relative importance of the deposition mechanisms are mainly the diameter and density of the particles. Large and dense particles are deposited more quickly due to sedimentation, whilst very small particles are transported to the surface more rapidly by Brownian motion (Nicholson, 1988). Figure 1.1 reproduces a figure from Nicholson (1988) (after Sehmel, 1980) showing how deposition varies strongly with particle diameter. Radionuclide material released from reactor accidents will typically have a wide range of particle sizes. However, very small or ultrafine aerosols (below 0.1 μm in size), termed nuclei mode, will rapidly coagulate and grow through vapour condensation to form larger aerosols. Similarly coarse aerosol (greater than about 3 μm) will be lost relatively quickly through sedimentation and other inertial processes. This results in a range between approximately 0.1 and 3 μm diameter, in which particles remain airborne for a longer period and can be transported for considerable distances (Warner and Harrison, 1993).

Electrical charge can also be important for the behaviour of aerosol particles. In general atmospheric aerosols possess little charge, but it is thought that aerosols released from nuclear accidents may have increased charge (Warner and Harrison, 1993). This may result in altered coagulation rates and also enhanced deposition, due to mirror charging of collecting surfaces. Additionally, the physicochemical properties of the aerosol may influence its behaviour, for example whether it is hydrophobic or hydrophilic will influence its rate of growth in the presence of water vapour.

Turning attention to the properties of atmospheric flows that influence particle dry deposition, it is clear that these flows are complex by nature and include a range of phenomena. Davidson and Wu (1990) provide a list of the properties of atmospheric flow that affect particle dry deposition:

- Flow separation
- Micrometeorological interactions with the surface, including:
 - Friction velocity
 - Roughness height
 - Zero-plane displacement
- Relative humidity
- Solar radiation
- Stability class
- Temperature

- Turbulence intensity
- Wind speed

These factors are not independent and there can be many interactions between them. For example, the amount of incident sunlight affects the surface temperature, which in turn influences the temperature profile with height. The temperature profile determines the degree of stability or convection in the atmosphere.

The third set of properties, that of the surface, influences the amount of dry deposition directly and indirectly. The surface vegetation, or land use, can directly determine the interception and impaction of aerosols, through its roughness and collection efficiency of individual collection elements. Additionally, the bulk shapes of the landscape influence the atmospheric flow. For example, an area of high ground can result in the speed up of flow over the top or diversion of the flow depending on the stability of the flow. The amount of turbulence within the flow will also be affected. Sufficiently steep topography can cause separation of the flow and areas of flow recirculation (Belcher and Hunt, 1998). These changes to the flow field can subsequently alter deposition.

In summary, the particle-atmosphere-surface system is complex and there are a number of factors that determine the rate of deposition. However, for the case of an accidental release of radionuclide material, the particle properties are fairly well defined and the influence of surface roughness has been investigated (Sehmel and Hodgson, 1980). This leaves the atmosphere and surface interactions as the main area of concern, in particular the effect of surface landscape features on the flow and deposition.

1.3.2 Influence of topography on dry deposition – field studies

Many authors have dealt with the subject of deposition of particles in one form or another. There is a wide range of reported data on deposition rates of atmospheric particles from field studies. For example, the concern over acid deposition to sensitive areas has generated a great deal of interest in the deposition of particles (Davidson and Wu, 1990), (Ruijgrok *et al.*, 1995).

The traditional approach to quantifying particle deposition rates is the use of a deposition velocity, V_d , defined as:

$$V_d = \frac{\text{deposition flux}}{\text{concentration at reference height}} \quad \text{Equation 1.1}$$

The use of a deposition velocity allows the influence of the landscape on larger scale dispersion and hence concentration and the local deposition enhancement or reduction to be separated.

Davidson and Wu (1990) and Nicholson (1988) provide reviews of experimental studies of particle deposition velocities. As pointed out by Ruijgrok *et al.* (1995), one of the problems with field determinations of deposition velocity is that the particle size ranges are often not determined, nor meteorological conditions fully reported. This creates a problem when comparing model results with experiment, because deposition velocity is strongly dependent on particle size. The choice of surface for collection also influences the results.

Deposition on a local scale can be subject to considerable spatial variation. For example, change of vegetation type can have a significant effect. A number of authors have studied the effect of forest edges on deposition and have found increased particulate deposition compared

to that to the body of the forest (Draaijers *et al.*, 1988; Hasselrot and Grennfelt, 1987). However, probably the biggest disadvantage of the deposition velocity approach is its inability to deal with the spatial heterogeneity caused by complex topography. In the review by Nicholson (1988) of experimental measurements of small particle dry deposition, no studies that include the effect of complex topography are reported.

There are a few published studies that have examined the dependence of dry deposition of dust in arid environments to complex topography (Biryukov, 1998), (Goossens and Offer, 1990), (Offer and Goossens, 1995), (Goossens, 1995). However, the particle size is generally larger than that which is important for the deposition of radionuclide material. The results from these studies are examined in more detail in the next section.

Although studies of particle deposition in complex topography are limited, a number of authors have studied the dispersion of pollutants and turbulence properties within complex landscapes, for example Cionco (1989).

1.3.3 Influence of topography on dry deposition – wind tunnel studies

The difficulties inherent in obtaining accurate deposition velocities for particles to a range of topographies and vegetation are an incentive for experimenters to carry out studies in controlled environments. The wind tunnel offers the opportunity to fix the characteristics of the landscape, the flow, and the airborne concentration of the particles and their properties. However, there are new problems that are introduced when using a wind tunnel, such as scaling issues and the choice of surface.

In the field of aeolian geomorphology, a variety of research has been carried out on the deposition of wind blown particulate material in complex topography using wind tunnels. The

principal material considered is loess, equivalent to silt (4 - 63 μm) and finer fractions. Although the focus has been on understanding the laying down of geological deposits and erosion of arid landscapes, some of this work is interesting from the standpoint of understanding the topographical influence on environmental particle deposition. A number of relevant papers are discussed below.

The sedimentation characteristics of dust in the wake of symmetrical hills were examined by Goossens (1988b). A model of a single hill was exposed to natural dust in a wind tunnel and the pattern of deposition was examined. A sharp maximum of deposition was observed on the concave part of the windward slope, followed downwind, by a minimum coinciding with the apex of the hill, followed by a smoother more elongated maximum. The deposition influence of the hill was presented as the difference from the flat case, rather than the ratio to the flat case. This makes applying the data slightly more difficult, particularly without the flat data as a reference.

Studies of the deposition of dust onto a range of hills were carried out by Goossens using a wind tunnel (Goossens, 1996). A series of permutations of hill height and length-to-height ratios were studied. The patterns of deposition over a range of six hills were compared with those for single hills.

Goossens and Offer investigated the deposition of desert dust in complex terrain (Goossens and Offer, 1990). Field measurements of gross loess deposition were carried out and compared with wind tunnel studies of a 1:2500 horizontal scale model, with a vertical exaggeration factor of 1.86. Deposition was found to occur most strongly on the windward slopes of the hills and little or no deposition on the leeward. The pattern of relative deposition agreed between the wind tunnel and field experiments.

An article in 1995 presented results from a comparison of wind tunnel experiments and field measurements of dust deposition on conical hills (Offer and Goossens, 1995). Short-term dust deposition was measured for a hill in the Negev Desert. A scale model was prepared and used in a wind tunnel experiment to compare deposition patterns. The wind tunnel model was found to adequately predict the field pattern.

Goossens also produced a conceptual model for the deposition of loess onto curved surfaces (Goossens, 1988a). The controlling factors were concentration and turbulence within the flow. The concentration was linked to the convergence and divergence of streamlines and these were related to different parts of the flow over a hill. A similar approach was used to different parts of the flow with different turbulence levels. The conclusions drawn were as follows:

- “
- *very much sedimentation on the concave part of the windward slope*
 - *a clearly less important, but still considerable sedimentation on the convex part of the windward slope*
 - *very little sedimentation on the leeward slope*
 - *near the summit of the hill, the sedimentation quantity is dependent on the position of the separation line. If this line is situated upstream of the summit line, the latter is situated in the separation zone and there will be very little sedimentation. If, on the other hand, the separation line is situated downstream of the summit line, there will be much more sedimentation than in the previous case.*” (Goossens, 1988a)

Neither the turbulence, nor the concentration dependence on the curvature of the hill, used in the model above, should be specific to the particle sizes studied. Therefore, the same parameters may be expected to control the variation in small particle deposition.

In summary, the papers discussed above provide a number of very useful insights into dust behaviour above complex topography. No detailed explanations are presented for the mechanism of increased or decreased deposition, although turbulence and concentration are determined as being important parameters. It is not clear how the results would vary for smaller particles, such as those released from a nuclear accident, although the conceptual model approach suggests that they would be similar. Applying the data to general data is problematic, because it is presented as difference from, rather than ratio to, the flat case.

Studies of specific scenarios of dust emission and deposition have also been carried out in wind tunnels. Xuan and Robins (1994) studied the emissions from coal stockpiles at a coal plant in Beijing and the resulting patterns of deposition. The authors concluded that complex topography increases the mean level of deposition and changes the distribution of the deposition. They also note that complex terrain produces wake vortices, which greatly increase the transfer of energy to particles from the mean flow.

Wind tunnels have been used to study particle deposition in flows without complex topography as such, but in the presence of obstacles and other features. Early studies have used wind tunnels to study the impaction efficiency of particles to simple geometries (May and Clifford, 1967). The capture of water droplets by cylindrical obstacles has been studied in a wind tunnel by Schatzmann (1999) as a model for trapping of atmospheric fog by woodland at high elevation. Dai *et al.* (2001) studied particle transport and deposition in turbulent boundary flows behind an obstacle. The authors found that particle deposition was greater in the region up to 20 times the obstacle height downwind, compared to the region beyond this. They also concluded that particle deposition in turbulent flows is complex.

Chamberlain (1984) studied the deposition of gases and particles to widely spaced roughness elements and found a pattern of increased deposition, with peaks at the forward face of the roughness elements and also in the wake of these elements. Zufall *et al* (1999a; 1999b) studied the dry deposition of particles to wave surfaces using wind tunnel studies and CFD. They found that particle deposition was greatest to the upslope portion of the wave surface, and reduced at the crest and downslope. They attributed the upwind increase to a combined effect of turbulence and impaction, and the reduced effect on the downwind slope to slower or negative flow. On average, particle deposition was 80% greater compared to a flat surface.

Further removed from the area of dry deposition, but of some relevance to wind tunnel modelling of complex topography, is a paper on the wind tunnel studies of aeolian processes on the planet of Mars and their effect on crater shapes (Greeley *et al.*, 1974). The patterns of erosion and deposition observed are of interest and show the spatial dependence of deposition phenomena on complex topography, albeit under very different conditions. There are also examples of work on particle deposition, from accidental releases, being studied in wind tunnels in the absence of complex topography. Hall *et al.* (1998) examined the deposition of particles of size ranging from 4 – 183 μm , released from a scale model of a building fire. The conclusions of the work were that large particle deposition could be studied with a scale wind tunnel model, and that particle deposition behaviour is complicated and depends on particle falling angle, particle inertia and downwash effects from the building.

In summary, wind tunnels have been widely used to study particle behaviour and deposition above scale models. However, few studies have been carried out of deposition for the particle size of interest (0.1 – 3 μm).

1.3.4 Flow over complex topography – wind tunnel studies

While the literature regarding small particle deposition to complex topography in a wind tunnel is relatively small, a great deal more has been written about the wind tunnel studies of flow over complex topographies. A selection of the more relevant papers are summarised below.

Finnigan *et al.* (1990) studied the turbulent flow over a two dimensional ridge, using a scale model in a wind tunnel. The authors used a gravel-covered surface to ensure aerodynamic roughness of the flow. Detailed measurements of the mean and turbulent velocity were presented, and the authors noted that streamwise turbulence was strongly coupled to the acceleration of the flow, and that the cross term and vertical turbulence were related to the curvature of the ridge. Trombetti *et al.* (1995) reported an analysis of the turbulence features for wind tunnel studies carried out on two-dimensional hills (ridges) and valleys. The authors concluded that the turbulence was dominated by pressure gradients near the surface and streamline curvature became more important with height. Takahashi *et al.* (2002) carried out their own wind tunnel study of flow over a two-dimensional hill and investigated the effect of windbreak fences on the flow. They reported detailed turbulence measurements and their results showed similar patterns of turbulence to those reported by Finnigan *et al.* (1990).

In addition to investigations of turbulence in such flows, there is interest in peak wind speeds at high elevations for transport and building design. Baker *et al.* (1985) compared field measurements and wind tunnel data for a real landscape and found reasonable agreement for speed up factors. Wind tunnels have also been used for studying the effect of hill shape and surrounding vegetation on flows for siting wind-power turbines (Neff and Meroney, 1998).

Related to the study of the properties of flows over complex topography, the dispersion of gaseous pollutants in such flows has also been studied in a number of wind tunnel experiments. For example the effect of three dimensional hills on dispersion from sources downwind of the hill has been investigated (Castro and Snyder, 1982). The authors found significant increases in downwind surface concentration, as high as 11 times for one position within the recirculation zone. The height of the source was also found to be important for the ratio of the maximum surface concentration relative to the flat case. The work was advanced with a similar study examining the effect of wind angle (Castro *et al.*, 1988).

Okabayashi *et al.* (1996) looked at the effect of variation in wind direction on gas dispersion over complex topography, including both a simplified geometry and a scale model of real terrain. The experiments involved sources both upwind and downwind of a model ridge and at two different heights. The authors used the results from the wind tunnel studies to derive relationships between variation in wind angle and maximum concentration. Cermak (1984) reported on a series of modelling studies over real complex topography, in which non-neutral atmospheric stability conditions were also included. Wind tunnel derived concentrations were compared with field measurements. Good agreement was achieved for neutral and unstable conditions, but less agreement was found for the stable case. Vosper *et al.* (1999) tackled the problem of stably stratified flow by using a stratified towing tank. Details of the flow past hemispheres and cones were investigated. In addition to determining drag values, the presence and shape of separated regions of the flow were also recorded.

1.3.5 Flow over complex topography – field data and theoretical work

The study of flow over complex topography is, of course, not limited to wind tunnel studies and there is a great deal of field data and theoretical work on this subject. Taylor *et al.* (1987) provided a review of work carried out on boundary layer flow over low hills that summarised a number of field experiments carried out over different hills. Taylor and Teunissen (1987) reported a comprehensive set of field measurements made over the low hill, Askervein on South Uist, Scotland, which has acted as a benchmark for a number of modelling studies.

From a more analytical viewpoint, Belcher and Hunt (1998) published a review of the mechanisms that control turbulent neutral boundary-layer flow over hills. They identified a number of general concepts that can be applied to such flows:

- Flow over even moderately sloped hills accelerates over the top. The effect is amplified by the wind shear with height. E.g. for a slope of 1/5 a speed-up of 1.5 times can be expected.
- Hills cause an increase in the surface drag on the bulk flow.
- The mean streamlines over hills in some cases approach the surface and in others recirculate in wake regions. Turbulence in the flow is greatly influenced by passing over hills, particularly in the wake. This has important consequences for the “*dispersion, deposition and chemical transformation of pollutants*” (Belcher and Hunt, 1998) amongst other things.

When hill slope is low, the resulting flow can be viewed as a perturbation to the flat case, for example, by considering relative speed-up and changes to the levels of turbulence. However,

when the slope is large, non-linear processes become important. Regions of separating flow can develop in the lee of such hills. The exact position of separation and reattachment in such flows depends on the slope of the hill. The depth of the recirculating region varies up to values comparable with the hill height (H) for steep slopes. The distance that the separating region extends downwind, extends from 12H for flows with low turbulence, to 3H for very turbulent flows (Belcher and Hunt, 1998).

Numerical work has been carried out by some researchers to determine what slopes are necessary for the onset of separation in flow over hills (Giostra *et al.*, 1989; Tampieri, 1987; Wood, 1995). The results of this work compared well to the small amount of field observations and wind tunnel data. The critical maximum gradient for a sinusoidal ridge or hill required to create separated mean flow was between 0.2 and 0.5. A steeper gradient is required to produce separation for a smoother surface. It should be noted that these results are for neutral conditions only.

Belcher and Hunt (1998) point out that care should be taken in interpreting separated flows. Such flows have often been modelled in two dimensions and this can disguise the fact that, for the case of real 3 dimensional hills, the separated region is open and the mean streamlines may enter and leave the recirculating region.

“Thus the concept, advanced in the earliest papers, of a separated-flow region with closed streamlines and a separation bubble is not really appropriate. However, contaminants in some flows do tend to behave as if they are trapped because the recirculating streamlines delay downwind transport and dispersion for a time scale of about $3L_R/U_B(H)$.” (Belcher and Hunt, 1998) Note: L_R is the length scale of the recirculating region and $U_B(H)$ is the velocity at hill height.

Mason (1996) provides a somewhat earlier summary of boundary-layer flow over hills. This summary includes the effects that atmospheric stability can have on such flows. One such effect is the indirect impact that stability has on the mean velocity profile. Unstable conditions reduce the wind shear and stable conditions increase it. The speed-up of the mean flow over the crest of the hill is dependent on the wind shear, and as a result, stable conditions will increase speed up. The stability will also influence the free-stream turbulence.

One measure of the degree to which stability affects flow over topography, is the Froude number, F . In the case of a stably stratified flow over a hill this can be expressed as:

$$F \approx \frac{U}{NH} \quad \text{Equation 1.2}$$

where U is the mean wind speed, H is the hill height and N is the Brunt-Väisällä frequency (a measure of the frequency of the restoration of stable fluid to a perturbation) defined by:

$$N = \left(\frac{g}{\theta} \frac{\partial \bar{\theta}}{\partial z} \right)^{0.5} \text{ seconds}^{-1} \quad \text{Equation 1.3}$$

Where g is the acceleration due to gravity, θ is the temperature and z is the vertical height. The Froude number can be viewed as expressing the ratio of the flow kinetic energy to the potential energy required to raise fluid to the hill height, H . For values less than one, the flow will tend to pass around the obstacle rather than over the top.

In addition to the direct effects that hills cause as a result of providing an obstacle to the flow, topography can also have indirect effects on the boundary layer. For example, the incident sunlight per unit area for a sloping surface will vary depending on the slope and orientation. Differential heating of adjacent areas with different slopes can lead to thermally driven flows,

such as those in valleys (Oke, 1987). Thermally driven flows can be important in predicting dispersion over complex topography, since they can cause drainage flows that move in alternative directions to the mean flow, and carry pollutants with them.

Flows in, and over, valleys are also affected by the stability of the boundary layer. Different regimes of flow have been observed over the same valley for different stability conditions. Holden *et al.* (2000) found that in strongly stratified conditions (with a Froude number ≤ 2) flow normal to the valley axis became detached from the flow within the valley. The separated flow within the valley then developed a downvalley drainage flow. For less strongly stratified conditions (with a Froude number ≥ 2) the flow remained attached and followed the cross-sectional shape of the valley.

The above review shows that a great deal of field, theoretical and wind tunnel work has been carried out on atmospheric flow over complex topography, particularly for simplified geometries. Some work has been carried out on the effects on pollutant dispersion caused by complex topography in field and wind tunnel studies. However, for the case of deposition of particles, there is much less information available. The main source of directly relevant data is the research group of Goossens *et al.*, for example (Goossens, 1996). However, this work deals with the deposition of aeolian dust, which is larger than that of primary interest for this project. As an alternative means of gaining such information, the literature surrounding the prediction of particle dry deposition was examined, and this is discussed below.

1.3.6 Predicting dry deposition

Empirical and process models

There is a wide range of wind tunnel and field data available on dry deposition to different flat surfaces, and a summary is provided by Nicholson (1988). Several authors have sought to produce correlations of this data to predict dry deposition, for example Schack *et al* (1985). Slinn (1978) provided a good overview of the parameterisation of dry deposition terms for particles for determining radiation doses. The author describes the deposition process in terms of a series of stages; from transport through the free atmosphere, the boundary layer, canopy and the surface layer. Using this approach, the total deposition can be characterised by resistances to deposition for each stage. However, the estimates are only order of magnitude accuracy and become less reliable for averaging periods less than a year, as individual meteorological events become more significant. The author notes that for dry deposition to smooth surfaces, the transfer across the surface layer would be expected to be the controlling factor. However, for rough surfaces the deposition may be rate-limited elsewhere in the atmosphere.

Ruijgrok *et al.* (1995) considered a range of models of particle dry deposition for use in mapping particle deposition over Europe. The authors divided the models they considered into two groups:

- Process oriented models, which attempt to quantify each of the mechanisms important to deposition, and;
- Bulk resistance models, which consider the resistance to transfer for each stage of deposition.

The authors concluded that the data requirements for process models are too large to be useful for mapping applications. The majority of these models also apply only to neutral atmospheric conditions. Considering the alternative bulk resistance models they noted that no well-established models exist for particle deposition. The authors finished by noting that:

“Little is known about the dependence of v_d [deposition velocity] on vegetation type, roughness characteristics, roughness transitions and stability conditions of the atmosphere.” (Ruijgrok et al., 1995)

It would be reasonable to add that even less is known about the variation in deposition with complex topography.

The turbulence within the flow clearly influences the rate of transfer of particles through the atmosphere to the surface. Although the particles will not follow every turbulent eddy, they will be driven by drag force in the same direction as the instantaneous velocity. It is expected that the vertical component of velocity will be most important for the vertical transfer of material. In many cases detailed vertical turbulence measurements are not available and friction velocity is frequently used as a scaling parameter in their place in particle deposition studies (Lai and Nazaroff, 2000; Schack *et al.*, 1985; Sehmel and Hodgson, 1980; Zhang and Ahmadi, 2000).

Empirical and process models appear unable to predict localised particle deposition over complex topography, because they produce a uniform deposition velocity based on the assumption that the surface characteristics do not vary spatially. They can be applied in a patchwork manner to different surface types, but cannot account for complex topography. Therefore, to successfully model particle deposition over complex topography, it is necessary to model the spatial variation of the mean and instantaneous flow properties, their interaction

with the surface and the resulting effects on particle transport and deposition. In other words, the interaction of these features should be coupled together in any model used.

Coupled models of flow, dispersion and deposition

To create a coupled model of landscape, flow, dispersion and deposition, the first step is the use of an appropriate model for predicting flow over changing topography. There are a number of ways to tackle this problem and they can be broadly divided into three modelling approaches: analytical models, numerical meteorological models, and computational fluid dynamics models.

Analytical models describe the flow using a series of mathematical equations that are based on properties of the flow. They involve some degree of simplification and are generally appropriate for a specific range of cases. The limited range of applicability and the lack of detail of turbulent properties of the flow, are the principal reasons for not considering these models for coupled particle deposition models.

The term “numerical meteorological model” covers a wide range of models, including those used for large-scale weather prediction. Of particular interest for the study of flow over topography, are those models that focus on relatively complex regional flows. Peilke *et al.* (1992) provide details of an example of such a model and its typical areas of application, which include mesoscale atmospheric dispersion. These types of models typically solve the governing equations for a number of parameters, for each area of a discretised domain. Because the focus of these types of models is on meteorological variables, temperature and humidity are modelled alongside pressure and velocity. Heat and moisture transfer within the surface are also important features. However, the typical domain size for these models is of

the order of hundred of kilometres, with cell sizes of around 1-2km. Whilst this scale can capture the important features of very large topographic features, they do not provide sufficient resolution to study the fine details of flow over complex topography.

Computational fluid dynamics (CFD) models also use a discretised domain over which they solve the equations of fluid flow, and are closely linked to meteorological models, with some areas of overlap. However, CFD models can be considered to be more generalised in their design and offer greater flexibility, particularly with regard to mesh generation. The principal equations of fluid flow solved by CFD models are the conservation of mass, momentum and energy, although other equations may be included to deal with specific problems such as the transport of pollutants. CFD models have been historically developed for dealing with engineering scale flows. However, with increased development, popularity and computing power, they have become more frequently used for a broad range of problems involving fluid flow.

CFD models offer several advantages for smaller scale problems. They are capable of modelling arbitrarily complex geometry at an arbitrary resolution, which can be adapted according to the properties of the problem under consideration. Both numerical meteorological models and CFD rely on turbulence models to close the set of equations for practical problems. CFD models offer a range of turbulence models that can be selected according to the needs of the problem. Importantly, CFD models include particle modelling coupled to the fluid flow solution.

Of the three tools described, CFD has a great deal of flexibility and appeared to be an appropriate tool to study the interaction of flow and particle deposition with complex

topography. Published studies using CFD for similar problems were reviewed and a summary of their main features is presented below.

1.3.7 Computational fluid dynamics and flow over complex topography

CFD modelling has been used to study atmospheric flows for some time. In particular, it has been used to study the interactions of buildings and the winds around them, in parallel with wind tunnel studies. Specifically, it has been used to determine wind pressures on different regions of buildings, for example Richards and Wanigaratne (1993), and to model the dispersion of pollutants, close to buildings (Cowan *et al.*, 1997) and in urban street canyons (Sagrado *et al.*, 2002). A review of the use of CFD for environmental flows is provided by Kim and Boysan (1999), who focus on the modelling of airflows around buildings, but also discuss flow over hills and the importance of turbulence modelling.

Computational fluid dynamics (CFD) and wind tunnel studies have been used to model atmospheric flows over complex topography by a number of authors. Kim *et al.* (1997) studied the flow over two-dimensional hills and compared the results for several turbulence models. The authors found good agreement for mean velocity results from CFD and wind tunnel experiments. They also found that the RNG k-epsilon performed better at predicting the reattachment point than the standard k-epsilon model. Maurizi (2000) compared CFD calculations of flow over two-dimensional valleys with wind tunnel experiments and concluded that the results for mean flow were in good agreement, for a number of turbulence models. The best agreement for turbulence characteristics was achieved with the RNG k-epsilon model.

CFD models of flow over complex topography have also been compared with field data. Kim *et al.* (2000) compared CFD results with standard and RNG k-epsilon models for four sites. The authors found good agreement for mean velocity and also good agreement between the RNG k-epsilon model and reattachment point for a valley site. In addition to comparisons with field and wind tunnel data, CFD has been used to examine potential sites for wind power generation (Carpenter and Locke, 1999) and the effect of hills on pollutant dispersion (Castro and Apsley, 1997).

1.3.8 Computational fluid dynamics and dry deposition modelling

The range of recent literature, described in the section above, suggests that CFD is capable of reasonable prediction of, at least, the mean properties of flows over complex terrain. However, in order to accurately model the pattern of particle dry deposition, it is necessary to model the important physical processes of particle behaviour in these flows.

As a starting point, it is useful to note that CFD has been used to model the dispersion of gaseous pollutants by a number of researchers, both close to buildings (Cowan *et al.*, 1997), (Meroney *et al.*, 1999) and in the vicinity of hills (Castro and Apsley, 1997). The modelling of gaseous dispersion has a number of parallels to the particle behaviour in such flows. However, atmospheric particles behave differently from gaseous pollutants in certain respects and these differences need to be considered. A number of authors have tackled particle behaviour in such flows with computational models, often using a combination of Eulerian and Lagrangian models. It is worth briefly examining the differences between these model types.

Eulerian Models

Eulerian models choose a static frame of reference that is fixed relative to the ground rather than to the mean flow. The domain under consideration is subdivided into a grid of connected cells. Wind and pollutants are assumed to move through the grid as a result of advection by the mean wind, diffusion due to the turbulent component of the wind and molecular diffusion and to fall due to gravity. Pollutants can also enter or leave the domain from sources or sinks. Molecular diffusion is normally insignificant in comparison to turbulent diffusion and is often ignored. The equation for transport of pollutants is then solved for every cell in the grid. However, the nature of the equations means that an analytical solution cannot be found for every timestep, and numerical computational methods must be used. This results in a large computational demand, and this is one of the main disadvantages of Eulerian methods. Also, the accuracy and resolution of the solution is dependent on the size of the grid cells used to subdivide the domain.

Lagrangian Models

Lagrangian models choose a frame of reference that is moving relative to the ground. Lagrangian particle models follow the motion of a number of particles. The forces acting on the particles may be derived from measured, or modelled, atmospheric motions that are in an Eulerian frame. This type of model is therefore part Eulerian and part Lagrangian. The dispersion and resultant concentration of pollutants can be calculated from the trajectories, and final positions of, a large number of particles. These types of models require a description of the turbulent velocity component and there are two approaches to obtaining this: a statistical approach and a deterministic approach. The statistical approach uses a weighted random function and a simple Markov process to simulate the effect of turbulence. The

deterministic approach uses the local turbulence field to estimate the dispersion of the pollutant and therefore the concentration. The benefit of Lagrangian particle models is that they use a grid model for calculating wind speed, yet the movement of particles is independent of the grid and so the smaller scales of motion can be modelled.

Reynolds (1999) describes a Lagrangian stochastic model for the deposition of heavy particles in turbulent flows. The model is based on the momentum equation for particles and includes shear induced lift and turbophoresis. The model is used to repeatedly calculate the trajectories of particles until an average picture of their concentration and deposition is built up. Direct numerical simulation (DNS) of the equations of fluid flow and particle trajectories has been used to examine particle deposition to a surface in turbulent channel flow by van Haarlem *et al.* (1998). The authors used a similar technique for the prediction of particle trajectories, integrating the equation of motion for the particles, over a series of time steps. Repeated calculations were carried out to build up statistical information. However, no comparisons to experimental results were provided for particle deposition.

Shams *et al.* (2000) describe a more applied piece of work, examining the deposition of particles of diameter from 10 nm to 50 μm . Their model of particle motion included gravitational, Brownian and lift forces, in addition to the drag force due to the fluid. They studied a fixed flow regime of a vortex close to a wall as a model for the sublayer of a turbulent boundary-layer flow. The authors used a calculated trajectory to predict limiting trajectories for impaction of larger inertial particles and multiple solutions to obtain probability of deposition for those particles subject to significant Brownian forces. Reasonable agreement was found with experimental data for deposition.

Zhang and Ahmadi (2000) used direct numerical simulation (DNS) solutions for turbulent flow in horizontal and vertical ducts to study particle deposition. The particles were subjected to the same range of forces as above (nonlinear drag, Brownian, lift and gravitational forces), and a sample of several thousand particles was tracked. Again, the results were in close agreement with experimental data and with empirical model results. The importance of various forces was also examined and, as expected, lift and drag were the most important forces for large particles, whereas Brownian force was significant for smaller particles.

Goharrizi (1998) used a similar approach to calculate particle trajectories for flow past a surface-mounted ribbon. For this work, the flow field was solved using a Reynolds averaged Navier Stokes (RANS) solution and a k-epsilon turbulence model. The collection efficiency was calculated using limiting streamlines of the particles rather than stochastic tracking of multiple particles. Reasonable agreement was seen when compared to experimental data, deviating slightly for smaller particles. Because of the use of limiting streamlines, rather a stochastic approach to particle tracking, the effect of turbulence on the particle trajectories is limited to the effect of turbulence on the mean flow.

A RANS CFD solution was used with a similar particle model to study the transport and deposition of particles, released upwind of a small building by Ahmadi and Li (2000). The particle tracking model was slightly more sophisticated in this study and although it considered the same forces, the instantaneous velocity field used for the particle drag calculation was modelled explicitly. This was calculated using a continuous Gaussian random field, scaled by the turbulent intensity. One thousand particle trajectories were modelled to provide statistical information for each case studied. This approach appears to be a good compromise between the very computationally intensive DNS method and choosing to neglect the effect of turbulence on trajectories entirely.

CFD has been used to model the dispersion and deposition of droplets from an orchard sprayer, by Xu *et al* (1998). The authors used a k-epsilon turbulence model, and porous three-dimensional zones to model the flow from an air-assisted sprayer in an orchard. The trajectories of the spray droplets (volume median diameter 120 μm , standard deviation 50 μm) were calculated using a stochastic Lagrangian approach. The deposition was determined using an empirical probability function. Good agreement was seen between experimental and modelled spray distributions.

CFD and particle tracking have also been used for the study of particle deposition to wave surfaces as described in an earlier section (Zufall *et al.*, 1999a; 1999b). The authors also carried out wind tunnel comparisons and the work has strong parallels to the study of flow over smooth complex topography. Good agreement was seen for the fraction of material deposited to different parts of the wave.

In summary, there is a range of examples of CFD models being used to model complex flows. There are also examples of CFD being combined with particle tracking methods to model the behaviour and deposition of particles in complex flows. However, no reference could be found to the deposition to complex topography.

1.4. Summary

There is a need to better understand the relationship between complex topography and particle dry deposition for accidental scenarios, and indeed for routine and continuous releases. Particle dry deposition is a complex process governed by many factors. Deposition is reasonably well quantified for uniform landscapes, but this is not the case for complex

landscapes, where the interaction between the surface topography and the atmosphere is complicated and varies spatially. To provide advice on relative dry deposition in emergency situations, more data is needed that accounts for this interaction.

Wind tunnel experiments have been used for similar studies and are well proven for the study of atmospheric flow over complex topography. Numerical techniques have also been used to study such flows. In particular, computational fluid dynamics has been used for studying small-scale atmospheric flows, including those over topography. CFD has also been combined with particle tracking to model particle behaviour and deposition in complex flows. The set up and execution of CFD models is time-consuming and not suited to use during an emergency. However, they can be used to model specific scenarios of interest prior to such an event.

For the purposes of this work a programme of combined experimental and modelling work was followed. The focus of the experimental work has been to demonstrate, whether or not flow over complex topography has a significant effect on dry deposition (Chapter 2). Additionally, the work was intended to act as a validation for further CFD studies. The CFD work has been used to extend and parameterise the limited number of cases studied with wind tunnel experiments. The modelling approach was based on a RANS CFD solution of flows over complex topography, combined with stochastic particle tracking and deposition modelling within those flows (Chapter 3). A wind tunnel (Chapter 4) and computational study (Chapter 5), into the effect of turbulence on deposition, was also carried out to provide more insight into this relationship. Modelling has been used to assess the effect of a series of landscape geometries, and related parameters, on dry deposition (Chapter 6). The results from these geometries have been used to derive a set of rules for predicting deposition around landscape features. An example, automated system has been developed incorporating these

rules to produce maps of deposition risk for real landscapes (Chapter7). Conclusions are then drawn about the influence of landscapes on particle dry deposition and the value of the approach used (Chapter 8).

Because of the large number of figures in this thesis, the text, figures and tables have been presented separately. The figures and tables can be found after the main text, and are indexed immediately after the table of contents.

2. PARTICLE DEPOSITION TO LANDSCAPES – WIND TUNNEL EXPERIMENTS

2.1. Introduction

In order to examine the relationship between complex topography, flow and particle deposition, the relative deposition to a number of idealised scale model landscapes was studied in a wind tunnel. The experiments aimed to answer three questions:

1. Does landscape have an effect on particle dry deposition?
2. If it does, which areas are most affected?
3. In the areas affected, is there an increase or decrease in deposition rate relative to the flat case?

Wind tunnel experiments have been used by other workers to investigate particle deposition and some of these studies are described in Chapter 1. However, there is limited literature on the deposition of small particles to landscape features, although the work of Goossens and co-workers is informative for larger particle sizes (Goossens, 1988b; Goossens, 1995; Goossens, 1996; Goossens and Offer, 1990). In addition to answering the questions above, it was hoped that the results from these experiments could also be used to test the validity and effectiveness of computational fluid dynamics (CFD) models in simulating the variation in particle deposition to landscape surfaces.

Two sets of experiments were performed. The first set were carried out using a point source of particles released upstream of the model landscape, equivalent to a localised source close to

the landscape feature. A second set was carried out using multiple particle sources. A nearly uniform profile of particle concentration was achieved in the crosswind direction and in the vertical direction for the lower part of the boundary layer. This source was representative of a distant source of particles, already well dispersed, with a plume width large compared to the landscape feature. In addition to producing different patterns of deposition, there are a number of experimental consequences of the different source types and these are discussed below.

2.2. Methodology

2.2.1 Wind tunnel characteristics

All of the experiments described in this chapter were carried out in the same wind tunnel, an open-return, square cross section design, driven by a centrifugal blowing fan. The working section of the tunnel was square in cross section, 2.5 m on each side, approximately 10 m long and capable of wind speeds in excess of 10 m s^{-1} . The relatively large size of the wind tunnel was necessary to ensure a sufficiently high Reynolds number in the model flow as discussed below. The sides of the wind tunnel were smooth with a small number of obstructions, including a door handle and window on one side and several tubing connections on the opposite side. Temperature stratification of the incoming air was not possible with this wind tunnel, and as a result only neutral stability flows were simulated. The exhaust air from the tunnel passed through a filter bank to remove particles. The inlet air was unfiltered. The wind tunnel was originally built at Warren Springs research laboratories, was subsequently moved to AEA/Harwell before being acquired by the University of Birmingham.

2.2.2 Flow measurements

Velocity and turbulence measurements were made with a pulsed wire anemometer using the technique described by Bradbury and Castro (1971). The instrument uses one central wire and two detector wires, perpendicular to, and to either side of the central wire. The central wire is pulsed and causes the surrounding air to be heated. The heated air is transported by the velocity of the flow and causes a response in the detector wire when it is reached. The velocity is calculated according to the formula:

$$V = \frac{x}{t} \quad \text{Equation 2.1}$$

Where V is the velocity, x is the separation of the sensor and signal wires and t is the delay between sending the pulse and its detection in the sensor wire. The ability to measure the direction of the flow is extremely useful for the flows in this study, where regions of recirculating air are present.

The instrument probe had dimensions of approximately 10 mm in the direction transverse to the flow and 5 mm in the direction parallel to the flow. The size of the probe limited the spatial resolution of the instrument to a similar scale of the probe. The pulsed nature of the instrument, which differentiates it from the continuous output of a traditional hot-wire anemometer, introduces a limit to the maximum frequency of velocity fluctuations that can be measured. For this instrument the sampling rate was approximately 100 Hz.

The measurements were controlled and logged by a personal computer. Calibration of the pulsed wire anemometer was carried out using a pitot-static tube and a micro-manometer.

Vertical and horizontal profiles of streamwise velocity and streamwise turbulent velocity were

measured at a number of locations upwind of, over and downwind of the model landscape. A small number of measurements of the vertical turbulence component w'^2 and also $u'w'$ were made at one location over the flat landscape. The absence of a traversing apparatus made these measurements extremely time consuming and they could not be performed over each geometry. The streamwise turbulence, calculated from the same data as that used to provide the mean streamwise velocity, was therefore used as an indication of the turbulence within the flow. Measurements of $u'w'$ allowed comparison with friction velocity calculated from the vertical streamwise velocity profile.

The streamwise turbulent velocity, σ_u , was calculated using the following equation:

$$\sigma_u = \sqrt{u'^2} \quad \text{Equation 2.2}$$

where u' is the difference between the instantaneous and mean streamwise velocity. The turbulent velocity can also be expressed as the turbulence intensity, I , using the following equation:

$$I = \frac{\sigma_u}{U} \quad \text{Equation 2.3}$$

where U is the mean streamwise velocity.

2.2.3 Landscape shapes

Three simplified model landscapes and a flat control case were used in the experiments. Two of the model landscapes were effectively two-dimensional, having a uniform cross-section, whilst the third was three-dimensional. The two-dimensional landscapes were both flat-sided

ridges of slope 1 in 1 (45°) and 1 in 3 (18.4°). The ridges were of height 0.1 m and of lateral width 2.5 m, equal to the width of the wind tunnel. Figure 2.2 shows the ridge of slope 1 in 1 installed in the wind tunnel. The three-dimensional landscape was conical in shape and of height 0.2 m, with a slope of 45° . The shapes of the model landscapes were chosen to be representative of sections of real hilly or mountainous topography, and to possess sharp changes in gradient, so that the effect of flow separation could be examined. Table 2.1 summarises the geometries studied.

2.2.4 Model construction

The two, two-dimensional model landscapes were constructed from a wooden frame of MDF cross-sections, joined by softwood batons and overlaid with sheets of hardboard. The three-dimensional landscape was constructed from a series of overlaid polystyrene sections, cut to approximate shape, and finished by covering with plaster. Both the two-dimensional and three-dimensional landscapes were covered with the same roughness material as the surrounding area, which is described further below.

2.2.5 Scaling considerations

It was intended that the flow above, and deposition to, the model landscapes should be representative of full-scale landscapes. The similarity criteria of Snyder (1972) were used as a guide for choosing suitable model parameters for representative modelling of flow and dispersion. The issue of similarity of particle deposition is less well studied. Reference is made to the snow drifting work of Kind (1986), the dust emission and deposition work of Xuan and Robins (1994) and the loess deposition work of Goossens and Offer (1990). Some discussion of other particle scaling parameters is also included.

The model landscapes were created with geometrical similarity to the full-scale, at a scale of 1:1000. The criteria for similarity described by Snyder (1972) are based on a number of dimensionless parameters of the flow. These are considered in turn below.

Rossby number

The Rossby number, Ro , is a measure of the ratio of advective to Coriolis accelerations and is defined as:

$$Ro = \frac{U}{L\Omega_R} \quad \text{Equation 2.4}$$

Where U is the velocity, L is the length and Ω_R is the angular velocity. The size of this parameter depends most strongly on the scale of the model being studied. Snyder (1972) concluded that, for models representing full-scale distances less than 5 km, similarity of this parameter can be neglected. The total length of working section available, after boundary layer generation, was limited to 4.5 m equivalent to 4.5 km at full-scale. Similarity in Rossby number was therefore neglected in this study.

Reynolds number

The Reynolds number is a measure of the ratio of inertial to viscous forces. It is defined as:

$$Re = \frac{UL}{\nu} \quad \text{Equation 2.5}$$

where ν is the kinematic viscosity. Because of the small scale of the model, it is impossible to achieve similarity between the Reynolds number of the model and the full-scale flow. Fortunately flow structure is similar at all sufficiently high Reynolds numbers (Snyder, 1972).

The characteristic height for this study is the height of the landscape features. To achieve a sufficiently high Reynolds number this height should be large. However, the size of the landscape features modelled within the wind tunnel was limited by the size of the wind tunnel (2.5 m x 2.5 m cross-section, 10 m working section). To minimise the blockage area caused by the models, whilst maintaining a high Reynolds number, a height of 0.1 m was chosen for the ridges, which extended the width of the cross-section, blocking an area of 4 % of the total cross-section. The three-dimensional cone was chosen with a height of 0.2 m, producing a blockage ratio of 0.64 %. The height also determined the number of hill heights downwind that the deposition could be measured.

The Reynolds numbers of the flows, using the hill height as the characteristic length, were 33,000 for the two ridges and 66,000 for the cone. The critical Reynolds number, above which the flow is independent of the Reynolds number, is not well reported for the model shapes in question. Snyder (1972) quotes a value of 11,000 for sharp edged buildings. Chatzipanagiotidis and Olivari (1996) used a value of 11,000 for a wind tunnel study of a two dimensional ridge, quoting a critical Reynolds number of 5,000 for rough sharp objects. Therefore the values used in the experiment are believed to be large enough that the flow features are independent of Reynolds number and therefore similar between model and full scale.

Peclet and Reynolds-Schmidt product

The Peclet number is defined as:

$$Pe = \frac{UL}{\kappa} \quad \text{Equation 2.6}$$

and the Reynolds-Schmidt product as:

$$Re.Sc = \frac{UL}{\nu} \cdot \frac{\nu}{\alpha} \quad \text{Equation 2.7}$$

where κ is the thermal diffusivity and α is the molecular mass diffusivity. These parameters are the product of the Reynolds number and the ratio of momentum diffusivity to thermal diffusivity (Peclet number) or to mass diffusivity (Reynolds-Schmidt number). When the Reynolds number is large, turbulent diffusion dominates the diffusivity of mass and temperature. Therefore, these parameters can be neglected when the flow is Reynolds number independent (Snyder, 1972).

Froude number

The Froude number is a measure of the ratio of inertial to buoyancy forces, and can be expressed in the form given by Equation 1.2. The flow considered is of neutral stability, and there is no temperature variation with height. As a result the buoyancy forces in the flow are zero. Therefore, the Froude number is infinite in both cases and similarity is achieved.

Surface roughness

In this simulation, Jensen's criterion has been met. In other words, the ratio of the model surface roughness to the full-scale surface roughness is equal to the ratio of model to full-scale length scale. The model surface roughness Reynolds number ($u \cdot z_0 / \nu$) was equal to 3.1 for the flat case and greater than the criteria of 2.5 (Sutton, 1949), ensuring that the surface flow was fully rough and similar between model and full-scale. It should be noted that the surface roughness used was not an exact replica of typical rural roughness features. A fetch of cubic roughness elements (see below for details) was followed by a uniform textured surface covering to achieve the suitable roughness length.

Particle scaling

Kind (1986) provides an overview of similarity criteria for modelling the drifting of snow, a process related to modelling of particle transport. The author identified the important parameters as the densimetric Froude number, the equality of the reference to friction velocity ratio between model and full-scale and the correct modelling of ejection of particles from the surface. The short duration of the deposition processes studied in this work (30 - 90 minutes), the small amount of deposited material and the small particle diameters used (0.75 - 2 μm), mean that resuspension was not a significant factor and the last parameter can be ignored. To support this assertion, a brief consideration of the forces involved in attachment/detachment of particles is useful. Hinds (1999) gives values for typical adhesive forces between particles and surfaces for individual particles. For a 1 μm particle the adhesive force is approximately 50 times greater than the force due to an airflow past the surface, even at 10 m s^{-1} . Therefore:

“individual particles less than 10 μm are not likely to be removed by common forces”

(Hinds, 1999)

The possibility of particle bounce should also be considered as a source of re-emitted particles. Using the critical velocity approach (Hinds, 1999), even for the largest particles used and worst-case coefficients, particle bounce does not occur below 6.5 m s^{-1} . Therefore, both particle bounce and resuspension, and therefore ejection velocity, can be ignored in this study.

Xuan and Robins (1994) modelled a more relevant case of the emission and deposition of coal dust in complex terrain. They indicate that the following are important for dust *emission* modelling: equality of density ratio (particle:air), equality of emission threshold velocity, equality of terminal velocity ratio, sufficiently large roughness-height Reynolds number. They also note that the reference velocity ratio and Froude number should be the same, in order to model the particle motion and aerodynamic flow simultaneously. Because resuspension is not being modelled, the emission threshold velocity ratio is not required to be similar in this case.

Goossens and Offer (1990) have studied the deposition of loess to complex topography. The authors do not consider similarity parameters in detail, only stating that:

“To ensure fluid-particle interaction in the experiment identical to that in the field, particles should be kept the same, regardless of whether the topographic model is to scale or not.” (Goossens and Offer, 1990)

Their work is referenced here, however, because the authors performed both wind tunnel and field studies of deposition to a hill and found good agreement between the two at a scale of 1:1342.

Particle deposition behaviour is strongly dependent on particle size. Fig 1.1 shows a graph of deposition velocity against particle diameter that illustrates this clearly. Very small particles are dominated by Brownian diffusion whilst large particles are dominated by sedimentation. Scaling the particle diameter would change the physical mechanisms responsible for the deposition process. For example, scaling down the diameter by a factor of 1000 would require the use of large molecules rather than particles, for which Brownian diffusion would be the dominant mechanism. If the particle size is kept constant between full and model scale, the ratio of particle size to the landscape will be larger for the model scale. However, because of the small size of the particles this ratio will be very large in both cases. The following equation (Tennekes and Lumley, 1972):

$$\frac{\eta}{l} \approx Re^{\frac{3}{4}} \quad \text{Equation 2.8}$$

relates η , the scale of the smallest turbulent eddies to l the scale of the largest eddies. Using this equation it is estimated that the size of the smallest eddies at model scale will only be a factor of 6 smaller than those at full scale, and several hundred times larger than the particle size. The smallest turbulent eddies will therefore be much larger than the particle size at both model and full-scale and their interaction will be expected to be similar in both.

The approach used in this set of experiments has been to use representative particles, having a similar size and density as those in the field. Equality of the particle density ratio (ρ_p/ρ_f where ρ_p is the particle density and ρ_f is the fluid density) between model and full scale is therefore met. The surface roughness has been scaled by the same ratio as the geometry. Assuming a log-law velocity profile of the form:

$$U(z) = \frac{u_*}{\kappa} \ln\left(\frac{z}{z_0}\right) \quad \text{Equation 2.9}$$

where $U(z)$ is the velocity at height z , u_* is the friction velocity, κ is the von Karman constant and z_0 is the roughness length, then the reference velocity is proportional to the friction velocity. This is discussed in more detail in Xuan and Robins (1994). The reference velocity is equal between model and full-scale and therefore the terminal velocity ratio (U_F/u_* , where U_F is the particle terminal velocity and u_* is the friction velocity) will also be equal because both U_F and u_* will be equal between model and full-scale. The roughness-height Reynolds number, calculated using the formula of Kind (1986) ($u_*^3/2g\nu$ where g is the acceleration due to gravity and ν is the kinematic viscosity), is equal to 40 and greater than the criteria of 30 (Kind, 1986).

The reference velocity ratio (U/u_*) is met as both reference, and friction velocity are equal between model- and full-scale. Because of the equality of reference wind speeds, the Froude number is not equal. Xuan and Robins (1994) argue that this criterion can be relaxed for emission and deposition studies because of the short saltation trajectories for coal dust. Because saltation is not being considered in this study, the only influence of gravity will be on the fall angle ($\arctan(U_F/U)$ where U is the reference velocity) of particles when sedimentation is a significant mechanism. Because the particle size is small in this study, sedimentation will be a minor mechanism of deposition. Estimates of the angle of fall for a 2 μm particle are of the order of 6×10^{-4} degrees in the flow above the scale model. Therefore the effect of variation in Froude number on the particle trajectory will be insignificant.

Although not mentioned in the above references, another scaling parameter for particle motion is the Stokes number, Stk , defined as:

$$Stk = \frac{S}{L} \quad \text{Equation 2.10}$$

where S is the stopping distance and L is a characteristic length (Hinds, 1999). The stopping distance is the distance travelled by a particle entering stagnant air with an initial velocity, before coming to rest. It is defined as follows:

$$S = \frac{\rho_p d^2 C_c U_0}{18\mu} \quad \text{Equation 2.11}$$

where ρ_p is the density of the particle, d is the diameter of the particle, C_c is the Cunningham correction factor, U_0 is the initial velocity of the particle and μ is the dynamic viscosity of the air.

The Stokes number is a measure of the likelihood of impaction into an obstacle. When the Stokes number is above a critical value, the particle is unable to follow the flow streamlines and will impact onto the obstacle. When below this value, the particle will move with the fluid around the obstacle and avoid impaction. The critical Stokes number varies depending on the geometry, but for impaction to a plate from a nozzle, where the flow turns through 90° , the critical Stokes number is 0.24 – 0.59 depending on the geometry.

It is worthwhile examining the Stokes numbers for the flows used in this study. The highest Stokes number for the scale model would be of the order of 0.001 and for the full-scale case 1×10^{-6} . Therefore, impaction is extremely unlikely to occur as a result of the flow around the

landscape features, at either scale. The amount and pattern of deposition will, therefore, not be sensitive to this parameter.

In summary, all of the important similarity criteria have been met for the aerodynamic flow and the deposition of particles to the surface. The densimetric Froude number is not similar between model and full-scale, but for the particle size studied, where terminal velocity is low, this will not be significant. The results obtained from the scale model can therefore be expected to be similar to those for the full-scale case.

2.2.6 *Boundary layer simulation*

In order to achieve a realistic simulation of an atmospheric flow, it was necessary to produce a scaled-down boundary layer in the lower part of the wind tunnel flow. A turbulent boundary layer was developed with characteristics representative of a neutral atmospheric boundary layer at a scale of 1:1000, and with a free stream velocity of 5 m s^{-1} , and varying according to Equation 2.9. A target roughness length (z_0) of 0.2 m at full scale was chosen as representative of rural area roughness, using values from a review of the meteorological literature by Counihan (1975). Although neutral atmospheric boundary layers only exist in a limited range of meteorological situations, the deposition behaviour in these conditions is a starting point for further study.

The use of triangular spires, followed by a fetch of roughness elements, is a well-used approach to generating a model atmospheric boundary layer (Irwin, 1981) and was used in this study. The dimensions and spacing of the spires were calculated using the formula from Irwin (1981) to generate a boundary layer of depth 0.8 m. Five spires were constructed of height 1 m, base width 0.12 m and a spacing of 0.5 m between the centres of the spires. These

were placed at a distance of 1.0m downwind from a large turbulence generating grid at the upstream end of the working section. The spires were followed by a series of roughness elements, to a distance of 2.35 m downwind of the spires. The initial size (0.02 m) and spacing (0.15 m) of the roughness elements was chosen to achieve a suitable model roughness length ($z_0 = 0.2$ mm) using the calculation of Irwin (1981).

The fetch of the roughness elements was limited by the practical arrangement of the wind tunnel. The doorway providing access to the wind tunnel prevented the ideal positioning of the landscape features. Placing these features further downwind would not have allowed sufficient downwind distance for deposition measurements. The landscapes were therefore placed immediately upwind of the access door shortening the fetch of the boundary layer development region. The boundary layer was developed more quickly by adding three rows of larger roughness elements. These were placed between the spires and the 0.02m sized roughness elements. Additional strips of shallower roughness element were added after the main section of roughness elements.

The final arrangement was varied by trial and error, to achieve a velocity profile that fitted a log-law velocity profile consistent with the desired roughness length of 0.2 mm (model scale). The arrangement used was seen to produce a boundary layer that was reasonably consistent with downwind distance. The arrangement of the spires and roughness elements in this section is shown in the diagram in Figures 2.1 and the photograph in Figure 2.2. To maintain the developed boundary layer flow, a textured material was applied to the surface of the landscapes and the flat control. This surface was also applied to the floor area upwind and downwind of the model landscapes. The material used was a textured wall covering with an array of uniform raised bumps with a height of approximately 0.5 mm.

The walls of the wind tunnel were smooth, with the exception of a small number of minor obstacles downwind of the landscape features. Therefore, the boundary layer developed adjacent to the vertical walls would be expected to be smaller than that developed over the floor of the wind tunnel. To minimise the effects of the walls on the dispersion and deposition of particles, the surface sampling locations were situated at least 0.5m from the walls.

2.2.7 Particle generation

The original experimental design involved the use of a spinning disc aerosol generator to produce monodisperse sodium fluorescein aerosol. However, trials using this method proved that it was incapable of producing sufficient numbers of particles for the detection of their deposition. As an alternative, sodium fluorescein particles were generated using a medical nebuliser (Acorn II®, Marquest Medical Products, Inc., Englewood, CO, 80112, USA. Ref 124014, Lot 703E), containing a solution of 25 g L⁻¹ sodium fluorescein. This generated particles at a much greater rate. The flow rate of air through the nebuliser was approximately 5.7 L minute⁻¹.

For the point source experiments, the output from the nebuliser was fed into a 25 mm diameter tube leading downwind from the nebuliser, and entering the boundary layer at a point located 0.21 m from the end of the boundary layer development section, with its centre 12.5 mm above the floor of the wind tunnel. The tube allowed the point source to be located close to the model landscapes (~0.9 m and 1.3 m upwind of the peak of the ridges and cone respectively) without the body of the nebuliser disrupting the flow. Particles were released for 30 minutes for the point source experiments.

The particles released were characterised with a light-scattering particle monitor (GRIMM Technologies Model 1.105). Approximately 90 % of the particle volume was in the size fraction from 0.75 – 1 μm diameter and 10 % was in the size range 1 – 2 μm diameter. Although the particles were not monodisperse, a nebuliser was used in preference to aerosol generators with a narrower range of particle sizes, because of the higher aerosol concentrations possible. There is relatively little difference in the deposition velocity between particles in this size range and therefore, the lack of monodispersity should have little effect. In addition, the use of a flat reference case eliminates any spatial bias due to particle size. Particle concentrations at the plume centreline, immediately upwind of the landscapes, were in the order of 160,000 particles L^{-1} .

To produce the broad source of particles upwind of the landscapes, six release points were used in place of the single source. The spacing and upwind distance from the landscapes was estimated using a simple Gaussian model for the dispersion of a gas. The locations used were equally spaced across stream and placed at a height of 0.2 m above the floor and at a distance 1.0 m downwind of the boundary layer generating spires. The release points were connected to a larger manifold by 15 mm tubing. The manifold was fed by a set of eight nebulisers of the same design as used for the first experiments. Although eight nebulisers were used for this experiment, their output was spread over a wider area than for the point source and the resulting concentrations and depositions were therefore reduced. The release time for the source was increased from 30 to 90 minutes to compensate for this.

2.2.8 Particle deposition measurement

To measure the deposition of particles, 25 mm Whatman GF/A filters were placed on the textured surface, using double-sided adhesive tape, at intervals along the centreline of the

wind tunnel and also across the width of the tunnel at several locations. Once the filters were positioned, the flow within the wind tunnel was started and the motor allowed to stabilise for a period of 10 minutes. The particles were then released from the source for a period of 30 minutes. Following exposure the filters were collected and shaken with 20 mL of pH 7 buffer in a 50 mL beaker for 10 minutes. The resulting solution was quantified by fluorimetric analysis with a fluorometer (Perkin Elmer 1000M), pre-calibrated with standard solutions of known concentrations.

The positions of the collecting filters and the arrangement of the other elements in the wind tunnel are shown in Figure 2.1 for the two-dimensional ridge with 1 in 1 slope. The filters were placed in similar positions for the other landscapes, with additional filters placed on the surface of the cone and in its wake. As noted above, the sample locations were restricted to the central area of the wind tunnel, with none placed closer than 0.5 m from the walls.

Attempts were also made to visualise the deposition pattern using illumination of the area with an ultraviolet lamp (1000 W UV flood lamp, UV Light Technology Limited, Birmingham). Photographs of the area were taken using a yellow photographic filter to eliminate all but the fluorescent light emitted by the deposited sodium fluorescein. However, the attempts were not successful because the fluorescence of the sodium fluorescein salt was dependent on the chemical being in the aqueous phase. Spraying the area with demineralised water was tried as a last resort and did, briefly, reveal the deposited material. However, this was impractical as it caused the surface covering to buckle and the deposited material to be washed away. Such a visualisation could be carried out using a non-aqueous form of fluorescein or a similar dye, with care taken to ensure even illumination of the surface.

2.3. Results

2.3.1 Flow measurements

In the following section all longitudinal (X) distances are given as distance downwind from the peak landscape height, with the exception of the flat case where they are given from the particle source. All lateral distances (Y) are given as distance from the wind tunnel centreline, increasing to the left hand side when looking downwind. All vertical distances (Z) are given as height above the flat landscape surface. The velocity profile for the developed boundary layer fitted a log-law profile of the form given in Equation 2.9, as shown in Figure 2.3 for varying distances downwind of the release point. The velocity profile varied very slightly with downwind distance, giving values of u_* of 0.22 - 0.24 m s⁻¹ and z_0 of 0.22 - 0.19 mm at model scale. This surface roughness at full-scale is typical of atmospheric boundary layer flow over rural terrain (Counihan, 1975). The vertical profile of streamwise turbulence intensity is shown in Figure 2.4. The values in the lower part of the boundary layer agreed well with typical streamwise turbulence values for the lower part of atmospheric boundary layers (Stull, 1988). Farell and Iyengar (1999) present a review of wind tunnel simulation of atmospheric boundary layers. Amongst the data presented is a graph of streamwise turbulence intensities, from a range of sources, for slightly longer roughness lengths than modelled here. Figure 2.4 agrees well with these results, with turbulence intensities slightly lower, as would be expected for the lower roughness length. For example, the turbulence intensity at a full-scale height of 50 m was 18 % in this study compared with a range of approximately 14 - 28 % reported by Farell and Iyengar (1999).



Table 2.2 shows values for the streamwise, vertical and cross-term turbulence measured at 0.05m above the flat surface. As expected the vertical turbulence component is lower than the streamwise component. Using the relationship in Equation 2.12 below, the friction velocity was calculated from these measurements. A value of 0.20 m s^{-1} was calculated, in reasonable agreement with the range determined from the log-law profile described above.

$$u_* = \sqrt{-\overline{u'w'}} \quad \text{Equation 2.12}$$

Figures 2.5 (a-c) show the effect of the landscapes on the vertical profiles of longitudinal velocity at varying downwind distances. The vertical profiles at the peak of the hills ($X = 0.0 \text{ m}$), and in the immediate wake show a region of increased velocity in the upper part of the boundary layer. This is more pronounced for the ridges, which extend across the width of the tunnel and have a larger projected area, than for the three-dimensional cone. In the wake behind the hills, the velocity above the hill height is higher than the upstream value, but changes rapidly towards the surface, with a region of recirculating flow close to the surface. The velocity profiles further downwind ($X = 1.55 - 1.95 \text{ m}$) show a recovery back to the upwind profile. Figures 2.6 (a-c) present the same data in a more intuitive way, with the velocity normalised to the free stream value, with the y-axis of the graph at the measurement location and the cross section of the landscapes indicated.

Figures 2.7 (a-c) show the streamwise velocity measured at 0.05 m above the surface (model scale), along the centreline of the wind tunnel, for each case. There is a clear region of speed-up on the upwind face of the slope, followed by a sudden reduction in velocity and reversal in flow direction in the wake of the hill before the velocity returns to a positive value further downwind. The recirculating region is smaller for the ridge of shallower slope, although measurements at 0.02 m above the surface identified the reattachment point at 0.4 m from the

peak, suggesting a shallow, elongated region of recirculating flow. Note that, the velocity in the wake of the cone recovers more quickly than the ridges, despite the extra height of the cone (0.2 m), because of its limited extent across the width of the wind tunnel. Figures 2.8 (a-c) show the profiles of turbulent velocity measured at 0.05 m above the surface. All three graphs show an increase in the wake, with the more steeply sloped ridge and cone showing a small minimum in the immediate wake. The cone also shows two maxima, one immediately behind the peak and one in the wake. The local minima are thought to be a result of the measurement point moving below the area of high turbulence created at the peak, before it re-enters the turbulent wake advected downwind from the peak. In the case of the three-dimensional cone, the secondary peak in turbulence may be caused by vortices shed from the sides of the cone, that merge behind the cone.

2.3.2 Particle concentration results

Lateral and vertical profiles of the relative particle concentrations immediately upwind of the landscapes are shown in Figures 2.9 and 2.10, for the point source and for the broader source. Although the broader source does not result in a concentration that is constant with lateral position it falls off much more slowly than for the point source. The fall off towards the edges for the broader source is believed to be due to losses in the manifold, resulting in less particles being released from the points further from the manifold inlet. There is no evidence of effects due to the boundary wall even at 0.3 m from the wall. The vertical concentration profile is also much more constant with height than for the point source, and is a more representative of a plume from a distant source.

2.3.3 Particle deposition results

Experimental deposition rate for the flat case is shown in Figure 2.11. There is a strong decay with increasing distance, due to the reduction in concentration as the aerosol is dispersed with increasing distance from the source. The local variations in deposition rate were thought to be due to experimental error as discussed later in this chapter. A power law curve was fitted through the points and used to normalise the deposition to the landscape cases. Lateral samples also showed that the deposition reduced strongly with distance from the centreline, as shown in Figure 2.12. This is expected from the concentration profile in Figure 2.9. There was evidence of a slight asymmetry in the flow, with the plume centreline moving towards the negative Y direction with increasing downwind distance. This is particularly noticeable for the distances $X = 2.84$ and 3.84 m. This may be due to effects from the boundary layer from the sidewalls becoming more noticeable at further downwind distances. The door for wind tunnel access was on the negative Y side and may have caused increased mixing on this side. The flat case was used as a baseline against which to compare the deposition to the model landscapes. The use of the flat case to normalise the deposition will reduce the importance of small asymmetries in the deposition.

Figures 2.13 (a-c) show the ratio of deposition rate relative to the flat case for the three landscape cases. For all three cases there is a similar pattern: a small reduction in deposition upwind of the landscape feature, a significant increase (up to 1.7 times) on the windward face and a reduction (as low as 0.07 times) in the immediate wake which recovers back to the upwind value with further distance downwind. Figures 2.13 (b-c) appear to show the relative deposition rate increasing with additional distance downwind. However, this is thought to be

an artefact of the calculation of relative deposition rate. This is discussed in more detail below.

The graph for centreline deposition for the 1 in 1 cone shares the same general features as the two dimensional landscapes. However, the increased deposition to the upwind face is significantly increased and the reduction in the immediate wake in the experimental results is not as significant as that for the ridges. The less significant region of reduced deposition behind the cone may be due to particles travelling around the sides of the cone and the smaller region of recirculation (in three dimensions) compared to the two-dimensional cases.

In addition to the samples taken along the centreline of the cone, a number were also taken on the cone surface and in the wake, up to a distance 1 m (5 hill heights) downwind of the peak. The resulting deposition rates at these locations are presented in Figure 2.14, which shows that there are areas of increased deposition to the sides and base of the windward face of the cone, in addition to the peak. Note, that this graph shows actual deposition rather than the ratio to the flat case. In the wake, the centreline deposition values are lower than those to each side. There is also some asymmetry in the pattern of deposition rate, with those at negative Y values showing slightly increased deposition relative to positive Y values. This agrees with the values seen in Figure 2.12 for the lateral deposition for the flat case. It is believed that this may be due to some slight asymmetry in the flow in the wind tunnel as described above, causing increasing deposition to one side.

Figure 2.15 shows the variation in deposition with downwind distance for the flat case with a broad particle source. It is clear that the fall off in rate with distance is much slower than for the point source (Figure 2.11). The magnitude of the deposition rate is smaller for the broader case ranging from $0.013 - 0.045 \mu\text{g m}^{-2} \text{s}^{-1}$ compared to $0.026 - 1.76 \mu\text{g m}^{-2} \text{s}^{-1}$. A three-fold

increase in release time was used to increase the total deposition for the broad source case. Figure 2.16 shows the lateral variation in deposition. This graph echoes the concentration profile in Figure 2.12 with its shallower fall off from the centreline. There is clearly some experimental noise in Figure 2.15 and also evidence of asymmetry at larger downwind distances in Figure 2.16, as seen in Figure 2.12. These are explored further in the discussion below.

The results for deposition to the 1 in 1 sloped cone with a broad source are presented in Figure 2.17, normalised to the flat case deposition. There is some experimental noise evident. However, the pattern of deposition close to the cone is very similar to that measured for the point source, with a large increase on the windward face (2.1 times), followed by a drop in the immediate wake (0.46 times) and then a second peak, before settling back towards a ratio of 1:1 with the flat case. It is worth noting that the peak downwind of the cone for this case is greater than one, compared with a value less than one for the point source for this geometry. This may be due to the enhanced mixing down of particles at a greater height towards the surface.

Figure 2.18 shows the deposition rate for the surface of the cone and the immediate wake. A number of features are apparent from Figure 2.18:

- Increased deposition to the top and centre of the windward face
- Reduced deposition on the lee side of the cone
- Enhanced deposition to each side of the centreline in the wake

There also appears to be some asymmetry to the deposition, but it is not clear if this is due to experimental noise or slight asymmetrical flow in the wind tunnel. These influences are described further in the discussion below.

One possible explanation for the variation in deposition rate in the presence of the landscape, is the variation of concentration at different locations because of effects of the landscape on the dispersion of pollutants. In order to determine whether this was the main cause of the differences in deposition rate, concentration measurements were made over a section of the cone at a number of points where deposition rate was also measured. Measurements were made using two light-scattering particle monitors (GRIMM Technologies Model 1.105). One was used to measure the concentrations at each point and a second to provide a correction for any variation in nebuliser output during the measurement period.

By combining the deposition fluxes and measured concentrations, deposition velocities were calculated according to Equation 1.1. Figures 2.19 and 2.20 show the deposition velocities calculated for a section of the cone using the deposition rates and measured concentrations. Figure 2.19 shows the variation with downwind distance along the centreline of the wind tunnel, from a distance 2.25 hill heights (-0.45 m) upwind of the peak to 4.75 hill heights (0.95 m) downwind of the peak. The change in deposition velocity shows a very similar pattern to that for the ratio of deposition rate to the flat case in Figure 2.17. This suggests that the variation in deposition rate is not due to variation in concentration alone. Figure 2.19 appears similar in shape to the graph of streamwise turbulence (Figure 2.8(c)). This suggests a relationship between the two. Although deposition velocity appears to be offset slightly upwind compared to the Figure 2.8(c), this is due to the lower measurement height of the concentration ($Z = 0.02$ m) and deposition flux ($Z = 0.00$ m), compared to the turbulence ($Z = 0.05$ m).

Figure 2.20 shows the variation in deposition velocity laterally in the wake of the cone at a distance of 2.75 hill heights (0.55 m) from the peak. It is clear that there is a minimum at the centreline with a maximum at either side. Again, this confirms the pattern seen in Figure 2.18 for the ratio of deposition rate to the flat case.

2.4. Discussion

The wind tunnel experiments described in this chapter are limited in scope. The wind tunnel is of course at model scale and the measured particles are at full scale as discussed in section 2.2.5. The experiments only consider a neutral boundary layer and a small number of representative geometries. Instrumental limitations have restricted the available turbulence components measured and the vertical resolution of the measurements. Some of the data from large downwind distances also indicate the presence of some asymmetry in the wind tunnel flow, possibly due to the effect of small obstacles on the entrance (negative Y) side of the wind tunnel. Despite these limitations, the experiments show some clear results and these are summarised below.

The model landscapes had a significant influence on particle deposition. A number of general features were identifiable:

- A slight decrease in deposition upwind of the raised topography
- A maximum on the upwind face close to the peak
- A region of decreased deposition on the leeward face, extending into the immediate wake and gradually recovering with distance to upwind levels

In the case of the three-dimensional cone there is a notable pattern of deposition on the surface of the cone with a minimum at the centreline in the lateral cross-section of deposition in the wake. The peak in deposition in the wake of the cone (Figures 2.13 (b), 2.17 and 2.19) coincides with a peak in the streamwise turbulence.

The results appear to be in qualitative agreement with wind tunnel studies for larger particle sizes to the ridge itself (Goossens, 1988b), although the present data shows no rise in the wake because of the difference in source characteristics. The two-dimensional results are also in broad agreement with wind tunnel, and CFD studies, to wave surfaces (Zufall *et al.*, 1999a; 1999b).

Although the deposition to the cone with a broad source is similar to the point source there are three points of particular note:

1. The ratio of deposition to the upwind face is higher for the broader source, peaking at around 2.1 times the flat case compared to 1.7 times for the point source. This is possibly a result of the greater vertical extent of the particle plume from the broad source and increased turbulent mixing in this region.
2. The secondary peak in deposition in the immediate wake of the hill has a ratio greater than one for the broad source, and less than one for the point source. In other words, deposition will be enhanced where the source is further away from the hill and higher up, and reduced when close to the hill and lower down, when compared to the flat case. A physical explanation may be that, for the point source, the hill partially blocks the low plume and mixes it with cleaner air from above. In the case of the broader source, the air above contains similar particle concentrations to that lower down and, therefore, the concentration behind the hill remains high. Figure 2.19 indicates that the local deposition

velocity is high in this region and therefore if the concentration is the same as the upwind value, deposition will be increased. This supports the view that, for the point source, the concentration may be lower behind the cone.

3. There is increased deposition to each side of the centreline in the wake of the cone. There was some evidence for this from the point source experiment, but the broader source shows this more clearly. The results from Offer and Goossens (1995) for deposition of larger particle sizes to a conical hill show a similar pattern, but over the body of the hill itself. The authors of that paper also discuss the presence of horseshoe vortices shed from the sides of the cone. It is thought that these areas of increased turbulence may be the cause of the deposition pattern in the wake of the cone.

The calculation of deposition velocities is particularly informative. They indicate that the effects on deposition rates relative to the flat are not due solely to the change in local concentration because of the landscapes. This suggests that there is a change in some property of the flow that is responsible for the increased deposition. This is most likely to be the local turbulent mixing and the vertical turbulence component in particular. The area in the wake of the cone is particularly interesting and suggests some association with turbulent structures caused by the cone.

Some discussion of experimental error is required. It was necessary to use of a point source close to the ground and close to the model landscape to achieve a large enough concentration to perform the experiment in a reasonable time. As a result the concentration, and therefore the deposition rate, fell sharply with distance. Whilst the deposition rate fell with distance downwind, the absolute experimental error remained constant. Therefore the relative error in the results increased with downwind distance. For the point source where this effect was most

exaggerated, the relative error based on variation in the unexposed filters was estimated as varying from 0.09 - 0.28 % relative standard deviation for the highest values close to the source, up to 5.5 - 10.0 % relative standard deviation for the lowest values at the far downstream locations. For the broader source, where the concentration fell less with distance the range varied less from 3.7 % to 5.5 % relative standard deviation for the upstream and downstream measurements respectively. An additional source of error, not included in these estimates, was the loss of small, but variable amounts, of the collecting filter onto the adhesive tape used for mounting the filters. Were the experiments to be repeated the error could be improved by using a stronger particle source to reduce the background variation, and either an alternative filter mounting system with duplicate smaller filters or multiple repeated experiments.

Despite the presence of the experimental error discussed above, comparison of the size of the deposition velocities with field, wind tunnel and model results was encouraging. The values in Figure 2.19 give a deposition velocity between 0.01 and 0.02 cm s⁻¹ for the area not affected by the landscape feature. Zhang *et al.* (2001) quote a range of values for field studies, although none have such a narrow range of particle sizes. The closest comparison is a mean value of 0.05 cm s⁻¹ for a rural surface and particle size 0.09 - 2.5 µm. Because the 0.75 - 2 µm region is expected to have the lowest deposition velocity the field values will be weighted by other sizes, resulting in a larger deposition velocity for the field values. With this in mind the results from this experiment appear in good agreement with field values. Predicted values for a similar friction velocity (0.2 m s⁻¹) and particle size (1 - 2 µm) are 0.05 - 0.10 cm s⁻¹ according to the predicted values by Sehmel and Hodgson (1980). Values quoted by Slinn (1978) for wind tunnel work over a range of roughness lengths and friction velocities, ranged from 0.01 - 0.03 cm s⁻¹ for this small range of particle sizes. The wind tunnel results are

therefore in good agreement with previous wind-tunnel results and full-scale measurements and in reasonable agreement with the model of Sehmel and Hodgson (1980).

2.5. Conclusions

The wind tunnel experiments described in this chapter have modelled the spatial variation in the dry deposition of particles to scale landscapes. Measurements of the flows established in the wind tunnel, indicate that they are a good approximation of a neutral atmospheric boundary layer flow. The landscape features produced significant influence on the modelled flows, with varying sized regions of recirculating flow in the wake of the ridges and the cone. Streamwise turbulence close to the ground was also strongly influenced by the landscapes.

The measured deposition rates were clearly affected by the presence of the landscapes and the ratios of deposition rate relative to the flat 'control' case were calculated. These showed regions of increased deposition, typically on the windward face of the landscape and regions of decreased deposition on the leeward face and the immediate wake. More complex effects were seen in the case of a three dimensional cone, with a minimum in deposition along the centre of the wake, but maxima to each side.

The importance of the source geometry was also investigated and some differences were seen using a broader source. Measurement of concentrations and calculation of deposition velocities also indicated that the variation in deposition rate is not attributable to variations in concentration alone. There appears to be a relationship between the local deposition velocity and turbulence.

To answer the questions posed in the introduction to the chapter:

1. Landscape shape does appear to influence dry particle deposition.
2. The windward and leeward faces, and the immediate wake appear to be most affected.
3. Deposition rates appear to increase on the windward face and decrease on the leeward face and in the wake for a point source close to the ground. An increase in the wake was seen for the broad source. Other, more complex effects were seen for the three-dimensional cone.

The results from these experiments indicate the effect that such landscape features can have on dry deposition. There is clearly a consistent pattern evident between the cases, although the source geometry does have an influence, particularly in the wake. The scaling considerations described at the start of the chapter suggest that these results are applicable to the full-scale case. The wind tunnel results have been used as validation data sets for the CFD modelling of dry deposition, and that work is described in the next chapter.

To predict the effect of deposition in the field, these results can be combined with wet deposition calculations that are straightforward, when the amount of rainfall is known. The cases here all assume a neutral boundary layer. Deviation from neutral stability would be expected to alter the pattern of deposition, primarily by altering the flow regime over the landscape features. The influence of surface roughness may also have an influence, particularly where it varies spatially over the landscape features. The interaction of multiple features would also be expected to complicate matters further. This last influence has been explored in Chapter 6.

The results of the three point source wind tunnel experiments presented in this chapter have been published in *Atmospheric Environment*, together with a selection of the computational

fluid dynamics results from Chapter 3 (Parker and Kinnersley, 2004). A copy of the paper is included in Appendix 1.

3. PARTICLE DEPOSITION TO LANDSCAPES – COMPUTATIONAL FLUID DYNAMICS STUDIES

3.1. Introduction

The principal aim of this work was to predict variation in particle deposition over a local area close to landscape features. Experimental studies of model landscapes can provide results for a limited number of cases, but wind tunnel experiments are expensive and time consuming. To make predictions over a wide range of cases, a mathematical model is needed. As discussed in the introduction, analytical models of particle deposition have been developed by a number of authors for flat topography. However, none have dealt with the variation due to changes in the geometry of the surface. The physical properties that are believed to be important in modelling the dry deposition of particles are as follows:

- Wind speed
- Turbulence
- Curvature of the flow
- Particle inertia
- Gravitational force

In order to model particle deposition successfully any model used should include these processes. Where appropriate, they should be able to model the interaction with the geometry being studied. In Chapter 1, the choice of model type was discussed, and the benefits of a

computational fluid dynamics (CFD) model were highlighted. Namely, that CFD models offer flexibility in the choice of scale, turbulence model, mesh generation and include detailed particle tracking. This type of model has also been used by other workers to study particle deposition, and this is dealt with in some detail in Chapter 1. For the work described below, the commercial CFD software package Fluent 5, was used. This particular software package was chosen based on its general purpose nature, the inclusion of suitable particle and turbulence models and also its local availability.

CFD models are designed to be used for many different types of flows including engineering, aerodynamic and environmental applications. Because of their general nature, it was necessary to develop and validate a suitable methodology to ensure that the results obtained were appropriate for typical atmospheric flows. In addition, the particle deposition predicted by the CFD had to be validated against experimental measurements of particle deposition in real flows. The first part of this chapter deals with the development of a method for predicting atmospheric flows, and the turbulence within them, around geometric shapes. The second part deals with the development of a method for predicting the particle deposition in flows over different geometries.

3.2. Predicting atmospheric flows

CFD has been used by a number of researchers to model atmospheric flows. This is typically for one of three reasons:

- to predict the wind loadings on newly built structures (Richards and Wanigaratne, 1993),
- to predict wind speed up over topography (Carpenter and Locke, 1999),
- to predict the dispersion of pollutants from sources in close proximity to complex buildings or groups of buildings (Cowan et al., 1997).

CFD has become a tool used in conjunction with scale model wind tunnel studies for these purposes. It allows the detailed investigation of the flow properties and the effects of variations in geometry and other parameters. There are a number of commercial and custom developed CFD codes used for this purpose. The variety of models available, and the complexity of the inputs to these models, have caused some concern over the suitability of the results for such purposes, particularly when used without validation. The validation of such models is dealt with below, after a discussion of some of the important features of CFD models.

3.2.1 CFD basics

Physical models

Computational fluid dynamics is based upon three physical laws that govern the motion of fluids. These are the conservation of mass, the conservation of momentum derived from

Newton's second law of motion and the conservation of energy from the first law of thermodynamics (Versteeg and Malalasekera, 1995). For some flows the conservation of energy can be neglected. For a Newtonian fluid, the viscous stresses are proportional to the rate of the fluid deformation, and the Navier-Stokes equations for fluid flow can be derived from these three sets of equations. The equations for the conservation of momentum in the x, y and z directions respectively, can be written as follows (Versteeg and Malalasekera, 1995):

$$\rho_f \frac{Du}{Dt} = -\frac{\partial p}{\partial x} + \text{div}(\mu \text{ grad } u) + S_{Mx} \quad \text{Equation 3.1}$$

$$\rho_f \frac{Dv}{Dt} = -\frac{\partial p}{\partial y} + \text{div}(\mu \text{ grad } v) + S_{My} \quad \text{Equation 3.2}$$

$$\rho_f \frac{Dw}{Dt} = -\frac{\partial p}{\partial z} + \text{div}(\mu \text{ grad } w) + S_{Mz} \quad \text{Equation 3.3}$$

where ρ_f is the fluid density, p is the pressure, μ is the dynamic viscosity and S_{Mx} , S_{My} , S_{Mz} are additional sources of momentum in each direction.

The Navier-Stokes equations can be applied to each individual element of fluid, and form the basis of the CFD technique. Analytical solutions to these equations are only possible for a few limiting cases. For general flow problems, a numerical approach must be used.

By integrating these equations over finite control volumes within the fluid, discretised equations can be derived. By dividing the model domain into a set of finite volumes, a series of simultaneous equations can be produced, which can be solved using linear algebra techniques to calculate the flow properties throughout the domain. An iterative approach is needed to couple the pressure and velocity solutions together. For the majority of flows of

interest to CFD, and in the case of atmospheric flows, the fluid flow is turbulent. This results in a very wide range of length scales that are impractical to resolve directly. A model of the turbulence is therefore required and this is discussed below.

There are a number of distinct steps involved in carrying out a CFD analysis. These can be broadly divided into pre-processing of the model, solving the equations and post-processing or analysing the resulting data. Versteeg and Malalasekera (1995) provide a useful overview of these steps and this has been partly reproduced below:

Pre-processing

- Definition of the geometry of interest, the computational domain.
- Sub-division of the geometry into a number of smaller, non-overlapping sub-domains to produce a mesh of cells.
- Selection of the physical and chemical phenomena that need to be modelled
- Definition of fluid properties
- Specification of appropriate boundary conditions at the edges of the domain.

Solving

- Approximation of the unknown flow variables by means of simple functions.
- Discretisation by substitution of the approximation into the governing flow equations and subsequent mathematical manipulations.
- Solution of the resulting algebraic equations.

Post-processing

- Visualisation of computed results using a number of different graphical techniques.
- Direct numerical output.

The software used, Fluent 5, in common with the majority of the commercial CFD solvers available, is based on the finite volume method of solving the governing equations.

Mesh generation

The generation of a suitable mesh to resolve the important features of the flow can be one of the most time consuming parts of a CFD analysis. Different types of mesh are available with which to subdivide a domain. For a cuboidal domain with the mean flow normal to one face, hexahedral cells are a natural choice, as the mean flow will be normal to two of the cell faces. The spacing of the cells can be adjusted to provide better resolution in certain areas. However, too large a ratio of the longest to shortest edge, can present problems to the solution.

A uniform array of hexahedral cells is termed a structured mesh and in the past was the only type of mesh available within some CFD packages. Advances in mesh generation have provided the option of unstructured meshes that are more suitable for more complex geometries, where the mean flow direction may not be clear or it may be impossible to subdivide the region into hexahedral cells.

Boundary conditions

In order to solve the equations for the fluid flow, the initial conditions at the boundaries of the domain must be set. It is also necessary to set the initial values within the domain. For the

CFD solver to give useful results the boundary conditions should be set to realistic values. Typical boundary conditions include no-slip walls at which the velocity is set to zero at the boundary, velocity inlets at which the velocity and turbulence parameters are defined and outlets where neither is defined and the values are extrapolated from within the flow domain. Symmetry boundaries are also possible where there is a plane of symmetry within the domain. These can be used to reduce the number of cells needed to model the domain, or alternatively, increase the resolution for the same number of cells.

Turbulence models

The ratio of inertial to viscous forces for a particular flow is described by the Reynolds number, Re , as defined in Equation 2.5. As Re increases, the nature of fluid flow changes from predictable laminar flow to unsteady, chaotic turbulent flow. The turbulent nature of many flows, including those within the atmosphere, result in eddies with a wide range of length and time scales. To calculate the motion of the eddies at every scale within a turbulent flow is beyond the ability of present day computing power, for all but the simplest flows. In practice, for many purposes the prediction of the individual turbulent motions is unnecessary and a statistical measure of such turbulence is sufficient. By separating the flow properties into their mean and fluctuating components, the Navier Stokes equations can be expressed in terms of the mean components and additional Reynolds stresses. These forms of the equations are termed the Reynolds averaged Navier Stokes (RANS) equations. However, a consequence of this approach is the introduction of a further six unknowns, the Reynolds stresses, into the equations. In order to solve these equations a model of the turbulence must be used. There are a number of different approaches of varying complexity that can be used to model turbulence.

The various benefits and disadvantages of these are described in Section 3.3 below and in more detail in Chapter 6.

Solving

Once the boundary and initial conditions have been defined, the CFD solver is set to iterate towards a solution. A number of options are available which determine the manner in which the governing equations are solved. As the solver iterates, information on the progress of the solution is available in terms of residuals. These are a measure of, either the imbalance in the continuity equations for segregated solvers (momentum, continuity and energy equations solved sequentially), or the rate of change of variables for coupled solvers (momentum, continuity and energy equations solved together). As the solution progresses and approaches a stable solution it is said to converge. The degree to which the solution has converged can be judged from the residuals, with lower values indicating better convergence. Residuals do not diminish to zero because of rounding errors within the computer implementation of the calculations (Fluent, 1999e).

Post processing

When the solution has converged sufficiently, the solved flow has to be presented in a meaningful way. There is a wide variety of ways that information regarding the flow can be viewed, and these range in complexity. The simplest might be the numerical value of a scalar value such as the mean velocity in a given direction, at a discrete point. The same information could be presented for a line in the domain (for example, the inlet in a two-dimensional domain) by plotting it on a XY graph. Velocity information can be presented as a series of vectors for a subsection of the domain. Contours can also be plotted to represent scalar values

over a two-dimensional surface. Other methods are also available, such as plotting streamlines, iso-surfaces and particle tracks. Appropriate techniques can be used to identify particular features of the flow, particle behaviour and deposition from the flow.

Limiting factors

The accuracy of the CFD solution is limited by a number of factors that include:

- Inclusion of appropriate physical forces and geometry
- Spatial resolution of the mesh
- Choice of turbulence model for turbulent flows
- Rounding errors

Without modelling the physical processes that control the phenomena of interest, the model cannot produce useful results. In this case the fluid flow, turbulence, its interaction with complex geometry and particle behaviour are important. These are described in more detail below. To ensure sufficient mesh resolution, cells were focussed close to the surface where the flow properties have the highest spatial gradients. The effect of mesh resolution was examined in each set of studies and is described later in this chapter and again in Chapter 6. A variety of turbulence models were investigated and an appropriate choice was made for the type of flow. The models considered are discussed below and also in Chapter 6. Rounding errors were minimised by solving all flows until the residual values were low and stable.

3.2.2 Computational Wind Engineering 2000 competition

As discussed above, one of the biggest obstacles to acceptance of CFD as a valid tool for studying flows of all types is the scarcity of validation of such flows with experimental results. Even where particular CFD solvers have been shown to produce close agreement with experiment, the great variety in choices of software, models, options and input parameters may mean that a suitable solution may not be guaranteed from different approaches to the problem. Where experimental results are available beforehand, there may be a suspicion that the CFD processes have been optimised to produce flows that agree well with experiment.

In an attempt to test the validity of the results from a number of CFD practitioners modelling atmospheric flow past a bluff body, a comparison of CFD results and field measurements was carried out as part of the Computational Wind Engineering 2000 (CWE2000) conference. CFD practitioners were asked to model the atmospheric flow around a 6m cube with well-defined boundary conditions and to submit their results to the competition organisers. These results were then compared with the field measurements, made around a real 6m cube constructed for the purpose. Comparisons with wind tunnel experiments published in the literature were also carried out.

The competition was entered by the author, as an exercise to develop and test an approach to be used for modelling atmospheric flows. Although the competition was focussed on atmospheric flow past a bluff body rather than landscape features, it also provided insights into modelling of atmospheric flows in general and flows involving flow separation. The approach used, and a summary of the comparison with the full-scale results, are presented below. The results of the comparison were published in the literature (Richards *et al.*, 2002) and a copy of the paper is included in Appendix 1.

Methodology

Choice of model

The outputs required by the competition were time-averaged values for velocity, pressure and turbulent kinetic energy and therefore a Reynolds averaged Navier Stokes (RANS) code was used. A k- ϵ turbulence model was chosen because of its well-validated nature and widespread use for such flows. In order to avoid the widely reported over-prediction of turbulence at the windward face of bluff bodies with the standard k- ϵ model (Castro and Apsley, 1997), the RNG k- ϵ model was used as an alternative. Whilst this is an improvement on the standard k- ϵ model, it still does not distinguish between the different turbulent stresses and may not be expected to capture all of the three dimensional flow features around an obstacle. More details on the differences between turbulence models are provided in Section 3.3 below.

Grid generation

The information supplied for the competition gave the location of the cube and a number of smaller structures some distance from the cube. The cube and these structures were all included in the modelled domain. The non-symmetrical nature of the building arrangement forced the choice of an unstructured grid close to the cube and other buildings. An area of structured mesh was used outside of this area. Full details of the mesh are provided in Richards *et al.* (2002), a copy of which can be found in Appendix 1. In retrospect, the distance between the other structures and the cube was sufficient to disregard their effect on the flow. This was the approach used by the other modellers, and allowed a simplified grid to be used.

Boundary conditions

For the case of an atmospheric flow the location and type of boundaries are not immediately obvious. The ground was assumed to be a no-slip wall for which the velocity is zero. The upstream boundary may be defined as an inlet with fixed velocity and turbulence parameters. The downwind boundary was set to be an outlet. If the domain is large enough, the sides and top boundaries can also be set to be boundaries with fixed velocities and turbulence parameters. For this study, a velocity inlet was used for the upstream boundary and also for the sides and top, and an outlet for the downstream boundary. The size of the domain was chosen to be large enough that there was sufficient spacing around the obstacles, that they did not block a large proportion of the cross-stream area.

The velocity at the inlet was defined using a log law, with coefficients derived from the data supplied by the competition organisers. The mean wind speed was equal to 10 m s^{-1} at 6 m above the ground. For the turbulent kinetic energy, a curve was fitted through the experimental data and interpolated to provide the boundary conditions.

Hardware

The grid generation, flow solving and analysis of results were carried using one of two computers: a Compaq Alpha XP1000 Workstation with EV6 processor and 512MB RAM and a shared DEC Alpha server with dual EV6 processors with 1GB RAM shared between a number of users. Both computers were running Compaq Tru64 Unix. Pre- and post-processing was carried out interactively, whilst the majority of the flow solving was carried out in batch mode.

Results

Results for pressure, velocity and turbulent kinetic energy were reported at the locations required for the competition, which included a number of points over the surface of the cube, and also at the inlet and outlet. The full results are not reproduced in the text as they can be found in the paper in Appendix 1. A plot of velocity vectors in a plane passing through the cube is included in Figure 3.1 to provide a visual indication of the flow around the cube.

Discussion

When comparing the choice of boundary conditions between the different CFD studies, as described in Appendix 1, one significant difference was the approach used to describe the turbulence intensity at the inlet. The approach used by the author was to match the turbulent kinetic energy profile to that measured experimentally. The result was a boundary layer that was not in equilibrium with the surface and developed across the domain, causing some speed up near the surface. The two other modellers used a different approach, based on a relationship with the friction velocity, u_* , put forward by Richards and Hoxey (1993), that results in a homogenous logarithmic velocity profile when used with the k- ϵ model. The relationships between the turbulent kinetic energy and the dissipation rate given by Richards and Hoxey are reproduced in Equations 3.1 and 3.2 below:

$$k = \frac{u_*^2}{\sqrt{C_\mu}} \quad \text{Equation 3.4}$$

$$\epsilon = \frac{u_*^3}{\kappa(z + z_0)} \quad \text{Equation 3.5}$$

Where k is the turbulent kinetic energy, ϵ is the turbulent dissipation rate, C_μ is a constant of the k - ϵ model, κ is the von Karman constant, z is the vertical height and z_0 is the roughness length.

The reason for a discrepancy between the full-scale turbulence and that needed for a consistent solution for the CFD is believed to be a result of significant low frequency turbulence measured in the field which is not present in the flows, with which the k - ϵ model was developed (Richards *et al.*, 2002). Despite this difference in the boundary conditions, the measured flow properties around the cube were very similar to CFD results, most probably because the turbulence generated by the cube dominated any turbulence present upstream.

The results from the comparison with the field measurements and the other CFD studies were encouraging, and the author's competition entry, in fact, came first. In general, the approach used showed good agreement with the velocities measured close to the cube and good agreement for prediction of the recirculating region, proving slightly better than the other CFD studies. Surface pressures on the cube were reasonably well predicted, but showed some areas of significant difference. Surface pressures are more important for building design than for studies of dispersion and deposition, although they do indicate a limitation of the CFD approach. The turbulent kinetic energy was not as well predicted as the velocities, and it is thought that this may be due to the fluctuating nature of the separation zones.

The results from the CFD also compared reasonably well with wind tunnel results. Although the CFD performed slightly less well than the wind tunnel results at predicting full-scale flow, they fell within the range of values from the wind tunnel, for 8 of the 9 values compared. Taken as a whole, the CFD model showed that it could provide valuable information about atmospheric flow although there were regions of discrepancy. However, this was also the case

for wind tunnel studies. The approach used by the author proved to be of equal validity to the other approaches used and performed slightly better in some instances. The approach used for setting the turbulent kinetic energy at the input was identified as requiring revision, using the relationship of Richards and Hoxey (1993) and it was hoped that this would improve the performance further.

3.3. Predicting particle deposition in atmospheric flows

Having established a suitable method for modelling atmospheric flows past obstacles, the modelling of particle deposition within these flows was developed. It is believed that particle deposition is affected by the local properties of the flow, and that models developed for particle deposition in equilibrium flows would not be suitable for capturing the local variation in particle deposition caused by landscape features. A model which implicitly included the local effects of variations in the speed, direction and turbulence of the flow, was required. The CFD package used, Fluent 5, included the ability to model particle trajectories. The model used a Lagrangian approach to model particle trajectories and took account of particle inertia, hydrodynamic drag due to the fluid, and the force due to gravity (Fluent, 1999d). The fluid velocity used to calculate the particle drag includes a component due to the turbulent motions of the flow. These are calculated using a Gaussian distributed random velocity component, scaled by the calculated turbulent kinetic energy. The turbulent motions are treated as discrete eddies with either a constant or randomly varying lifetime. This model was also capable of modelling deposition to surfaces when the particle trajectories came within one particle radius of the domain boundaries. Because the trajectories of the particles are influenced by a random

component due to turbulence, they can be calculated repeatedly to build up an average concentration field and statistical pattern of deposition.

To test this approach to modelling particle deposition, the wind tunnel experiments described in Chapter 2 were modelled using this approach and the results compared between the predicted and measured values. The details of the computational study are given in the following section.

3.3.1 Methodology

The particle trajectory model in Fluent 5 was used, together with the solution to the flow over the specified geometry also calculated with Fluent 5. A summary of the approach used is given below:

- Definition of the geometry of the landscape feature of interest
- Creation of a model domain which encloses the feature
- Sub-division of the domain with suitable grid
- Definition of boundary conditions consistent with atmospheric flow
- Set solver and turbulence model options as described in previous section
- Solution of flow to convergence
- Definition of particle source and particle model options
- Repeated calculation of particle trajectories and deposition using solved flow
- Reporting of predicted flow and particle behaviour

Specific details for each step are given below.

Domain choice and grid selection

The flow over each of the three landscapes and the flat control case, studied in the wind tunnel and described in Chapter 2, were modelled with CFD. The width of the modelled domain was equal to the width of the wind tunnel (2.5 m). It extended to a length of 6 m, and a height of 1 m. The downwind extent of the domain was equal to approximately 50 hill heights for the two-dimensional cases and 20 hill heights for the three-dimensional case. A height of 1 m, sufficient to include the boundary layer rather than the full height of the wind tunnel, was chosen.

A hexahedral grid was chosen because of the relatively simple geometry. This also provided more economy in the number of cells used, compared with a grid based on tetrahedra. The grid was “adapted” in the area surrounding the point source and the area downwind, including the landscape features. This process doubles the resolution in each direction for the treated area. The resulting grids had hexahedral cells of horizontal spacing 0.01 m close to the area of the ridges and cone and increasing to 0.05 m away from this area. The vertical spacing started at a size of 0.005 m at the surface, increasing geometrically by a factor of 1.1 with each cell. This is equivalent to a y^+ value of just under 35 for the lowest cell, slightly greater than the lower limit and in the range recommended for CFD solvers (ERCOFTAC, 2000; Fluent, 1999c). The total number of cells for each domain ranged between 390,000 and 645,000. A preliminary coarse grid of 110,000 cells was also produced to provide information on grid resolution dependence. In addition to the landscape shapes, a flat case was modelled to allow the ratio of the deposition to be calculated.

Boundary conditions

The upwind boundary was defined as a velocity inlet, with a log law profile with u_* and z_0 determined from experimental measurements (0.23m s^{-1} and 0.22 mm respectively). The turbulent kinetic energy and dissipation rate were assigned profiles based on the value of u_* after Richards and Hoxey (1993). These were used in preference to experimental values for the reasons described above. Although experimental values were available in this case, it was intended to develop a method that could be used for a range of landscape shapes in idealised flows for which experimental values would not be available. The sides of the wind tunnel were defined as smooth no-slip walls. The floor of the wind tunnel was defined as a no-slip wall with a roughness height of 0.001 m and a roughness constant of 0.5 , equivalent to the textured roughness used on the surface. Note that the roughness height is the height of the roughness element as opposed to roughness length, z_0 . The top of the modelled domain was defined as a symmetry boundary. The downwind boundary was defined as an outflow boundary.

Solver details and turbulence model

The flows over the landscapes were modelled using a commercial CFD solver, Fluent 5.5.14. The flows were solved using steady state Reynolds averaged Navier Stokes equations. A number of turbulence models were tested including: standard k-epsilon, Renormalization Group (RNG) k-epsilon and Reynolds Stress Model (RSM). Preliminary studies showed that the RNG k-epsilon approach predicted the position of the reattachment point of the recirculating area with the most accuracy. The RNG k-epsilon turbulence model has also been shown to perform well by other workers, for studies of flow over complex topography (Kim et al., 2000; Maurizi, 2000). This turbulence model was therefore chosen for the remaining

studies. However, as discussed above, this model is isotropic in nature and may not capture some three-dimensional features of the flow where anisotropy of the turbulence becomes important.

One specific option that was included in the model was the 'velocity gradient correction'. This was an update to the software that dealt with the interpolation of the velocity used for predicting the particle phase trajectories. Runs carried out with and without this option showed that, when switched on, it produced results closer to the experimental results.

Particle source details

A point particle source was modelled for each case and also a broad source for the three-dimensional cone geometry. The lower surface of the domain was defined such that particles coming within one radius distance were trapped and recorded as deposited. Resuspension of deposited particles was not considered since this was likely to be small for the particle size used (Hinds, 1999). For these studies, the number of particles tracked was 1×10^7 . A particle diameter of $1 \mu\text{m}$ was used, particle density was 1000 kg m^{-3} and the Cunningham correction factor used was 1.16632.

3.3.2 Results

Modelled flow

The results described in this section show both the CFD results and those from the wind tunnel experiments. Comparison of the CFD and experimental profiles of velocity showed that the CFD predicted the flow field reasonably well. The modelled flows all showed regions of reversed flow of similar proportions to the experimental flow. The points of reattachment

also compared well, and these are presented in Table 3.1. Note that, use of the pulsed-wire anemometer to assess reattachment and reversal of flow required the measurements of velocity to be made slightly above the surface. The use of a hot-wire anemometer with a smaller probe head would have allowed measurements to be made closer to the surface, but was not available for this work. However, the use of CFD allows extrapolation to the surface for comparison with other values as detailed below. Values from the CFD solution are presented for the heights used in the experimental study and also for the velocity in the cell adjacent to the wall. Table 3.2 presents some reported values for other experimental (Arya and Shipman, 1981) and computational results for reattachment behind a ridge (Jung, 1994; Kim and Patel, 2000; Mouzakis and Bergeles, 1991). All values were taken from Kim and Patel (2000). The values for both the wind tunnel and CFD results from this study are in line with the reported values, particularly when the wind tunnel value is adjusted to surface value using the CFD results.

Two statistical measures were used to compare the predicted values with the wind tunnel values; the fractional bias (FB) and the normalised mean standard error (NMSE). These were modified from equations in Hanna *et al.*, (2004) and are defined below:

$$FB = \frac{(\overline{X_{CFD}} - \overline{X_{WT}})}{0.5 * (\overline{X_{CFD}} + \overline{X_{WT}})} \quad \text{Equation 3.6}$$

$$NMSE = \frac{(\overline{X_{CFD}} - \overline{X_{WT}})^2}{\overline{X_{CFD}} * \overline{X_{WT}}} \quad \text{Equation 3.7}$$

where $\overline{X_{CFD}}$ and $\overline{X_{WT}}$ are the mean CFD and wind tunnel measurements respectively.

Figure 3.2 compares the vertical profiles of streamwise velocity between the CFD and the wind tunnel measurements for the cone of slope 1 in 1. The CFD does well in achieving the same profiles. The values of FB were -0.0087 , -0.22 and -0.071 for the three vertical profiles respectively ($X = -0.75, 0.25$ and 1.55m). The NMSE values for each profile were calculated as 0.00039 , 0.038 and 0.011 respectively. The CFD over predicts the vertical extent of the recirculation region in the immediate wake by approximately 50 %.

Figure 3.3 compares the longitudinal profile of streamwise velocity, measured at a height of 0.05 m above the surface, between the CFD and wind tunnel. The general pattern and the maxima and minima of the velocity coincide for the experimental and modelled case. However, there is some difference in the magnitude of the velocity, which appears to grow with distance downwind. The FB of the CFD results is -0.26 and the NMSE is 0.093 . However, the magnitude of the FB and NMSE increase with downwind distance, with values of -0.13 and 0.035 respectively upwind and -0.35 and 0.13 downwind. This may be due to the over-prediction of the vertical extent of the recirculating region.

Particle deposition

Figures 3.4 – 3.5 show the ratio of deposition rate relative to the flat case for the two two-dimensional landscape cases with a point source release. The two-dimensional cases show very good agreement. The FB of the CFD results relative to the wind tunnel is 0.11 and the NMSE is 0.11 for the 1 in 1 slope case (Figure 3.4), these values are -0.15 and 0.11 respectively for the 1 in 3 slope case (Figure 3.5). There is some over-prediction by the CFD on the windward face of the ridges, which is more apparent for the steeper 1 in 1 slope case. This may be due, in part, to the lower spatial resolution of the wind tunnel deposition samples, particularly for the ridge of slope 1 in 3 (Figure 3.5). There is also a slight

divergence in results at large distances for the 1 in 3 slope ridge, and this is believed to be due to increasing experimental error with distance in the wind tunnel case, as discussed in Chapter 2.

Figure 3.6 shows the graph for centreline deposition for the 1 in 1 cone, which shares the same general features as the two dimensional landscapes. The agreement between the CFD and experiment is not as good for the three-dimensional case with FB between the model and experiment of -0.32 and NMSE of 0.53 . However, the important features are the same between the CFD and wind tunnel results. As for the two ridge cases, the deposition to the upwind face is slightly over predicted by the CFD on the lower part of the cone.

However, the main difference between this case and the two-dimensional cases is that the deposition in the wake region is consistently under predicted. It is believed that this is due to a combination of two reasons. Firstly, the over-prediction of deposition to the windward face removes a significant proportion of particles from the flow, which are then unavailable to deposit further downwind. Secondly, there is evidence of slight asymmetry in the wind tunnel flow and therefore the pattern of deposition. The experimental and CFD pattern of deposition showed that deposition along the centreline, in the wake, was reduced compared to that on either side. A slight asymmetry in the experimental flow would have moved this region of lower deposition away from the centreline, resulting in increased deposition along the sampled centreline, compared to the CFD.

Figure 3.7 shows the results for the same geometry, the 1 in 1 sloped cone, but exposed from a broader source of particles. The concentration field reaching the geometry had a much smaller spatial gradient in comparison to that from the point source. Further details of the source arrangement are described in Chapter 2. There are areas of disagreement between the

two sets of data, but again they do contain similar features. The FB is 0.34 and the NMSE is 0.32. There is an increase in deposition to the windward side of the geometry. The CFD did not capture the peak value seen in the wind tunnel data, but there is good agreement in the general location of the increase. There is a region of reduced deposition downwind of the peak in both the wind tunnel and CFD results, although the minimum predicted by the CFD occurs slightly later than that in the experimental data. This is consistent with the point of reattachment predicted by the CFD occurring further downwind than seen in the wind tunnel (Table 3.1). There is then a peak, followed by a reduction, in both the experimental and CFD results. The CFD did not reduce to as low a level as found in the experiment. However, within a distance of 1.5 peak heights the results from the two techniques were very similar, allowing for experimental error in the wind tunnel results. The agreement at these distances is much better than for the point source for the reasons described above.

Figure 3.8 shows a comparison of the deposition ratio for the cone geometry for a broad particle source. Again there are many areas of agreement between the two, although the details differ. The differences are partly due to the much sparser spatial resolution in the experimental samples, compared with the CFD. There is a peak of deposition increase on the windward face, followed by a reduction on the leeward face. The pattern in the wake of the hill shows a split along the centreline, with both sets of data showing higher deposition to either side of the centreline. The wake area in general appears to be over-predicted by the CFD, but with distance this difference becomes less, as shown by the plot along the centreline in Figure 3.7.

A series of runs were carried out at a coarser resolution (110,000 cells) and the results from these runs showed some differences in the pattern of deposition. The principle difference was a larger over-prediction on the windward face, with ratios as high as 4.5:1 for the cone with a

point source. However for the other areas, including the wake, there was relatively little difference. The good agreement between the two-dimensional cases with higher mesh density and the wind tunnel results suggest that the resolution is sufficient. This is supported by further mesh resolution studies in Chapter 6.

3.3.3 Discussion

The streamwise velocity and reattachment lengths of the flow over the landscape features were predicted well by the CFD approach used. There are some slight differences in the shape and size of the recirculation zone as shown by the vertical profiles of velocity and Table 3.1. Comparison with values reported in the literature show good agreement with other work (Table 3.2).

For the prediction of relative deposition rates, the results above show that the CFD has performed very well for the two-dimensional cases, with good agreement between the wind tunnel and CFD. The only points of discrepancy for these cases are the peak values, and the values at larger distances downwind. The difference at the peak values is partly explained by the lack of spatial resolution in the experimental samples. The values further downwind do not agree with the wind tunnel results as well, because of the increasing experimental error at these locations, as discussed in Chapter 2.

The three-dimensional case does not agree as well as the two-dimensional case. The data from the point source release shows a significant under-prediction by the CFD in the wake. This is believed to be due to asymmetry in the wind tunnel flow, causing the area of increased deposition to either side of the centreline to stray over the centreline, resulting in increased deposition in the experimental case. The use of a broader source improved the agreement in

the further wake, but there was still some difference in the near wake, in particular the location of the secondary maximum.

Preliminary mesh dependency studies showed that the majority of the results were not strongly dependent of mesh resolution, apart from the region surrounding the landscape peak.

3.4. Conclusions

The first part of this chapter indicates that CFD is a useful and valid tool for studying the flow past bluff bodies, and is comparable with results produced in wind tunnel studies. The particular modelling approach used, and the choice of turbulence model (RNG k-epsilon) also appear to be suitable for these types of flows, particularly for the two-dimensional cases.

The CFD results presented in the second part of this chapter support the conclusions from Chapter 2, that landscape features affect the dry deposition of particles. The main findings, namely, an increase to the windward side of the peak and a decrease on the leeward side and in the wake, are all predicted by the CFD results. The numerical agreement in deposition ratio compared to a flat landscape was very good for the two-dimensional geometries studied. The results for the three-dimensional geometry agreed less well with some areas of difference, and FB values of -0.32 and $+0.34$ and NMSE of 0.53 and 0.32 . However, the predicted patterns were still qualitatively correct.

Although this study is based on a limited number of cases and conditions, the results show that CFD is a useful tool for predicting ratios of deposition due to flow around landscape shapes. CFD has been used to study the effect of free-stream turbulence on deposition and is described in Chapter 5 and compared to the experimental data from Chapter 4. It has also

been applied to the more detailed investigation of landscape influence on deposition in Chapter 6.

4. PARTICLE DEPOSITION IN UNIFORM TURBULENCE – WIND TUNNEL EXPERIMENTS

4.1. Introduction

The comparison of wind tunnel experiments and CFD predictions for particle deposition to landscape features provided encouraging evidence to support the use of CFD for modelling particle deposition. The results suggested that turbulence was an important variable influencing particle deposition, with areas of greater local turbulence showing some correspondence with areas of greater deposition velocities. To investigate this observation and to further validate the use of CFD for studying particle deposition, a series of experiments was carried out to study the particle deposition from flows of varying levels of turbulence. The experiments carried out were similar in design to the studies of May and Clifford (1967) on impaction of larger particles to similar sized obstacles. However, this previous work did not include the effects of turbulence on deposition.

The experiments were conducted in a smaller wind tunnel than the one used for the landscape studies, and relied on the well-studied phenomenon of decaying grid turbulence (Comte-Bellot and Corrsin, 1966). Deposition was measured onto a cylinder and a plane in a range of turbulence levels, to investigate whether there was any correlation between the level of turbulence intensity and the amount of deposition. The same experiments were then modelled using CFD, and the results were compared. Discussion of the CFD study, and comparison between the experiment and modelled data, can be found in the next chapter.

4.2. Methodology

4.2.1 Wind tunnel design and characteristics

The wind tunnel was an open-return, square cross section design, driven by a centrifugal fan at the outlet. The working section was 0.2 x 0.2 m in cross-section with a length of approximately 2.0 m. The side and upper surfaces of the working section were made of Perspex, and the lower surface from laminated board. HEPA filters were attached to each end to prevent particles from entering or leaving the wind tunnel. An adjustable aperture at the exit of the centrifugal fan controlled the wind tunnel velocity. The layout of the wind tunnel is presented in Figure 4.1.

The range of mean velocities achievable in the wind tunnel was measured using a pitot-static tube and micro-manometer (DP Measurements TT570 SL, 0.01 m s⁻¹ resolution between 1 and 9.99 m s⁻¹) for velocities above 1 m s⁻¹. For velocities below 1 m s⁻¹ a thin-film omnidirectional transducer (Danctec 54T21, range 0.05 – 1 m s⁻¹) was used. The tunnel calibration results are presented in Figure 4.2. For the deposition experiments, a mean streamwise velocity of 5 m s⁻¹ was used.

4.2.2 Producing and measuring turbulence

To examine the relationship between turbulence and particle deposition, it was necessary to establish a reliable method of generating the required levels of turbulence. It is well known that the flow of fluid through a grid of bars generates turbulence, which decays with distance downstream. This phenomenon was used to generate turbulence in the flow. An overview of experimental turbulence generation in air behind grids of different geometries is provided in

Comte-Bellot and Corrsin (1966). This paper provides empirical relationships for the variation of turbulence intensity with grid geometry, spacing and distance downstream from the grid. The turbulence intensity is dependent on M , the distance between mesh centrelines, U_0 the mean speed for the same mass flow through an equivalent empty area and t , the time of travel from the grid.

From a distance of 40-50 M downwind of the grid, the turbulence is homogeneous and shows only a small degree of anisotropy (Comte-Bellot and Corrsin, 1966). A suitable mesh size was chosen to produce homogeneous turbulence within the distances achievable within the constraints of the wind tunnel. By varying the distance of the grid to the position of the deposition sampling, the turbulence intensity at the sample location could be varied. The grid was made of hardboard and consisted of square apertures cut out of the board. A photograph of a section of the grid is included in Figure 4.3. The spacing between the mesh centrelines (M) was 0.015 m and the solidity (projected solid area per unit total area) was 0.56. The grid Reynolds number, defined as $Re_M = U_0 M / \nu$, where ν is the kinematic viscosity of the fluid, was approximately 5000. The mesh size was also chosen to provide significant variation in turbulence intensity within the distances available. In practice, the distance between the grid and the sampling location was varied by moving the grid and keeping the sampling position fixed.

Hot wire measurement of flows

The purpose of the experiment was to establish a relationship between the intensity of the turbulence and the amount of deposition onto a surface in that flow. In order to measure the turbulence intensity, a constant-temperature hot wire anemometer (CTA) was used. A single wire probe, with an additional temperature-compensating probe, was used to measure the

instantaneous streamwise velocity, from which the turbulence intensity was calculated. A Dantec hot wire anemometer system was used, consisting of a Disa (now Dantec) type 56C01 CTA unit fitted with a 56C14 CTA temperature compensated bridge attached to two 55P11 miniature wire probes (one for velocity measurement and the other for temperature compensation) each mounted in a 55H20 probe support.

The single output voltage from the hotwire system was connected to a data acquisition card (National Instruments PCI-MIO-16E-4/PCI-6040E) via a shielded connector block (National Instruments SCB-68). The data acquisition card was 12-bit resolution and capable of 500 kSamples s⁻¹ for single-channel sampling. The data acquisition card was installed in a personal computer running the laboratory automation software LabView (National Instruments). The output voltage was recorded at a frequency of 200 Hz for 30 s. The data acquisition card was set to an input range of 1 to 2.5 V to optimise the sampling resolution. The hot wire anemometer was calibrated using a pitot-static tube and a micro-manometer before each series of measurements. A 4th order polynomial fit was chosen, rather than a King's law equation, to give the best accuracy over the measured range. Velocities measured were far in excess of those at which convective flows induced by the hot wire are significant. A typical calibration curve is presented in Figure 4.4. The polynomial was applied within LabView to calculate the velocities for each sample voltage. The average and standard deviation of the sampled velocities were then calculated. It is worth noting, that six significant figures were required for the polynomial coefficients to ensure accuracy and that the calculated velocities did not oscillate significantly with increasing voltage.

A LabView 'virtual instrument' was constructed specifically for this work. The virtual instrument consisted of a number of sections, and these are outlined below:

- data acquisition section
- calculation of statistics of the sampled voltages
- conversion of the sampled voltages to velocities, using the coefficients for the polynomial curve fitted to the calibration curve
- calculation of statistics of the calculated velocities
- plotting of graphs of the raw data and their power spectra
- recording to a file of the raw voltages and calculated velocities

The interface to the virtual instrument is presented in Figure 4.5 and the underlying wiring diagram is presented in Figure 4.6. The sub-virtual instruments used within this diagram are presented in Figures 4.7, 4.8 and 4.9.

The constant temperature anemometer was used to measure the streamwise turbulence within the wind tunnel, with the grid located at different positions for the same wind speed of 5 m s^{-1} . It was necessary to adjust the speed control of the wind tunnel for different positions of the grid to achieve the same mean wind speed at the measurement point. Particle deposition was measured at the centre of wind tunnel cross-section. Horizontal and vertical traverses of the wind tunnel showed that the values of the wind speed and turbulence in the central 0.10 m of the cross section were within approximately ten percent of the value at the centre. In the absence of strong gradients of turbulence across this region, measurements of turbulence were made at the centre of the wind tunnel.

Comparison of measured turbulence levels and literature values

The turbulence was calculated from the measured velocities for a number of locations of the grid. The streamwise turbulence intensity, defined in Equation 2.3, was calculated for each distance and is presented in Figure 4.10. Turbulence measurements were originally made at 4 distances, from 0.62 m to 1.47 m from the grid. The distance of 0.62 m was chosen because it is approximately 40 mesh widths from the grid, and this is the distance at which grid generated turbulence typically becomes homogeneous (Comte-Bellot and Corrsin, 1966). Two closer distances were added later to achieve greater turbulence intensity, the closest at approximately 20 times the mesh spacing. At these closer distances the turbulence will not be expected to be fully homogeneous.

The measured turbulent velocities were fitted to the equation given in Comte-Bellot and Corrsin (1966). The authors of the paper give a general expression for the ratio of the square of the mean velocity to the mean square of the turbulent velocity for different values of travel time from the grid. The equation used is presented below:

$$\frac{U_0^2}{u'^2} = A \left(\frac{U_0 t}{M} - \frac{U_0 t_1}{M} \right)^n \quad \text{Equation 4.1}$$

Where U_0 is the mean velocity, u is the instantaneous streamwise turbulent velocity, t is the time of travel from the grid, M is the grid spacing, A , t_1 and n are constants. The authors of the above paper suggest calculating the coefficients for the equation by varying t_1 until the longest straight line can be achieved through a plot of $\log\left(\frac{U_0^2}{u'^2}\right)$ against $\log\left(\frac{U_0 t}{M} - \frac{U_0 t_1}{M}\right)$.

When plotted in this form (Figure 4.11) it became apparent that the turbulence values at larger distances were larger than predicted by the power law. This is likely to be due to the residual

turbulence of approximately 3% streamwise turbulent intensity, measured in the wind tunnel without the grid present.

The fitted line gave the following values for the coefficients in Equation 4.1: $n = 1.14$, $U_0 t_1 / M = 9$, $A = 11.2$. These values were within the range, but towards the extreme ends, of the values quoted from a number of studies in the paper by Comte-Bellot and Corrsin (1966). The principle differences between this experiment and those quoted are the smaller grid Reynolds number and higher area-blocking ratio used for this experiment. The majority of the velocities quoted were in the range of $10 - 20 \text{ m s}^{-1}$, with a minimum of 6.25 m s^{-1} , compared with the value of 5 m s^{-1} in this experiment. The grid Reynolds number was equal to 5,000 in this experiment, compared with 5,500 – 2,420,000 in the reported studies, with most of the order of 10,000. Although the value in this experiment is lower than the minimum reported (a necessity to maintain sufficient spacing from the grid at the required wind speed), it is certainly above the critical value required to generate turbulence as seen by the results in Figure 4.10. The lower Reynolds number would therefore not be expected to significantly change the behaviour of the flow. The blocking ratios ranged from 0.31 – 0.44, compared with 0.56 in this experiment.

Despite the slight deviation from the theoretical values, there was significant variation in turbulence with different distances from the grid. These values were well suited to a study of the variation in deposition rate with turbulence.

4.2.3 Particle generation

To allow an assessment of particle deposition to be made, aerosols of sodium fluorescein were generated using a medical nebuliser (Acorn II®, Marquest Medical Products, Inc.,

Englewood, CO, 80112, USA. Ref 124014, Lot 703E). A solution of 50 g L⁻¹ sodium fluorescein in water was used to supply the nebuliser. The aerosol produced by the nebuliser was polydisperse, with a volume median diameter of approximately 2 µm. A more monodisperse aerosol would have been more desirable, in order to isolate the effects of size. However, monodisperse aerosol generators such as the vibrating orifice aerosol generator or spinning disc aerosol generator both produce much lower concentrations and would have made the duration of the experiments impractically long.

The nebuliser was placed in the contraction section of the wind tunnel upstream of the working section. The spatial variation of the concentration across the working section at the point of deposition was measured using a light-scattering particle monitor (GRIMM Technologies Model 1.105). The concentration showed a marked fall off from the centre of the wind tunnel. To improve the dispersion of the aerosol a cone was attached to the nebuliser outlet (Figure 4.12). With the cone in place, the particle concentration was much more constant with cross-stream distance.

4.2.4 Deposition and concentration measurement

The deposition of the particles to two different geometries was measured; a vertical cylinder with its long axis normal to the flow and a vertical plane whose surface was parallel to the flow. 24 mm filters were placed on the surface of the collector for each case (Whatman GF/F). For the case of the cylinder, a single filter was placed with its centre on the upwind centreline of the cylinder. The diameter of the cylinder was 20 mm and its circumference was 62.8 mm. Therefore, the filter extended only part of the way around the upwind side of the cylinder. The filter was attached to the cylinder with double-sided adhesive tape between the cylinder and the filter.

The plane was 40 mm long and 1mm wide, arranged with the 40 mm faces parallel to the mean flow and the 1 mm faces normal to the flow. The plane extended across the full height of the wind tunnel (0.2 m). Two filters were used, one attached to each side of the plane. The filters were attached to the plane using electrical tape arranged vertically at the upwind and downwind edges of the filters, at a horizontal distance of 8 mm from the centre of the filter. The filters were taped at their edges for the plane case to prevent the edges from presenting a raised surface to the flow.

An isokinetic sampler was placed behind the sample collection point at a distance of 0.07 m, to obtain a reference concentration for the calculation of the deposition velocity. A stainless steel, thin-walled probe and filter holder assembly (Gelman 2220) was used with a 47 mm filter (Whatman GF/F). The internal diameter of the probe was measured using a micrometer and was equal to 8.4 mm. The required flow rate for isokinetic sampling was calculated to be 16.6 L min^{-1} for a mean velocity of 5 m s^{-1} . The flow rate through the probe was adjusted for each run using a bubble meter (Gilibrator Primary Air Flow Calibrator System, Gilian, using 2-30 L min^{-1} measuring cell) to achieve a value within 1% of this flow rate. This ensured an accurate sample volume and hence concentration. The location of the isokinetic probe was chosen to allow the filter assembly to be placed in the expansion section of the wind tunnel, and for the probe not to interfere with the flow close to the detectors.

The amount of sodium fluorescein deposited to the filters on the cylinder and plane, and filtered through the isokinetic probe, was determined using fluorimetric analysis of an aqueous extract using a fluorometer (Jasco 821-FP Intelligent Spectrofluorometer). The fluorometer was set to an excitation wavelength of 433 nm and an absorption wavelength of 533 nm. A linear calibration was determined using a series of sodium fluorescein standards of concentration from 6 to $60 \mu\text{g L}^{-1}$ made up in pH 7 buffer. The filters were extracted by

shaking in pH 7 buffer for 5 minutes. The samples from the isokinetic probe were further diluted to bring them into the calibration range. Results were recorded both from the digital readout of the instrument and from a chart recorder output. Concentrations in the extract solutions were calculated from the fluorometer response and the results of the calibration. The mass of sodium fluorescein deposited was calculated using Equation 4.2:

$$M_{fl} = C_{liquid} \times V_{liquid} \quad \text{Equation 4.2}$$

where M_{fl} is the mass of fluorescein, C_{liquid} is the concentration of fluorescein in the liquid extract and V_{liquid} is the volume of the liquid extract. The airborne concentration of sodium fluorescein was calculated using Equation 4.3:

$$C_{air} = \frac{M_{fl}}{V_{air}} \quad \text{Equation 4.3}$$

where C_{air} is the airborne concentration and V_{air} is the volume of air sampled (sample time multiplied by volume flow rate). The deposition velocity was calculated using Equation 1.1, the airborne concentration and the deposition flux (M_{fl} divided by exposure time).

4.2.5 Wind tunnel configuration

The arrangement of the wind tunnel during the experiment is presented in Figure 4.12. Note that the position of the particle source was fixed relative to the sampling location. The distance between the turbulence generating grid and the sampling location was varied to achieve different levels of turbulence intensity. The different levels of turbulence intensity upwind and downwind of the grid will have altered the dispersion of the particles from the source. However, any variations in concentration will be normalised for by the concentration

measurements from the isokinetic sampling probe. The experiment was run for a period of twenty minutes to allow the accumulation of sufficient sodium fluorescein for detection. The free stream velocity was set to 5 m s^{-1} for each run. This corresponds to a Reynolds number of 6,600 for the cylinder using the diameter as the characteristic length, and 13,200 for the plane using the length of the face parallel to the flow as the characteristic length. Streamwise turbulence intensities of 3.1, 4.0, 5.2 and 8.6 % were used.

4.3. Results

4.3.1 Cylinder

Figure 4.13 shows the measured deposition velocity for the deposition to a 20 mm cylinder in 5 m s^{-1} flow for varying degrees of turbulence. There is considerable scatter in the results. However, the results suggest that the level of turbulence has some influence on the deposition velocity, with a general rise with increasing turbulence, tailing off at higher values. Only two sets of measurements, for each value of the turbulence intensity, were carried out for this case.

4.3.2 Plane

Figure 4.14 shows the measured deposition velocity for the deposition to a vertical plane in 5 m s^{-1} flow for varying degrees of turbulence. Only three turbulence intensities were studied for this case, but three sets of measurements were taken for each value. The average of the deposition velocities to the two faces of the plane are plotted in this figure. The points on the graph represent the average over the three cases and the error bars, the range of these average

values. It is worth noting that there was some bias to one side of the plane, probably due to a slight asymmetry in the wind tunnel flow or in the mounting of the plane.

Figure 4.14 shows some variation with turbulence intensity, with an increase in deposition velocity with increasing turbulence. There appears to be a peak in deposition velocity at the intermediate turbulence value, but this may be a result of scatter in the results. Note that the absolute values of deposition velocity for the plane case are approximately a factor of ten smaller than those for the cylinder.

4.4. Discussion

The results from these two sets of experiments show the turbulence intensity of the flow has some effect on the deposition velocity to the surface. There appears to be a rise in deposition with increasing turbulence, which tails off at higher values. There is a clear difference in magnitude between the value of deposition velocity for the cylinder and the plane. This is to be expected as the filter placed on the cylinder varied between facing normal to the flow and a shallow angle to the flow. In comparison the filter on the vertical plane faced parallel to the flow and presented a much smaller area to the oncoming flow. With a collecting surface of finite size, there will also be an effect due to the deviation of the flow around the collecting surface. This may affect the shape of the curve relating deposition velocity to turbulence. This is investigated further in Chapter 5.

There is also a possible effect due to the location of the isokinetic sampling probe behind the sampling location. The depletion of particles, due to deposition onto the collector, will decrease the concentration sampled by the probe, which is downwind of the collector. This will introduce an error into the calculated deposition velocity, which should ideally be based

on the upwind concentration. Computational fluid dynamics was used to investigate this further as described in Chapter 5.

Given further time and resources a number of improvements to this experiment could be made. Rather than using a single isokinetic probe behind the sampling location, a set of probes, arranged around the sample location could be used. Prior to the actual measurement, the sample support could be removed and replaced by an isokinetic probe. The ratio of the concentrations from the probes around this central probe, to that from the central probe could be used during the measurement, when the central probe is removed and replaced by the sample support. This would give a more accurate measurement of the concentration at the sample location.

The results in Figures 4.13 and 4.14 are limited by the lower and upper limits of turbulence intensity achievable in the wind tunnel. Lower turbulence intensities would be useful to determine the lower limit of the deposition velocity. Practical steps to achieving lower turbulence levels might include a more smoothly designed inlet and contraction section to the wind tunnel, and elimination of small steps passing from the inlet to the working section. Alternatively, a flow straightener (e.g. honeycomb material) and gauze might be used to lower the turbulence level in the flow within the existing wind tunnel. To produce higher degrees of turbulence, a different type of grid might be used. Equation 4.1 suggests that a larger grid spacing (M) will yield larger turbulence intensities. One problem with this is the limit of space within the wind tunnel may only allow the sample to be taken in the non-homogenous region less than 40 - 50 mesh spacings downwind from the grid.

The maximum streamwise turbulence intensity generated in this study was 8.6 %, compared with a value of 18 % near the surface in the large wind-tunnel study for the boundary layer

over the flat surface. Local values of turbulence intensity reached higher values in the presence of the landscapes, but the presence of stagnation points makes the maximum turbulence intensity values in these cases misleading. The root mean square of the instantaneous velocity, in the presence of the landscapes, reached as much as double the values for the flat case. The local absolute turbulence values in the wind tunnel were therefore as much as four times the highest value used in this study. The local increase in deposition velocity of 1.5 - 3 times seen in the wind tunnel experiments is consistent with these results and the general upward trend in Figures 4.13 and 4.14.

A more complete study could also be made, using a range of different velocities and a range of different cylinder sizes. However, the portion of the cylinder's circumference covered by the filter would need to be kept constant, as the deposition rate will vary around the circumference.

An additional improvement to the experiment would be the use of a more tightly monodisperse aerosol, to test the sensitivity of different sizes to turbulent deposition.

Comparable studies of particle deposition in varying levels of turbulence could not be found in the literature. May and Clifford (1967) studied the impaction of aerosols onto a series of geometric obstacles including cylinders and ribbons (face normal to the mean flow). However, although their study used a range of wind speeds, no reported turbulence values are given. Their study also used larger particles than used in this experiment, with diameters ranging from 20 μm to 40 μm .

4.5. Conclusions

Preliminary studies of particle deposition to a cylinder and a plane show that there is some relationship between turbulence intensity and deposition velocity. Increasing turbulence intensity results in increasing deposition velocity. The relationship does not appear to be linear and the rate of increase in deposition is seen to decrease with increasing turbulence. The deposition velocities to a vertical plane are smaller than those to a vertical cylinder for the same turbulence intensity. CFD has been used to investigate these results further and is described in Chapter 5.

5. PARTICLE DEPOSITION IN UNIFORM TURBULENCE – COMPUTATIONAL FLUID DYNAMICS STUDIES

5.1. Introduction

The previous chapter described the experimental study of the effect of turbulence intensity on deposition velocity. In order to test the effectiveness of computational fluid dynamics (CFD) models at predicting the variation in particle deposition, these experiments were modelled using CFD. In addition to comparing the experimental and computational results, the calculated particle concentrations at the inlet to the isokinetic sampler were used to correct the experimental deposition velocities.

5.2. Methodology

The CFD software, Fluent v5.5.14, was used to model the flow of air around the collectors used in the wind tunnel experiment. The same software was also used to model the dispersion and deposition of the aerosolised sodium fluorescein in the flow. The general features of CFD have been covered previously in Chapter 2 and will not be repeated here.

A two-dimensional model of the area surrounding the collector was created. The domain covered an area 0.3 m long by 0.2 m wide, and was discretised into 4164 triangular cells for the cylinder and 9644 cells for the plane. Triangular cells were chosen to allow better fitting to the geometry of the collector and a range of cell sizes to be included. Figures 5.1 and 5.2 show the meshes used for the cylinder and plane respectively. Only the central region of the

wind tunnel was modelled and therefore, the boundary layers at the walls of the wind tunnel were not included. A uniform velocity of 5 m s^{-1} was defined at the inlet with uniform turbulence intensity. The value of the turbulence intensity was varied for each run and was equal to the values measured in the experimental study. The RNG k-epsilon model was used to model the turbulence intensity within the flow. For the particle tracking, a series of evenly spaced particle injections (79 injections at 2.5 mm spacing) were arranged parallel to the inlet, 0.01 m inside the domain, to represent a uniform concentration of particles.

The procedure followed was identical to that used to model particle deposition in the larger wind tunnel. Firstly, the flow around the collector was solved. Then the trajectories of a large number of particles were tracked within that flow, to build up a pattern of deposition to the surface. Deposition velocities were calculated based on concentrations upwind of the collecting surfaces.

5.2.1 Cases studied

The two types of collector geometry studied were a vertical cylinder and a vertical plane parallel to the flow. The details of the geometries are given below.

The cylinder had a diameter of 20 mm and was arranged vertically with its long axis normal to the flow. For the purposes of the two-dimensional CFD study, this was represented as a two-dimensional circle in the plane of the flow as shown in Figure 5.1. One of the benefits of computational fluid dynamics is the ability to investigate the influence of a number of parameters on the results relatively easily. Taking advantage of this, the size of the cylinder was varied to investigate the effect on deposition. The dimensions of the cylinder and the domain were reduced by one half to produce a model of a cylinder of diameter 10 mm. The

wind speed was held constant at 5 m s^{-1} . Deposition velocities were calculated for the same set of turbulence intensities.

A vertical plane of dimensions $1 \text{ mm} \times 40 \text{ mm}$ ($W \times L$), with the small dimension normal to the flow, was also modelled. This was represented as a rectangle in the plane of the flow for the purpose of the two-dimensional CFD model, as shown in Figure 5.2.

5.3. Results

5.3.1 Cylinder

Figure 5.3 shows the results from the CFD modelling of deposition to a cylinder with different levels of turbulence. There is a strong dependence on the downwind distance (X) as would be expected, with the windward edge ($X = 0.090 \text{ m}$) receiving the greatest amount of deposition. The deposition reduces with increasing distance from the leading edge, but secondary maxima are apparent. For all but the most turbulent cases, there is a strong peak immediately upwind of the centreline at $X = 0.099 \text{ m}$, corresponding roughly to the location of maximum velocity and streamline convergence, and a smaller peak at $X = 0.106 \text{ m}$. The distribution for the most turbulent case is slightly different, with a single less well-defined secondary maximum at $X = 0.095 \text{ m}$.

The position of the filter and its width is shown on this graph and it is clear that the filter covers the area where the majority of the deposition occurs. Figure 5.4 focuses on the area covered by the filter, and with this added detail it is apparent that there is increasing deposition with increasing turbulence intensity for most of this area. However, at the two

most upwind points of the cylinder, the deposition for the highest turbulence case is lower than for the other cases.

Figure 5.5 presents the data as a polar plot and shows the upwind area of the cylinder more clearly. The pattern of deposition for the three less turbulent cases all appear similar, but the pattern for the most turbulent case shows a change in pattern, with a slight reduction at the upwind side but an increase between 20 to 80°. The difference in deposition for the most turbulent case suggests that the use of a filter on the upwind side of the cylinder may not capture the change in total deposition well. This is investigated in the discussion below.

There is an interesting pattern of maxima and minima for all four cases. It was not clear whether this was due to the properties of the flow, or the use of a series of discrete particle sources that preferentially deposit in certain locations. To investigate this further a series of runs were carried out with finer spacing of the particle injections. The results of these runs are presented in Figure 5.6 and show that, although the finer spacing reduces the size of some of the peaks, there is no gradual decrease with increasingly fine spacing. The pattern of maxima and minima remains and is therefore likely to be a feature of the interaction between the flow and the cylinder.

Figure 5.7 presents plots of the turbulent kinetic energy for the least and most turbulent cases around the cylinder. The turbulence close to the surface is another possible cause of the local deposition maxima and minima. Careful examination shows that the region close to the surface of the cylinder varies through high to low and back to high turbulence values with increasing downwind distance. It is useful to compare this with Figure 5.5. The areas of high turbulence close to the cylinder at the upwind face, and in the wake, correspond with high

deposition. The other maximum at around 80° is probably a result of the concentration increasing as the streamlines converge in this area.

The results for the smaller cylinder are presented in Figure 5.8. The graph shows the deposition to the filter area only. The data show similar values to the larger cylinder for the less turbulent cases, but deposition velocities continue to rise with increasing turbulence. The variation with turbulence intensity appears to be approximately linear up to the 5.2% case, and starts to level off above this.

5.3.2 Plane

Figure 5.9 shows the results for deposition to the vertical plane. The graph shows deposition for each value of turbulence intensity, and also the location and width of the filter used in the experimental study. It is clear that the calculated deposition is noisier than for the cylinder. The deposition is greater to the upwind face and decreases with distance downwind for the more turbulent cases. For the less turbulent cases the deposition increases with distance before reducing again. There is greater deposition for higher turbulence intensity, although the difference between the cases gets smaller with downwind distance. There is no complex pattern of deposition as was the case for the cylindrical geometry. Figure 5.10 shows the CFD results for the plane and focuses on the area covered by the filter. The general trend for this region appears to be the same as that for the whole plane.

5.4. Discussion

5.4.1 Cylinder

The variation in deposition velocity with angle is clearly significant. An analogous area of study is the heat transfer from a circular cylinder. Early work reported in Schlichting (1968) shows a strong dependence on angle for heat transfer (Schmidt and Wenner, 1941). There is qualitative agreement between the turbulent kinetic energy close to the cylinder, plotted in Figure 5.7, and the heat transfer rate from a cylinder. However, there are clear differences, with the downwind transfer greater than the upwind for heat transfer. This is to be expected because of the inertial properties of particles and the variation of concentration around the cylinder. The same text also references work on the effect of free-stream turbulence on heat transfer rates (Kestin *et al.*, 1961). This work reports strong variation in this parameter with increasing turbulence, leading to increased heat transfer rate. The experiments showed a significant effect; with a 1% increase in turbulence intensity showing a 25% increase in local heat flux. It should be noted that these experiments were carried out at significantly higher Reynolds numbers than the present work. However, they support the importance of free-stream turbulence in controlling the transfer to or from the surface of a cylinder.

The raw CFD calculated deposition velocities could not be compared directly to those measured experimentally, because the filter area used in the experiment was smaller than the whole cylinder. The CFD model was two-dimensional, whereas the width of the filter in the experiment varied in the third dimension. In order to compare the two sets of results, the width of the filter in this dimension was calculated. Figure 5.11 shows the deposition velocity data for only the region covered by the filter in the experimental study. The filter width is also

presented in this plot. The CFD results need to be normalised for this filter width to predict the deposition to the filter as a whole.

It is worth noting that the upwind area of the cylinder, to which the majority of the deposition occurs, is weighted most heavily. The area where there is an obvious increase for the turbulent case is weighted less strongly. To examine this effect, the deposition velocity was calculated using the average of the deposition to the whole cylinder. These results are presented in Figure 5.12. Whilst the magnitude of the deposition velocity is lower for the whole cylinder because of the inclusion of areas of lower deposition, there is little difference in the trend with increasing turbulence.

For each point where the deposition value was reported from the CFD calculations, the filter width and separation of reported values were used to calculate the area of the filter that the CFD result represented. The CFD values were then weighted by this area, summed and normalised to the total area of the filter, to give a deposition value equivalent to that measured by the filter in the wind tunnel experiment. Figure 5.13 shows these values compared to the experimental ones. Note, that the trend of the experimental and computational results is the same, but the magnitude of the deposition velocities is different, with the CFD results over predicting by a factor of approximately 20. A similar over-prediction was seen in the earlier wind tunnel comparison, but again the relative deposition was predicted correctly. The cause of this over prediction is not immediately clear. It may be due in part, to the limited length scale of the steps of the particle trajectory model. Another possibility is the isotropic nature of the turbulence model used. Anisotropic turbulence will be generated close to the surface of the cylinder in the wind tunnel flow. These turbulent stresses will be treated as being isotropic in the CFD model, which will tend to over predict the normal stresses. These normal stresses are used in the particle tracking model and may over predict the deposition to the surface.

The results from the CFD analysis also indicated one area of potential improvement in the experimental design. The predicted concentrations upwind of the cylinder and at the location of the isokinetic sampler inlet were different. Those at the sampler inlet were lower by a factor of 0.65 to 0.73. The reduction in predicted concentration is thought to be due to removal of aerosol by deposition and disruption to the airflow by the cylinder. By using the ratio of the CFD calculated concentrations upwind of the cylinder and at the sampling location, the deposition velocity can be calculated based on the upstream concentration. These values are presented in Figure 5.14, and show a general reduction in deposition velocity but no change in trend.

To overcome the reduction of measured concentration because of removal by the cylinder or plane in the experimental measurements, an alternative approach could be used to measure the concentration. Multiple samplers located in the plane of the cylinder or plane could be used, including one in place of the cylinder or plane during a pre-run profile measurement, as described in the previous chapter.

The results above indicate that a smaller cylinder would be more appropriate for any future experimental measurement of deposition velocity, because there would be a greater difference in measured value with the variation of turbulence. The cause of this scaling property is not immediately obvious, but is thought to be due to the interaction of the turbulence in the bulk flow with the boundary layer around the cylinder. The nature of the turbulent wake, would be expected to change for a cylinder in this Reynolds number range (3300 – 6600) (Batchelor, 1967).

5.4.2 Plane

As for the cylinder case, it was necessary to take into account the area of the plane covered by the filter, in order to compare the experimental and CFD results. Using a similar calculation to that used for the cylinder case, the equivalent deposition velocity for the area covered by the filter was calculated. The results are presented in Figure 5.15. The general trend in the CFD results is similar to the experimental results with an increase in deposition velocity with increasing turbulence intensity. The CFD results do not match the apparent peak at a turbulent intensity of 5.2 %, but do fall within the range of experimental error. The CFD results again over estimate the magnitude of the deposition velocity by a significant margin. The reasons for the over prediction given above in Section 5.4.1 are also applicable here. The greater over-prediction to the plane than the cylinder lends more weight to idea that the anisotropy of the modelled turbulent stresses may be the cause of this, since the turbulent stresses in the wind tunnel are more likely to be anisotropic in this case

5.5. Conclusions

The results from the computational fluid dynamics studies show the same trend as the experimental studies, that deposition velocity varies with turbulence intensity and the higher the turbulence intensity, the greater the deposition velocity. However, the relationship does not appear to be a linear one, with the size of the effect depending on the level of turbulence and the scale of the geometry for the case of a cylinder. Although the CFD results correctly predicted the trend in deposition velocity, they over-predicted the magnitude by a significant. This over-prediction may be due to a lack of explicit modelling of the smallest scales of particle motion, or perhaps more likely, the effect of the isotropic nature of the turbulence

model used in the CFD failing to distinguish between the turbulence component normal to the surface and those parallel to it.

The CFD results allow an investigation into the details of the deposition. The spatial variation in deposition to a cylinder indicates that a number of processes are influencing the deposition. These most probably include the turbulence close to the surface, and the convergence and divergence of streamlines, and their resulting influence on concentration, as suggested in Goossens (1988a) for curved surfaces. Additionally, the location of the recirculation region will have an influence, because of its effect on concentration close to the cylinder.

Predicted concentrations suggest that the measurement of concentration in the experimental study could be improved by placement of multiple isokinetic samplers as described in the previous chapter. The variation in deposition with scale of the cylinder geometry also indicates that a smaller cylinder would provide a clearer demonstration of deposition enhancement with turbulence.

6. PARTICLE DEPOSITION TO LANDSCAPES – FURTHER COMPUTATIONAL FLUID DYNAMICS STUDIES

6.1. Introduction

In Chapter 3, the development of a suitable methodology for predicting atmospheric flows over obstacles, and the relative particle deposition from those flows, was described. In this chapter these techniques are applied to a range of similar cases. These cases involve two- and three-dimensional geometries. The influence of a number of parameters is examined using the two-dimensional cases, which are computationally more economical. The three-dimensional cases have been chosen to represent a few key landscape features.

6.2. Methodology

The computational methodology used is as described in Chapter 3. In addition, the influence of a selection of turbulence models has been investigated. There are some differences between the two-dimensional and three-dimensional cases. The three-dimensional cases are comprised of a greater number of cells, and in some cases have a lower resolution because of the need to limit the total number of cells, due to memory constraints of the hardware used. Details of the differences between the two- and three-dimensional cases are described in the section on three-dimensional cases below.

6.2.1 Two-dimensional cases

A wide range of two-dimensional cases was studied and an overview is given in Table 6.1. These were used to investigate the sensitivity of the results to model choices, as well as predicting variation in deposition for various landscape types. These cases are representative of real landscapes such as ridges, escarpments and valleys. Two-dimensional cases have the advantage that they need a smaller number of cells to represent the model domain. These cases can be solved with greater speed using a given computational resource. The results from these two-dimensional cases are also easier to interpret and present clearly.

General methodology

The flows were solved for each case until they reached convergence. Convergence was judged by monitoring the residuals for the calculated variables, and was taken as the point where the residuals reached a small, stable value (typically $10^{-6} - 10^{-8}$). The residuals were defined as the root mean square rate of change of the variables, normalised to the value after five iterations for the velocity and continuity. For the turbulent kinetic energy and dissipation rate, these were defined as the normalised imbalance in the continuity equation for these variables (Fluent, 1999e).

The particle release was then defined and a large number of trajectories (approximately 200,000) were calculated. Where the trajectories passed within one particle radius of the wall, the particles were recorded as deposited. The resulting concentrations and pattern of deposition were then reported. In general, a plane source of particles, representing a uniform vertical concentration was used. This was modelled using an array of discrete particle sources, with the mass associated with each calculated according to the vertical position and separation

of the particle sources. The mass output was scaled with the product of the velocity at the vertical position and the separation of the particle sources, to give a uniform concentration field. The individual particle sources were chosen so that they fell in the vertical centre of the grid inlet cells.

The main requirement of the modelling results was that they should predict the change in deposition arising from the flow over the landscape shapes. For the majority of cases the deposition rate was normalised to a flat case to give the relative variation in deposition rate.

Mesh density

In order to ensure that the mesh had a sufficient resolution to capture the important features of the flow and particle deposition, a series of cases were run with different mesh densities. The basic geometry studied was a two-dimensional ridge of slope 45° . This was chosen because it was one of the cases examined in the wind tunnel and incorporated the fundamental features of a landscape shape. The ridge was 50 m high and was located at a distance of 750 m downwind from the start of the domain. The dimensions of the domain were 4000 m in length (X-direction) and 1000 m in height (Z-direction). The domain was chosen to be long enough to capture the significant changes in deposition, and high enough that the height of the landscape features did not exceed 5% of the domain height for the two-dimensional cases and 10% for the three-dimensional cases.

Five different mesh densities were used and these were described as coarse, coarse_focus, coarse_focus_adp, medium, medium_adp. Two uniform resolutions were used: coarse and medium. The computational hardware enforced an upper limit on the number of cells that could be modelled. Therefore, rather than increasing the resolution alone, the resolution was

increased in the region of the ridge in some cases. In other words, focused in the area of more complicated flow. These cases are denoted by 'focus'. For two of the cases, the cell density was doubled in each dimension for a selected area, using the adaption feature of Fluent. This converts each two-dimensional quadrilateral cell into four new cells. These cases are denoted as 'adp'. The details of the meshes used are given in Table 6.2.

For the particle deposition comparison between the different mesh types, a point particle source was used both for computational efficiency and for better comparison with the wind tunnel experiments.

Particle trajectory step

The particle trajectory model within Fluent offers the option to set the maximum length of the trajectory step. This is the distance that the particle travels before the new velocity is calculated, based on the balance of forces at its new position. The particle trajectory is also recalculated on entry into each new cell, so where the path through the cell is smaller than the maximum step length, the trajectory will be calculated with a smaller step size. A range of step sizes was examined from 0.01 m to 10 m. The cell size varied from 5 – 25 m in the horizontal direction and the smallest cell was approximately 1m in the vertical direction. The flow over a two-dimensional ridge was used for the comparison, with the coarse_focus_adp mesh from the mesh density study. Again a point particle source was used for economy.

Turbulence model

The effect of turbulence model choice on flow and deposition was examined. Three models were used:

- Standard k- ϵ model (Std. k- ϵ),
- Renormalization group k- ϵ model (RNG k- ϵ),
- Reynolds stress model (RSM)

There is a wide range of turbulence models available for use with computational fluid dynamics solvers. The relatively simple, one-equation Spalart-Allmaras model for turbulent viscosity was discounted, on the basis that it may not be able to model sudden changes in length scale as may be experienced in regions of flow separation (Fluent, 1999a). More complicated models such as large eddy simulations (LES) were discounted because of the significant increase in computational cost involved without, in this case, any significant benefit. The time varying output produced by LES models would have no additional value for this application where an integrated result is required. Another practical reason for discounting this approach is that the particle tracking algorithm in the Fluent software is not compatible with flow solutions produced by the LES model.

The standard k- ϵ model was devised to model the dynamics of turbulence (Versteeg and Malalasekera, 1995) and is based on transport equations for the turbulent kinetic energy within the flow (k) and its rate of dissipation (ϵ) (Fluent, 1999b). The k- ϵ model has been used to model many types of flow, and variations of the model have been developed with the aim of overcoming some of its shortcomings. The standard k- ϵ model, and the RNG k- ϵ model, were both used in this study, and are described below.

The standard k- ϵ model, as devised by (Launder and Spalding, 1974), is a semi-empirical, universal model, capable of dealing with turbulent flows in many situations. It was derived based on the assumption of fully turbulent flow, which is a realistic assumption for

atmospheric flows. As described above, the model has been used to model many different types of flow and is the most widely validated turbulence model. This has led to its limitations being well established, one of which is its over-prediction of turbulent kinetic energy on the upwind face of bluff bodies, as discussed by Castro and Apsley (1997). This is a potential problem with such a model for the study of flows over landscape features, particularly where there is a sharp discontinuity in slope. However, this model has been included with those tested because it is so well validated.

One of the more recent variations of the standard k - ϵ model was a result of the application of statistical mechanics techniques to the problem. The Renormalization Group (RNG) k - ϵ model was developed by Yakhot and Orszag of Princeton University, and involves:

“removal of small scales of motion by expressing them in terms of larger scale motions and a modified viscosity” (Versteeg and Malalasekera, 1995).

A full review of the application of renormalization-group techniques to turbulence is presented by Smith and Woodruff (1998). On a practical level, it has the advantage of not requiring calibration to specific flows, as all but one of the coefficients come out of the mathematical treatment, compared with the five empirical coefficients required for the standard k - ϵ model. The RNG approach yields a differential equation for the turbulent viscosity which provides a more accurate treatment of near-wall flows (Fluent, 1999e). Additionally, it does not suffer from the over-prediction of turbulent kinetic energy on the upwind face of bluff bodies (Castro and Apsley, 1997). These features make the model attractive for the modelling of atmospheric flows and it has been included in the comparison.

Where the k - ϵ models predict only the turbulent kinetic energy within the flow, the Reynolds Stress Model (RSM), models the production and transport of all six of the Reynolds stresses

individually. As a result, this model requires greater computational resources because it involves the solution of seven equations, six for the Reynolds stresses and one for their dissipation rate, compared to the two equations required for the k- ϵ models described above. It has the advantage of being able to model three-dimensional (non-isotropic) effects more accurately. However, this model is less widely validated than the k- ϵ model. This model has been included in these tests.

To test the effect of the turbulence models on the predicted particle deposition, a series of model runs were carried out using each turbulence model for the case of a 45° ridge and a flat case. The predicted turbulence and the relative increase in deposition rate were compared. A point source of particles was used for computational economy.

Wind speed

In order to investigate the effect of wind speed on particle deposition, a series of model runs was completed with varying wind speeds. Both the ridge geometry used above, and a flat case, were studied. The vertical profile of velocity was given by a log law following Equation 2.9, with velocities at 10 m above the ground of: 2, 5, 10 and 20 m s⁻¹. The range of wind speeds was chosen to represent typical atmospheric conditions. The roughness length used was 0.192 m (equal to the full-scale equivalent of the wind tunnel value, measured at the hill locations) and the corresponding friction velocities were 0.20, 0.51, 1.0 and 2.0 m s⁻¹ respectively. The deposition rates were calculated using the solved flows for these boundary conditions and the results were compared to see the effect on deposition. A plane source of particles was used giving a uniform concentration of 0.1 $\mu\text{g m}^{-3}$. Note that greater source strength is required at higher wind speeds, to obtain the same concentration. For all other cases the wind speed was set to 5 m s⁻¹ at 10 m above the ground.

Particle diameter

The variation in deposition rate with particle diameter was also investigated. A series of runs was carried out with particle sources of 7 different diameters, ranging from 0.1 to 100 μm , of unit density ($\rho = 1000 \text{ kg m}^{-3}$). The range of diameters was chosen to represent particle sizes that have relatively low deposition velocities and are therefore of concern for dispersal and deposition. For each diameter, a flat case and a 45° ridge were modelled. The deposition rates were calculated using the particle trajectory model and these were compared between the different diameters. The ratio of deposition rate between the ridge and the flat case was also examined for each diameter.

Particle density

A similar set of computational experiments was carried out for particle density, following the same pattern as that for particle diameter. Particle densities of 800 – 50000 kg m^{-3} were modelled for a particle diameter of 1 μm . This range was chosen as it represents most of the typical material densities that might be released in the atmosphere, from organic materials at the lower end to high atomic weight, radionuclide material at the higher end (such as uranium at 19,050 kg m^{-3}). Two runs at each particle density were carried out, one with a flat geometry and one with a ridge. The ratio between the ridge and the flat case was compared.

Landscape slope

The examination of the effect of slope was carried out as part of a systematic investigation of landscape shape. The cases studied involved the examination of the effect of slope for a two-dimensional ridge. Five ridges of different slope were modelled and compared to the flat

geometry case. The height of the ridge was kept constant at 50m and the base was increased in size as the slope became less steep. The slopes ranged from the steepest at 1 in 1 (45°), to the shallowest at 1 in 5 (11.3°). The dimensions of the ridges are given in Table 6.3.

Landscape shape

To investigate the effects of landscape shape further, models were run with geometries of forward facing steps, sinusoidal ridges and a selection of valleys. The details of each of these are described below. Graphical representations of the shapes studied are included with the results to avoid duplication.

Forward facing step

Four different forward facing step geometries were examined each of height 50m:

- a vertical step
- a 45° degree step
- a concave step, and;
- a convex step

In addition to providing information about the deposition for these types of geometry, it was hoped that these shapes would also provide information on the parts of the shape that influence deposition and the effect of different types of curvature.

Sinusoidal ridges

To examine the effect of smoothly varying ridge height, two ridges with sinusoidally varying height were studied. The ridges were modelled with a peak height of $\frac{1}{2}$ and $\frac{1}{4}$ of the half-base

width. The results for flat-sided ridges of the same height and base length (slope 1 in 2 and 1 in 4 respectively) were compared with these results.

To create the sinusoidal ridges, the peak was assigned to the maximum of a sine curve at $\theta=\pi/2$ and the upwind base at the minimum at $\theta=-\pi/2$ and the downwind base at the minimum at $\theta=3\pi/2$. The equation used to produce the hill heights is given below:

$$Z = \left(\frac{A+1}{2} \right) \times peakheight$$

$$where: A = \sin \left(\frac{X - X_{peak} + \left(\frac{baselength}{4} \right)}{baselength} \times \frac{\pi}{2} \right) \quad \text{Equation 6.1}$$

where: Z (m) is the vertical height of the ridge at a downwind distance X (m),

X_{peak} (m) is the downwind distance of the peak,

peakheight is the maximum height of the ridge, in this case 50 m, and;

baselength is the distance from the upwind to the downwind edge of the ridge, in this case 200 m and 400 m respectively for the different cases.

The equation above was applied at 1m intervals of downwind distance to produce a smooth surface. The calculated heights were transferred to the mesh generating software Gambit, by creating a file of commands in the form 'create vertex coordinates X Y Z'. This file was read into Gambit and the resulting vertices were combined to create the sinusoidal surface.

Valley geometries

Three different valley geometries were studied: a V-shaped, a U-shaped and a sinusoidal shaped valley, each having a maximum depth of 100 m below the reference plane. The V-

shaped and the sinusoidal shaped valley extended for a distance of 200 m from the windward to the leeward edge. The U-shaped valley had the same geometry as the sinusoidal valley at each side, but had a horizontal section extending for 100 m at the bottom of the valley. The total distance between upwind and downwind edges was therefore 300 m for this geometry. The valley shapes can be seen in the results for these cases referred to later on in this chapter. The deposition rate relative to the flat case was calculated for each geometry. The choice of geometries is somewhat arbitrary, but it is designed to capture important features of the flow over a valley. Because only neutral stability was considered features present for more stable flows are not explored. This could be included in part of future work.

Multiple ridges

The effect of a number of consecutive ridges was examined by modelling four different arrangements of two ridges, and one arrangement of three ridges. All of the ridges were 50m high, flat-sided ridges of 45° slope.

The geometries of the cases with two ridges were as follows:

Ridges adjacent, bases connected (peaks 2 hill heights apart)

Ridge bases 2 hill heights apart (peaks 4 hill heights apart)

Ridge bases 8 hill heights apart (peaks 10 hill heights apart)

Ridge bases 18 hill heights apart (peaks 20 hill heights apart)

In the case with three ridges, the bases were separated by 2 hill heights distance from the adjacent ridge.

6.2.2 Three-dimensional cases

General methodology

The methodology used to model the three-dimensional cases was very similar to that used for the two-dimensional cases. The main differences were as follows:

- Increase in geometry height from 50 m to 100 m to compensate for decreased area presented to the flow.
- Generation of three-dimensional geometries and meshes. This is discussed in more detail below.
- Some coarsening of mesh to reduce the total number of cells to a manageable level.
- Increased number of particles tracked to ensure noise in deposition pattern was kept to an acceptable level. This was required because the number of cells to which the particles deposit is increased relative to the flat case. The number of particles tracked was increased, from approximately 200,000 particles for the two-dimensional cases, to between 1.68 - 2.76 million particles for three-dimensional cases.
- Use of a different computer platform with greater processing power and memory to carry out the modelling. The existing Compaq Alpha XP1000 workstation was replaced by a Hewlett-Packard HP-UX 12 CPU server, with 4GB RAM per CPU. This was made available as a trial service from University of Birmingham, Information Services.
- Interpolation of deposition results to a uniform grid for direct comparison with the flat case results. This was achieved using the contouring software Surfer (Golden

Software) to interpolate results to a regular grid, using a Kriging algorithm. However, because of the large numbers of data points, the choice of interpolation method is not particularly significant (Gittings, 2003). The interpolated results for the landscape shape were divided by the interpolated results for the flat case at the same locations to give the spatial pattern of deposition ratio.

To determine the most appropriate mesh density to use for the modelling of the three-dimensional cases, three different meshes were used to model a cone of slope 1 in 1. The three meshes were similar to those used for the two-dimensional cases, and are described in Table 6.4. The flow and deposition were modelled for each mesh and the choice of mesh density was based on a comparison of these results. This is discussed further in the results section below.

Cases studied

Five different geometries were studied in addition to a flat control case. The cases modelled are described in Table 6.5 and are represented as three-dimensional contour plots in Figure 6.1. The geometries were chosen to represent simplified examples of real individual hills in the landscape. For the case of the sinusoidal hill, an equation similar to equation 6.1 was used for both the downwind and crosswind directions. These values were multiplied together (Equation 6.2) to give a three dimensional hill of sinusoidal cross section.

$$Z \propto \sin(X) \times \sin(Y) \qquad \text{Equation 6.2}$$

For each case, a plane of symmetry, parallel to the mean flow direction and passing through the peak of the hill, was used to reduce the computational workload. For the presentation of

the results in the next section, the domain has been mirrored in the plane of symmetry to give an impression of the results for the whole geometry.

6.3. Results

6.3.1 Two-dimensional cases

Mesh density

The results of particle deposition for the different meshes are presented in Figure 6.2. The graphs become noisier with increasing mesh density. This is a result of a finite number of particles depositing to the surface. As the cell size becomes smaller, less particles deposit in each cell and the variation becomes larger. This is especially clear for the two cases where the mesh is focussed around the peak. In these cases (Figure 6.2 (b) and 6.2 (c)) there is a clear change in the noise at 1500 m, where the mesh density changes. All five graphs show the same general features: a peak on the upwind face of the ridge, a minimum on the leeward face and a more gradual peak in the wake. The main differences between the graphs, apart from the noise, are the sizes of the peaks on the windward face and the sizes of the minima in the lee of the ridge. The *coarse_focus* (Figure 6.2 (b)) and *medium* (Figure 6.2 (d)) meshes show a higher peak on the windward face, approximately 25% more than the lowest value. Comparison of the CFD and wind tunnel experiments in Chapters 2 and 3 showed that the deposition to this area was over-predicted by the CFD. This suggests that the higher values here may be less accurate than the lower ones. The increased mesh density for *coarse_focus_adp* and *medium_adp* does yield lower values for this peak. Note that the coarse

case also gives a lower value, but this is thought to be due to averaging because of the wider cells.

The area of the leeward face of the ridge appears to show higher deposition for the coarse and coarse_focus cases (approximately 40% higher than the other three cases) and this may be due to incomplete resolution of the recirculating flow. Figure 6.3 focuses on the area of the ridge, from the windward foot of the ridge at $X = 700$ m, through the peak at 750 m, to the leeward foot at 800 m. From this figure, it is clear that the coarse case does not have sufficient cells to resolve the features seen in the other cases. The suggested over prediction at the peak from the coarse_focus and medium cases is clear here. There appears to be little difference between the coarse_focus_adp and the medium_adp cases.

Particle trajectory step

Figures 6.4 and 6.5 show the calculated deposition rate with a range of maximum step sizes used in the particle trajectory calculation. There is very little difference between the results from the different step sizes. The small differences that are visible are most likely to be due to the stochastic nature of the particle tracking approach. Note that for this study the coarse_focus_adp mesh was used.

Turbulence model

Figure 6.6 shows contour plots of the predicted turbulent kinetic energy (TKE) calculated using the three different turbulence models. All three produce results that are qualitatively the same, showing a plume of turbulence stretching downwind from the peak of the ridge. The main differences between the solutions lie in the region close to the peak. The standard k- ϵ

model shows a significant increase in TKE upwind of the peak. The RNG k- ϵ model shows some increase upwind of the peak but only at a much lower level of TKE. The RSM model shows a lesser degree still. The RNG and RSM models also show a larger region of low turbulence in the lee of the ridge. The maximum values of TKE were similar between the models, with 1.11 for the standard k- ϵ model, 0.84 for the RNG k- ϵ model and 0.92 for the RSM model.

Figures 6.7 and 6.8 show the particle deposition rate to the surface, normalised to the flat case, for each turbulence model. Again, all three show the same qualitative result, however, there are some important differences between them. The standard k- ϵ model and the RNG k- ϵ model both show similar patterns, with the standard version of the model producing a slightly larger increase on the windward face. The RNG version produces a more significant decrease in the immediate wake. The pattern in the further wake is similar for both cases. The RSM model produces a similar pattern, but the increase on the upwind face of the ridge is significantly larger (a factor of 7.7 increase compared to 2.9 for the standard k- ϵ model and 2.3 for the RNG k- ϵ model). The maximum in the wake is also further away from the ridge.

Wind speed

Figure 6.9 shows the deposition rate for the four different wind speeds studied. There is a clear increase in deposition with increasing wind speed. To show this more clearly, the deposition velocity, averaged over the whole surface, was plotted against friction velocity in Figure 6.10. This graph shows a clear linear relationship between the two over this range of velocities. The ratio of the deposition rate to the 45° ridge compared to the flat case at the same wind speed is presented in Figure 6.11. It is clear that the graphs are qualitatively and

quantitatively the same, although there is scatter due to the stochastic sampling. Within the range considered, the wind speed does not appear to change the effect of the ridge on deposition rate relative to the flat case. The mean increase at the peak is 2.45 with a standard deviation of 0.15 between runs. The increase in the wake peaks at a factor of 2.0 between 10-14 peak heights downwind of the peak.

Particle diameter

Figure 6.12 shows the calculated deposition rate to the flat geometry, for the range of particle diameters modelled, assuming a density of 1000 kg m^{-3} . There is very little to choose between the results for diameters $0.1 - 10 \text{ }\mu\text{m}$. However, at $50 \text{ }\mu\text{m}$ the deposition rate has approximately doubled and at $100 \text{ }\mu\text{m}$ it is eight times the value at $0.1 - 10 \text{ }\mu\text{m}$. Figure 6.13 shows the deposition velocity averaged over each flat case, using the freestream concentration ($0.1 \text{ }\mu\text{g m}^{-3}$). This shows the trend more clearly, with a very slow rate of change from $0.1 - 10 \text{ }\mu\text{m}$, and rising much more quickly at larger particle sizes. Figure 6.14 shows the effect of a 45° ridge on the deposition rate. The pattern of increased and decreased deposition is similar for the particle diameters $0.1 - 10 \text{ }\mu\text{m}$, but for the larger particle sizes the effect is reduced in size, whilst still showing the same features.

Particle density

The predicted deposition rates varied little for the particle densities studied. The flat case and ridge case results were very similar to those for particle diameters $0.1 - 10 \text{ }\mu\text{m}$. As a result only the average deposition velocity is presented in Figure 6.15. It is clear that over the particle density range of environmental particles there will be little effect from density alone.

Landscape slope

Figure 6.16 shows the results of calculated deposition to ridges of varying slope. As the slope decreases there are a number of obvious trends. The increase in deposition on the windward face of the ridge decreases from an average of 1.9 to 1.2 and becomes broader. Maximum increases were higher than these values; with the difference greatest for the steeper ridges. The maximum values are also expected to be somewhat dependent on the stochastic method. The area of reduced deposition behind the ridge is only apparent for the two steepest ridges, disappearing for slopes of gradient 1 in 3 and less. The increase in deposition rate in the wake of the ridge is apparent for all slopes, but becomes less pronounced for shallower ridges, but is still present for a slope of 1 in 5. The maximum in the wake also moves closer to the peak as the slope decreases. The average increase over a range of 4 hill heights drops from 2.0 to 1.4.

Landscape shape

Forward facing step

Figure 6.17 presents the deposition results for the four different forward facing step geometries. The general pattern of deposition is similar between all four cases, with a peak of deposition occurring at the position of the step and a longer area of increased deposition downwind of this area. Figure 6.18 shows the same data in more detail, focussing on the region from 500 to 1500 m downwind of the start of the modelled domain. Note, that the top of the deposition peak for the vertical step has been omitted in this figure to provide more detail on the other graphs.

It is clearer from this figure that the peak in deposition occurs at the discontinuity in the slope. For the vertical step the peak is largest and corresponds with the change from horizontal to vertical and back to horizontal. For the 45° step there is some increase at the bottom of the step where the slope changes from horizontal to 45°, but it is larger at the top where it changes from 45° back to horizontal. This difference is thought to be due to the discontinuity at the top experiencing higher velocity flow than that at the bottom. This pattern is the same in the results for the other two cases. The concave case shows a sharper and higher peak, where the discontinuity is at 50m above the initial ground level, compared to the convex case where the discontinuity is at ground level. Note that for the concave and convex cases, the slope changes from horizontal to vertical, or vice versa, at the discontinuity.

For the vertical and convex cases there is also a small reduction in deposition immediately upwind of the step. All four step types, caused recirculating regions of flow at this wind speed (5 m s⁻¹ at 10 m above the ground). The vertical step caused a recirculation region approximately one step height long, upwind of the step, and another, approximately two step heights long, downwind of the step. The 45° step had a very small region of recirculation upwind and downwind. The concave case had no upwind region, but a downwind region of similar size to the vertical case. The convex case had an upwind region approximately equal to half the step height in length, but no downwind region. The reduction in deposition upwind of the step appears to correspond to the presence of a significant recirculation region. The downwind recirculation region appears to have no obvious relationship with deposition. The convex case, which exhibited no recirculation, shows the greatest decrease in deposition downwind of the step.

The increased deposition in the wake also varies for the different cases. The steps that end in a sharp discontinuity (the vertical and concave cases) show a larger effect in the wake with

deposition rates reaching twice the value for the flat case. The 45° slope, which ends in a 45° discontinuity, shows an increase in the wake, but it is not as large as for the vertical and concave cases. The convex case, which ends in a gradual change in slope, has a much smaller effect with only a slight increase compared to the flat case in the wake.

Sinusoidal ridges

Figure 6.19 presents the relative deposition rates to the two sinusoidal ridges, compared to the flat case. For ease of reference, the ridges of slope 1 in 2 and 1 in 4 are presented in the same figure. At first sight there is little difference between the sinusoidal and the flat-sided ridges. However, on closer inspection the deposition on the upwind face to the sinusoidal cases shows a smoother variation, compared to the sharp peaks that occur at the peak of the flat-sided ridges. The deposition to the upwind face also shows a higher maximum for the sinusoidal ridges at roughly the middle of the face, corresponding to the point of steepest gradient. The higher deposition in the wake also extends less far for the sinusoidal cases.

Figure 6.20 shows the same data, but highlights the region around the ridges. Plots of streamwise gradient of the ridge height are also included on these graphs. For the upwind face there seems to be a good agreement between the gradient and the relative deposition rate, with a change in slope of 0.5 corresponding to a change in the deposition ratio relative to the flat of 0.5. On the leeward face there appears to be good agreement for the more steeply sloped cases (sinusoidal ridge 1 in 2 (Figure 6.20 (a)) and flat sided ridge 1 in 2 (Figure 6.20 (b))), but this becomes less good for the shallower cases. The deposition to the leeward face is likely to be affected by the degree of separation of the flow and the turbulence. For the steeper cases, the region of separation will be larger and this will delay the deposition of the particles until further downwind. For the shallower ridges there will be a smaller region of separation and

the turbulence generated by the ridge will bring the particles closer to the surface and increase deposition in a shorter distance. It is also worth noting that, for the flat-sided ridges there is a peak in deposition at the ridge itself that corresponds with the discontinuity in the curve of the gradient.

Valley geometries

Figure 6.21 presents the results for the three different valley geometries. The pattern of deposition is similar for each case. There is a reduction in deposition from the upwind edge of the valley that recovers at the downwind valley edge. There is a peak of deposition at the top of the downwind valley edge, with a factor of 2.5 to 3.3 increase and little wake effect beyond this. The predicted flow for these valleys showed recirculation within the valley for each case. Therefore, most of the particles would be expected to bypass the valley floor and reach the downwind valley edge before some is recirculated into the valley.

Figure 6.22 presents the same data, but focuses on the valley region and includes the streamwise gradient of the valley height. Even at this scale, the differences between the geometries are subtle. The reduction in deposition for each case is similar on the upwind side of the valley and the lower half of the downwind side. The peak at the downwind edge is largest for the sharp discontinuity found in the V-shaped valley, followed by that for the U-shaped valley with its wider cross-section and finally smallest for the sinusoidal valley. Although the peak of deposition for the U-shaped valley is smaller than for the V-shaped valley, the integrated increase is greater, probably due to the wider valley cross section. There is some correspondence between deposition and the gradient of the valley, but it is not as clear-cut as for the flat-sided and sinusoidal ridges. In particular, the downwind side of the

valley shows a different pattern from the gradient. This is most likely to be caused by the recirculation pattern within the valley.

Multiple ridges

Figure 6.23 presents the results for deposition to consecutive ridges. The case for a single ridge is also included for comparison. The inclusion of a second ridge, adjacent to the first, creates a second peak in deposition rate of similar size to the first. Following the second peak, the remaining region appears to be very similar to that for a single ridge, with perhaps a slightly smaller increase in deposition in the wake.

For the case of two ridges 2 hill heights apart, the second peak in deposition rate is larger than the first, but again the deposition in the wake is very similar to that for the single ridge. Where the ridges are separated by 8 hill heights the second peak is larger and appears to be superimposed on the broader increase due to the wake of the first ridge. The increase in the wake region is now clearly lengthened compared to the single ridge case. With the separation increased to 18 hill heights the peak is still larger than that for the single ridge, but the wake effect from the first ridge is reduced at this point. There is a more definite separation between the wakes of the two ridges and the combined effect extends further downwind.

For the case of three ridges, the peaks in deposition rate increase with each ridge. The wake effect appears to remain the same as the single ridge case.

It appears from these results that consecutive ridges close together have little effect, except in the production of local peaks at the ridge peaks whose magnitude grows with each additional peak. Where the ridges are separated by a greater distance, the second ridge causes a second peak and an increase in the wake.

6.3.2 Three-dimensional cases

The five three-dimensional cases studied have been grouped together for the purposes of comparing the results between cases. Plots of velocity vectors, turbulent kinetic energy and deposition ratio relative to the flat are presented.

Figures 6.24 – 6.28 present velocity vectors at a height of 5 m above the surface for each geometry. There is a clear increase in velocity above the landscapes for each case, with a greater degree of speed up close to sharp edges in the geometry. For the steeper sloped geometries, the cone of 1 in 1 slope and the elongated cone of the same slope, there is a significant change in the direction of the flow over the windward face of the hill. A region of stagnation is also apparent for these cases. For the shallower geometries there is also some gentler alteration to the direction. In the wake of all of the hills there is evidence of recirculation of the flow. This is more obvious for the steeper and sharper edged hills, as would be expected. In the wake of the hills the effect on velocity is more varied, with only the elongated cone and the 1 in 1 cone showing significant effects downwind. It should be noted that the scale is not the same for each velocity vector plot (Figures 6.24 – 6.28).

Figures 6.29 – 6.33 show contours of turbulent kinetic energy plotted on planes normal to the mean flow, starting at the peak of the geometry and extending downwind to a distance of 1000 m from the peaks. The general pattern is similar for all cases, with a plume of turbulence extending from the peak downwind. The highest level of turbulence is seen for the elongated cone case, with the maximum occurring above the height of the peak of the hill. The cone of slope 1 in 1 also shows high turbulence levels, with an interesting double maximum in the wake. The maxima, in this case, are closer to the ground than in the case of the elongated cone.

Figures 6.34 – 6.38 show contours of the ratio of deposition to the hill case relative to the flat case. These plots have been produced using deposition data for the flat case and for each three-dimensional geometry case in turn. Because of the variation in the mesh arrangement between cases, it was necessary to interpolate the deposition data to a uniform grid. The values on this grid were then divided by the values for the flat case on the same grid. The results were plotted as contours in these figures. Note that the ratio of 1.1 times the flat case has been used as a contour value. This has been used in preference to 1.0 because the noise in the deposition values result in intermittent contours at 1.0. A ratio of 1.1 therefore provides a better cut-off for highlighting areas of increased deposition. The horizontal scale and the deposition scale is the same in each case to allow comparison between the cases. The areas of enhanced deposition at the edge of the domain in some plots, are artifacts of the normalisation and interpolation process, and should be ignored. The isolated patches of increased deposition are a result of the noise present in the stochastic process for calculating deposition. Whilst they may indicate a general area of increased deposition when grouped together, they should not be interpreted as individual ‘hot-spots’ when present on their own.

The deposition pattern for the cone of slope 1 in 1 shows increased deposition to the windward face of the cone, with the maximum close to the peak. Deposition to the leeward face is reduced compared to the flat case. There are two areas of increased deposition in the wake of the cone, to either side of the centreline. The pattern for the shallower cone is similar on the face of the cone, but with a lower rate of increase on the windward face. There is some area of increase in the wake, but it is not as clear as for the steeper cone. The elongated cone shows a very significant effect in the wake, with an increase in deposition extending downwind for some distance, in two broad areas leading from the crosswind edge of the hill. There is also significant increase in deposition to the windward face.

The deposition to the pyramid also shows an increase on the windward face of a similar order to the cone of slope 1 in 3. There is less of a reduction to the leeward face for this case. The pattern in the wake is not clear, showing separated areas above the 1.1 contour line. There is some suggestion that there is more increase to either side of the centreline, but this is not clear. Finally the sinusoidal hill shows increased deposition to the windward face, reduction to the leeward face, but almost no effect in the wake.

6.4. Discussion

6.4.1 Two-dimensional cases

Mesh density

The `coarse_focus_adp` mesh was chosen as a suitable density to use for the remainder of the cases studied, as it appeared to capture the important features of the deposition. The `medium_adp` mesh showed little advantage to justify the increased number of cells. At this point it is worth reiterating that the main objective was to predict broad patterns of increase and reduction in deposition relative to the flat, rather than a highly resolved map of deposition to specific shapes.

Particle trajectory step

The results for the different particle trajectory steps showed little difference between them. The second smallest step value of 0.1 m was chosen for the remaining cases, as a conservative approach.

Turbulence model

None of the turbulence models available were without their drawbacks. The standard k- ϵ model over-predicted the turbulence on the windward face, as would be expected from its recognised shortcomings for flow past bluff bodies. Both the standard and RNG k- ϵ models are isotropic and do not differentiate between the different Reynolds stresses. The isotropic nature of the turbulence models was suspected of causing over prediction of deposition in the results of Chapter 5. However, for the calculation of relative deposition rates this was not important. The RSM is less well validated than the k- ϵ models and in the cases studied here over-predicted the increase in deposition to the windward face. The CFD comparison with wind tunnel experiments, described in Chapter 3, had shown that the deposition to the windward face of the ridges was approximately correct using the RNG k- ϵ model. The higher deposition produced by the RSM model was, therefore, not supported by the experimental results. The RNG model was chosen as the best compromise between capturing the important flow features, avoiding regions of unrealistically high turbulence and avoiding over-prediction of deposition. It was also attractive because its formulation relies on only one empirical constant.

Wind speed

Wind speed was seen to be an important parameter for total deposition, with deposition velocity varying linearly with friction velocity. However, over the range of wind speeds investigated here, the *ratio* of deposition to the ridge compared to the flat case showed no variation. For shallower and smoother geometries there may be a change in pattern with a reduction in wind speed, when the Reynolds number of the flow becomes lower than a critical value, and the flow no longer separates in the wake of the hill. The critical Reynolds number

for this transition has not been investigated with the modelling studies because it will depend on the surface roughness and hill shape as well as the hill height and wind speed. A brief discussion of critical slope for recirculation of flow caused by hills is included in Chapter 1 and reference is made to Wood (1995).

Particle diameter

The variation in deposition velocity with particle diameter, seen in Figure 6.13 for the flat case, shows a fairly constant value for deposition velocity until a threshold diameter is reached. Above this value, approximately 10 μm , the deposition velocity approaches the gravitational settling velocity, which increases rapidly with diameter. A useful comparison can be made between this data and the diffusive flux based models of Sehmel and Hodgson (1980). The results in Figure 6.13 agree with the models of Sehmel and Hodgson for the case where the resistance below 0.01 m is neglected. In the case of the CFD model used here, the height of the cell at the boundary is larger than this value and, therefore, there is no explicit modelling of the effects at this scale.

The surface resistance in the model of Sehmel and Hodgson (1980) is derived from wind tunnel studies using uniform surface roughness, with z_0 values up to 0.06 m. The surface roughness used in the CFD calculations was 0.192 m, and therefore the deposition velocity will be expected to be higher than those seen in the results from Sehmel and Hodgson. The CFD predicted deposition velocities are of a similar order to those observed for rough ground cover and forest canopies (Zhang *et al.*, 2001). Where the depositing surface is smooth, the CFD approach used is likely to under predict the deposition velocity. However, for most cases of atmospheric deposition where the surface roughness elements effectively act to intercept airborne particles this layer will be less important. In these cases the deposition rate will be

controlled by the transport through the bulk flow, and will be well predicted by the CFD model. As discussed in Chapter 1, Slinn (1978) notes that for smooth surfaces, the transfer across the surface layer would be expected to be the controlling factor, but for rough surfaces the deposition may be rate-limited elsewhere in the atmosphere.

The purpose of this modelling study was to predict the relative change in deposition rate from a flat to a complex landscape. The absolute value of the deposition velocity is therefore not the parameter being predicted, only the relative deposition caused by a change to the landscape type. The principal effects of such a change in landscape geometry are to change the turbulence level in the bulk flow, and hence its diffusivity, and to change the concentration gradient by causing the streamlines to converge or diverge. These effects are implicitly modelled in these CFD models. The properties of the flow very close to the surface, which reduce the deposition velocity for smooth surfaces, are unlikely to be changed by the bulk landscape changes. The relative deposition effects are therefore unlikely to be affected by neglecting this small scale, even though the absolute deposition velocity may be over predicted. The effects of different surface roughness values on the relative deposition is something that has not been explicitly modelled in this study, but could be explored further in future work. In particular, the detailed study of the near-surface flow and its interaction with roughness elements and vegetative canopies could be used to develop a sub-model for the surface transfer, which could be applied within larger models.

The results for the variation in deposition to the ridge with particle diameter show that the effect of the ridge decreases with increasing particle diameter. This reduction in the effect of the ridge is most likely to be a result of the larger particles being less influenced by the turbulent flow caused by the ridge.

Particle density

The range of densities found in environmental particles is relatively small and is reflected by the cases modelled here. There is relatively little change in particle deposition rate for the different densities. This is to be expected as the varying density particles can be considered as particles of different aerodynamic diameter ranging from 0.89 to 7.1 μm . As could be seen from the results for particle diameter, there is little difference in deposition velocity over this range. Density would become more important for particles greater than 10 μm , where the rate of change of deposition velocity with particle size is greater.

Landscape slope

The slope of a two-dimensional ridge clearly has a strong influence on the deposition rate.

The steeper the slope:

- the greater the increase on the windward face,
- the greater the decrease on the leeward face
- the greater and further downwind the increase in the wake

The results presented in Chapters 2 and 3 from the wind tunnel studies, show differences in the relative deposition in the wake for different source configurations. The wind tunnel studies carried out with a point source, both experimental and CFD, do not show an increase in this region. The results presented in this chapter are produced using a uniform upwind concentration, representative of a distant source. With a uniform upwind concentration, the increased turbulence produced in the wake causes increased transfer of material from higher levels towards the surface and therefore enhances deposition. The one wind tunnel case with a

broader source supports these results and shows an increase in the wake, although this is complicated by the three-dimensional geometry.

The effects on deposition modelled in this chapter and summarised above, are most likely to be the result of a combination of effects. The contraction of streamlines caused by flow passing up over the hill increases the concentration gradient and hence the flux to the surface. The converse is true above the downwind side of the hill. A second effect is the increase of the turbulence in the flow caused by flow over the landscape feature. Increased turbulence results in greater mixing and greater transfer to the surface for the same concentration gradient. This is responsible for the increased deposition in the wake of the landscape features. Whilst these two effects help in the interpretation of the results it is difficult to apply them in isolation as the concentration gradient is strongly influenced by the flow and deposition upwind. In the case of flow recirculation, as was present in many of the studied flows, it becomes harder still to apply these ideas to landscapes. In such cases, the coupled modelling of flow and deposition using CFD is extremely valuable.

Landscape shape

The forward facing step models show the influence that the type and location of discontinuity has on deposition. Sudden discontinuities in height produce a sudden rise in deposition. Where they occur at height, they disrupt the flow and produce a turbulent wake, causing a further deposition increase downwind. Where there is a sudden change in gradient at ground level, as is the case for a convex forward facing step, the increase is less dramatic.

A study of flow and dispersion of pollutants over a cliff (Hill, 1994) was used for comparison to the vertical forward facing step case. The referenced work included wind tunnel and CFD

studies of dispersion from a point source upwind of a vertical cliff. The results from the CFD study showed a sharp discontinuity at the location of the cliff, with increased concentrations relative to the flat case. Although this is not directly comparable with the CFD studies reported here, because of the different source configuration, it is qualitatively similar. The referenced work also found recirculation at the base of the cliff, as was the case in this study.

The sinusoidal ridge case shows the effect that the curvature has on deposition. The rate of deposition increase shows a reasonable agreement with the gradient for the windward face. For the case of the valley geometries, this agreement is less apparent and this is probably because a different flow regime applies, dominated by the downwind edge of the valley.

It is informative to compare the results from these CFD studies to wind tunnel studies and field studies of particles that have been reported in the literature. A number of papers by Goossens and co-workers are of relevance here (Goossens, 1988a; Goossens, 1988b; Goossens, 1996; Offer and Goossens, 1995). Although these works focussed on wind blown dust of diameter less than 63 μm , and a median diameter of about 30 μm (although it is not specified whether this is mass- or number-median diameter and whether it is aerodynamic or actual diameter), they are still a useful comparison. A review of a number of these papers is included in the literature review in Chapter 1.

It is useful to compare the results for deposition to a symmetrical sinusoidal hill, reported by Offer and Goossens (1995), with the sinusoidal ridge modelled above. Figure 6.39 reproduces the results from this paper, and the pattern of deposition is clearly very similar to that predicted from the modelled results, for the sinusoidal ridge of slope 1 in 2. This provides additional validation of the CFD results calculated here and supports the results of the wind tunnel work described in Chapter 2. Although the particle size used in the work by Goossens

is larger than that considered here, the sensitivity studies carried out above, investigating particle diameter, showed that the results were insensitive to particle diameter below 10 μm for a density of 1000 kg m^{-3} , and of a similar pattern to those at 50 μm for the same density. This indicates that it is reasonable to compare the two results, although some differences should be expected. The conceptual model of Goossens regarding deposition and surface curvature (Goossens, 1988a), discussed in Chapter 1, is also of interest here. The main controlling features of the flow are identified as concentration (identified through converging streamlines) and turbulence. This would also appear to be the case in the present results. High deposition occurs where the streamlines converge and increase the concentration close to the surface, such as on the windward face. High deposition also occurs in the wake, where turbulence is high. However, the identification of high deposition to the windward concave parts of the slope, and low deposition to the windward convex parts, by Goossens (1988a), doesn't agree with the results in Figures 6.20 (a) and 6.20 (c). In these results, the opposite appears to be true, with increased deposition to the higher windward convex part of the hill.

Multiple ridges

The effect of multiple ridges can be divided into two broad classes of cases:

- those where the ridges are close together and the effect is similar to that of a single ridges
- those where the ridges are far enough apart that there are clearly two ridges with some overlap in deposition effect

For separation of 2 ridge heights apart, the effect is clearly of the first type, whereas for ridges 18 ridge heights apart it is of the second. For a separation of 8 hill heights the effect is not so

clear-cut. This result is in agreement with a general rule of thumb that hills that are 10 hill heights apart are independent in their effects.

As for the case of the sinusoidal ridge, useful comparison can be made with the wind tunnel data of Goossens (1996). In this paper he investigated various combinations of hills of different heights and slope, although not of different separations. An example of the results from this work is included in Figure 6.40. This graphs shows the same features for closely spaced ridges, where the deposition to successive peaks increases in magnitude. There is a difference though in this case, as the deposition to the second hill is shadowed by the first hill and this is different from that predicted for the CFD. This was not the case, however, for all the geometries studied by Goossens, with shallower hills not showing a shadowing effect. This difference may be due to the larger particle sizes in those studies, which would prevent the particles from recirculating with the flow into this region. It is also important to note that the spacing between the ridges is greater in the present CFD study with three hills.

6.4.2 Three-dimensional cases

The patterns of deposition for the three-dimensional cases are clearly more complex than those for the two-dimensional cases. There are obvious similarities between the two, with all the cases showing an increase on the windward face of the hill and reduction on the leeward face and into the wake for some. One feature that is clear is that the deposition ratio along the centreline is not representative of the overall pattern of deposition for the three-dimensional cases. For example, for the cone of 1 in 1 slope, the deposition ratio along the centreline includes the maximum at the peak, but does not capture the increased deposition to either side of the centreline in the wake. These areas of increased deposition are seen for the two cases with steep slopes, namely the cone and the elongated cone of slope 1 in 1. The plots of

turbulent kinetic energy suggest that these features are associated with high turbulence close to the surface. For these two cases the turbulent kinetic energy contours have a kidney shape, with lobes of high values on either side of the centreline and lower values in between. These areas of high turbulence are possibly associated with horseshoe vortices trailing from the hill, see for example Offer and Goossens (1995).

Comparison with work done on slightly larger particle size range is informative. Offer and Goossens (1995) studied the deposition of windblown dust to a conical hill in the field and made comparisons in a wind tunnel. The features are remarkably similar between their field and wind tunnel studies, and also show agreement with the features in the results for the cone of slope 1 in 1 presented here. Specifically, these are the increase on the windward face, peaking close to the summit, and reduced deposition on the leeward face. The wind tunnel results in the work by Offer and Goossens (1995) also showed a minimum in the near wake on the centreline, with higher deposition to either side. However, the area measured in the reported work did not extend far beyond the hill itself. The comparison of the CFD results with these wind tunnel results and, more importantly, the field studies, gives further confidence in the application of CFD to this type of problem. An interesting extension to this work would be the modelling of multiple three-dimensional hills with different separations and lateral offsets.

6.5. Conclusions

This chapter describes the use of computational fluid dynamics to study the dry deposition of airborne particles to landscape features. The validity of the modelling approach has been addressed by experimental work reported in previous chapters. The importance of different

modelling choices has been examined and a systematic study of two-dimensional landscape features has been carried out. A limited number of three-dimensional cases have also been modelled. The results have been compared with the limited experimental and field data available.

6.5.1 Modelling choices

The mesh density was seen to be an important variable. The meshes were all of reasonable resolution and differences were seen between the coarser and finer meshes. The coarsest mesh did not capture detail of deposition increase to the peak of a ridge, nor deposition reduction on the leeward face. The particle trajectory step has little obvious effect over the range studied and with the mesh used here. The choice of turbulence model was significant, with the biggest difference seen between the k-epsilon models and the Reynolds stress model (RSM). The RSM model showed significantly higher increase in deposition compared to the k-epsilon models, despite similar turbulent kinetic energy levels. The standard and RNG k-epsilon models differed in their prediction of deposition to the near-wake region. The RNG k-epsilon model gave the best compromise between the features of the three models tested. It avoided the known limitations of the standard k-epsilon model and provided better agreement with wind tunnel data than the RSM model.

In addition to the modelling choices discussed above, wind speed, particle size and particle density were examined. Particle deposition rate varied directly with wind speed, but relative deposition to a ridge compared to a flat case showed no change in quantity or extent with wind speed over the range examined. Particle diameter caused an increase in deposition velocity above a threshold of 10 μm . The results for variation in particle deposition showed some differences between data from the literature, due to no explicit modelling of the smallest

scales close to the surface. Particle density had little effect over the range of values found in environmental samples, for the particle size studied.

6.5.2 Landscape shape

Landscape shape had a significant effect on dry deposition, as expected. Deposition was seen to increase on the windward slope of a ridge by a factor as large as 2.5, decrease on the leeward face and in the near wake by as much as a factor of 0.25, to rise again in the further wake by as much as a factor of 2. Steeper slopes showed larger effects, with sharper peaks in deposition on the upwind face. Shallower ridges resulted in a less sharp increase in this area and absence of a region of reduced deposition below a threshold gradient (1 in 3 for the conditions studied). Results from a forward facing step showed that the nature of the curvature is important, with different results for a step change, concave, convex and 45 degree slopes.

Comparison of flat sided and sinusoidal ridges showed no large differences, but a slight change in pattern was seen due to local changes in gradient. The valley geometries studied showed a reduction in the valley and a peak of increased deposition on the leeward valley edge. Multiple ridges showed separate effects when sufficiently far apart and superimposed deposition patterns when closer together, with higher peaks as a result.

The three-dimensional cases showed similar patterns to the two-dimensional cases. All the geometries studied showed increased deposition to the windward face, and most showed a reduction on the leeward face, although this extended into the wake for the elongated cone. For the steeper sloped geometries there were regions of increased deposition in the wake and these were found to either side of the centreline.

In general the results showed strong patterns for landscape types and consistent results, with weak dependence on most of the parameters investigated. This makes the results useful for application to real landscapes. The limited comparisons available with the wind tunnel experiments presented in Chapters 2 and 3, published literature from wind tunnel, and field trials for larger particle sizes, show good qualitative agreement with these CFD results. The results suggest that near-surface turbulence, and concentration, are the controlling parameters for deposition, in agreement with the conceptual model of Goossens (1988a) for larger particle sizes. The interaction between surface landscapes and these parameters is not straightforward, and the use of a CFD model is a practical way to study these features, and their influence on particle dry deposition.

6.5.3 Future work

There are a number of further studies that could be undertaken. More three-dimensional cases could be modelled, in particular multiple hills in different arrangements and ridges at different angles to the flow. The modelling could also be extended to include non-neutral stability conditions. More detailed investigation of the interaction with and deposition to surface roughness could be carried out. This could be extended to the development of a sub-model for deposition to vegetative canopies. For further validation a field trial could be carried out, using either an artificial tracer or a natural aerosol. A potential natural aerosol would be sea salt that could be used in areas of complex coastal topography with the advantage of steady on-shore winds under certain meteorological conditions.

7. APPLICATION OF DEPOSITION RESULTS WITHIN A GEOGRAPHICAL INFORMATION SYSTEM

7.1. Introduction

The driving force behind the research into how landscape shape affects dry deposition, is a need to better understand the spatial variations in such ground deposition, following an accidental release of material to atmosphere. The wind tunnel and computational fluid dynamics studies have shown that landscape shapes do alter the local amount of deposition, and that significant changes can occur over a short region. To be of practical value, the results of this research need to be integrated into a system that can be used in an emergency situation. The system needs to guide the sampling of ground contamination in order to isolate areas exceeding threshold values. In particular, it should be possible to identify areas of isolated high deposition or ‘hot-spots’, which may fall outside of a general area of high deposition. The aim is not to predict actual deposition rates accurately, rather to indicate areas where the deposition will differ significantly from that for an area of uniform topography, with a view to informing sampling strategy “on the ground”.

The work presented in this chapter illustrates an example system based on the following steps:

1. Definition of rules governing increased or decreased dry deposition, surrounding landscape features.
2. Decomposition of a real landscape into landscape features.
3. Combination of rules and landscape features, together with meteorological information to produce a map of regions of increased and decreased risk of deposition.
4. Estimation of the area affected by plume of contaminant using meteorological information and a dispersion model.
5. Combine plume extent and map of deposition risk to produce a map of predicted areas of deposition, to act as a sampling guide.

These steps could be followed manually, or used in isolation to provide increased information in the absence of the full set of data. However, during an emergency situation sampling guidance is needed quickly, so that ground sampling can be completed within 24 hours. Therefore, for a dry deposition prediction technique to be valuable, it should form part of an automated system. Ideally, such a system should be able to produce results, from the supply of the required information, in a timescale of tens of minutes, or an hour at most. This short timescale is the main reason for following an approach based on simple rules, rather than using a complex CFD or detailed meteorological model with large information and processing requirements.

The system described here, is designed around the use of a computer-based geographical information system (GIS). Such a system can import and handle spatial data, perform calculations based on single or multiple data sets and produce graphical representations of the

results. A useful introduction to such systems is provided by Burrough and McDonnell (1998) who include a range of practical definitions of GIS, including the following:

“a system for capturing, storing, checking, manipulating, analysing and displaying data which are spatially referenced to the Earth” - (Department of Environment, 1987).

GIS systems have moderately large computer processing and storage requirements. Because of these, they have in the past, been used on more specialised computing platforms, typically with a Unix operating system. Progress in computing hardware has now produced very capable GIS systems based on personal computers, and such systems are capable of running a rule-based dry deposition model as described above. The basic data requirements for such a system are digitised topography data, meteorological data and concentration data from a dispersion model. These requirements are discussed in more detail below. To increase the speed of such a system the topographical data could be included beforehand, reducing the amount of data to be input or imported during an emergency situation.

The remainder of this chapter deals with the rules that can be derived from the CFD work undertaken so far, and the generation of an example GIS based system. The system has been produced as an example of how such a process might be undertaken. The system produced includes a range of simplifications for the purposes of producing a ‘proof-of-principle’ and is not intended to be a working system. To produce a robust system, field validation and further CFD work needs to be carried out on a greater range of landscape shapes, and under a wider variety of meteorological conditions.

7.2. Derivation of rules governing dry deposition surrounding landscape features

It has been discussed in several places above, that the principle aim is to produce a system that can quickly estimate areas of increased or decreased deposition, relative to a flat terrain case, rather than accurately predict deposition rates. The approach used, has been to study the relative deposition to a series of key landscape shapes and conditions using CFD and validate them against wind tunnel studies. The results from these studies have been simplified to a series of rules that can be applied by algorithms within a system, such as that described above. The use of a series of rules, rather than modelling the actual landscape itself, allows the process to be carried out much more quickly and places less demands for input information on the user during an emergency situation. Also, by simplifying the output of the CFD models, more emphasis is placed on the general trends present in the results, which are most applicable to real landscapes. An alternative approach would have been to map the quantitative deposition pattern predicted by the CFD. However, this would have been dangerous in terms of suggesting a fully quantitative prediction not necessarily applicable using rules based on a limited number of cases.

A summary of the results produced in Chapter 6 is presented in Tables 7.1 to 7.3. These have been used as the basis for a series of rules that can be applied to landscapes. There are a variety of results for individual landscape types and their implementation relies on being able to identify these features successfully. For the purposes of demonstrating this system, the effect of two key feature types, hills and ridges, have been used. Their identification, classification and resulting effect on deposition, are dealt with below. A complete system would require a greater range of landscape types.

The results from the CFD analyses of individual landscape shapes need to be formalised before they can be applied to the shapes identified in a landscape. The results presented in Chapter 6 cover a broad range of landscape types and includes complex patterns of increased and decreased deposition. These results need to be structured and simplified before they can be meaningfully applied to a real landscape. Additionally, there is a range of further parameters that could be investigated to extend the applicability of this approach. The aim of the work presented in this chapter, is to demonstrate how such a system might be developed. Rules have been derived and applied for peaks and ridges within a landscape and the specifics of the rules are presented below.

7.2.1 Peaks

Figures 6.34 – 6.38 show the different effects of three-dimensional hills. For this example system, no differentiation was made based on the shape of the hill because of the infinite variety of possible shapes and the problems in identifying different types using an automatic system. The hills or peaks have been divided according to their slope. Two classes of peak were distinguished: those with a slope of 1 in 1 or greater, and those with a lower slope. The areas of affected deposition were digitised from the figures of increased and decreased deposition to produce a vector outline of the areas likely to be affected. These could then be scaled and applied to peaks identified within a landscape, depending on their slope. The orientation of the affected area depends on the wind direction and needs to be included in the application of these areas. Although this is clearly an over-simplification, it demonstrates the principle of this approach.

7.2.2 Ridges

A similar approach was used for ridges as for peaks. The threshold of increased deposition of 1.1 times the flat case was used as a delimiting line, as for the peak data. The data in Figure 6.16 was used to determine the size of these areas. This data is summarised in Table 7.4. In this example, the small region of decreased deposition behind the ridge was not included, although this could be incorporated in an improved version.

7.3. Identifying landscape features

The rules above have assumed that individual landscape features can be identified for a real landscape. This may be done relatively easily by hand for a small area, either on the ground, or by viewing topographical information from maps. However, a manual approach would become time consuming for a large unfamiliar area. There are also likely to be areas that do not clearly fall within any category. The use of a system of landscape feature recognition within a GIS avoids these problems, by automating and formalising the procedure. This also makes decisions as to the classification of features traceable and hence auditable. The details of one such system are described below.

Information on the topography of a landscape is normally input into a GIS as a digital elevation model (DEM). This type of information is termed a raster format, providing a two-dimensional array of elevation values at regular spatial locations. There are a number of sources of DEMs at different scales available from different sources. These include GTOPO30 global 30 arc second data, of approximately 1km resolution, from the USGS, through to 7.5 minute DEM also from the USGS, which is only available for the United

States. Recently imagery from NASA's EOS system of satellites, has also produced fine scale, approximately 30 m, digital elevation model data (ASTER) for most of the globe.

However, for the UK a readily available source of DEM data is the Ordnance Survey. This comes in two formats, both derived from contours on topographical maps. Land-Form Panorama is derived from 1:50000 map data and has a 50 m horizontal resolution, whereas Land-Form Profile is based on 1:10000 map data and has a 10 m horizontal resolution. The Ordnance Survey data has the advantage of being in UK National Grid projection and, therefore, allows easy comparison with other UK spatial data, without the need to change the geographical projection. An example of Land-Form Panorama data can be found in Figure 7.1. All of the Ordnance Survey data presented in this thesis are © Crown Copyright Ordnance Survey and was supplied by EDINA Digimap/JISC. Further details of sources of digital elevation data can be found at the Digital Elevation Data Catalogue internet resource (Gittings, 2003).

Digital elevation model data only provides an array of elevation values, not a description of the type of topographical features present. To identify such features requires the use of a GIS algorithm. An example of such an algorithm is described in a PhD thesis on the subject (Wood, 1996). The approach used is to classify each part of the landscape into one of the following regions: pit, peak, channel, ridge, pass or plane. The classification is achieved by comparing each raster cell with its neighbours. This section of the surface is then approximated with a quadratic equation. This equation is used to calculate derivative quantities: slope, cross-sectional and longitudinal curvature and minimum and maximum convexity. These values are then compared with a series of rules to assign them a category. For example, a peak would have a slope of zero and positive convexities. This method can categorise a surface into the above features unambiguously, and has the advantage that the

resulting features correspond with our understanding of common landscape features. An example of the classification of a landscape using this method is presented in Figures 7.2 – 7.6.

Classification of the landscape into these features acts as a starting point for applying rules describing the relative deposition. To apply these rules, a set of linear and point features are needed, and the output of the classification algorithm described above, must be converted to data in this format.

7.4. Applying the rules within a GIS

In order to apply these rules within a GIS system in an automated way, it is necessary to program the GIS with a series of instructions. For the purposes of demonstrating this system, the GRASS GIS software was used. GRASS is an acronym for Geographic Resources Analysis Support System and was originally developed by the U.S. Army Construction Engineering Research Laboratories between 1982-1995. GRASS is available as Free Software / Open Source under the GNU General Public License. GRASS is used in many academic, commercial and government settings (GRASS GIS, 2003). The software incorporates a large number of utilities and geo-processing algorithms, contributed by a variety of users. GRASS was chosen in preference to commercial products, such as ESRI ArcView or ArcInfo, because of the flexibility available in programming and automation, and also the inclusion of feature extraction algorithms produced by (Wood, 1996) described in Section 7.3 above.

An automated system was developed in the form of a script of commands controlling GRASS. The programming language used to write the script was Perl; chosen for its ability to

perform mathematical manipulation of data and coordinates, to read and write configuration files with ease and to issue text commands to GRASS.

The practical process used to outline areas of affected deposition was divided into that related to peaks and ridges. There are a number of similarities between the two processes. Flow charts of the important parts of each process are included in Figures 7.7 and 7.8. The full text of both these scripts, and a short script to combine their output, is included in Appendix 2. The details of each process are described below.

Peak script

The script for identifying areas affected by the hills/peaks requires digital elevation model data and wind direction as input for this example. The digital elevation model is specified, by providing the name of the raster map containing this data, within the script. These data have been obtained from Landform Panorama data © Crown Copyright Ordnance Survey supplied by the EDINA Digimap/JISC service. The data was converted from OS NTF format to native GRASS raster format. For this example, a constant wind direction has been assumed over the region considered, and this is specified as a constant. However, the script has been written so as to allow a field of varying wind direction to be used. This would allow the use of data from a larger scale meteorological model to be used, by supplying a raster map of wind direction for each cell. No specification of wind speed is included because, within the range of wind speeds studied, there was no change in the relative effect on deposition, although absolute deposition does vary with wind speed.

The script next calculates the slope for every cell within the raster map, and the average elevation over the whole map. The landscape features are then identified using the algorithm

described by (Wood, 1996) which is included as a module in GRASS. There are a number of parameters that control the performance of this algorithm. In particular, the slope tolerance which determines the minimum slope that is used to identify non-planar features, was set to 1 degree. The window size, which determines how many cells surrounding the calculated cell in each direction are considered when fitting a curve to identify features, was set to 11. For digital elevation maps of 50m resolution, this is equivalent to a distance of 250m to each side of the calculated cell. The result of the algorithm is a map of different feature types including peaks and ridges.

The peaks are then selected from the resulting feature map and are converted to a different format, that contains only point representations. The coordinates of each peak are then read in turn, by making use of Perl's text handling facilities. For each peak, the elevation, average elevation and wind direction are then read from the appropriate maps, at the coordinates of the peak.

One of the problems in producing an automated system is determining the relative height of the landscape features. The elevation above sea level is provided by the digital elevation data, but the effective height above the surrounding area is more difficult to determine. For the purposes of this study the average elevation over the region considered, was subtracted from the elevation above sea level to give an effective height. This is not an ideal solution because it is not applicable to all landscapes. For example, it would not be suitable where there is a net slope across a wide region. This could be improved by calculating the average elevation within a distance from the peak.

It was also necessary to estimate the slope of the area surrounding the peak. The average of the slope within a circular area, of radius equal to the effective height of the peak, was used as

an estimate of the slope of the peak area. This is clearly an approximation, as it will introduce an error in the slope if the slope, is significantly different for the region outside this for shallower peaks.

The slope averaged over this area representing the hill, is then used to determine whether the template for a steep (>45 degree slope) or less steep hill (<45 degree slope) is used. The appropriate template is then scaled, depending on the effective height of the hill and the orientation is determined by the wind direction. This template is then added to a map of cumulative deposition effect. The next set of coordinates is treated in turn, until a map of all the areas affected by the peaks has been built up.

Figures 7.9 (c) and (d) show the output from the peak script applied to an area in the Scottish highlands. The figures show the same area with two different wind directions, 135° and 225° (direction wind is blowing from, clockwise from grid north). Note, that the size of area affected varies with the height of the peak, and also that the affected areas are rotated according to the wind direction. There are three different values for the resulting maps, yellow represents no effect, red an increase and blue a decrease in deposition. Where two regions overlap, the resulting value on the map is the sum of the two values. To distinguish between no effect and an area of mixed increase and decrease, the effect of increase and decrease are given different identifying values. For each region of increase, the nominal value of the map is increased by 1.0, and for each region of decrease, the value of the map is increased by 0.0001. This allows the effects to be separated using the 'Combine' script described below.

Visual inspection of the shaded elevation map suggests that there are more peaks than those identified in resulting figures. The use of a size window in the script has discriminated against

the smaller peaks. The value for this size window can be varied where the landscape type dictates that smaller peaks should be included.

Ridge script

The script used to analyse the ridges in the landscape is very similar to that for the peaks. However, some differences in the implementation are required because of the two-dimensional nature of the features. The differences between the two scripts are detailed below.

The increase in deposition due to a two dimensional ridge can extend to a reasonably large distance downwind of the ridge. To include this effect, the resulting map is extended by a distance of 10km in the downwind direction. The slope in the vicinity of the ridge is calculated in a different way to that for peaks. The slope is calculated at the start of the script for every cell using a range of different size windows. These raster data layers are used later in the script, together with a rough estimate of the slope for each ridge, to calculate the average slope of the ridge.

The ridges' features are identified and converted to a vector file. This vector file is then output as a text file, containing a list of the coordinate pairs for each point on the ridge. Each ridge in turn is then read into the script and analysed. The overall angle of the ridge is calculated. An assumption is made that, if the angle of the ridge is less than 45° to the wind direction, it should be disregarded. Those ridges at an angle greater than 45° are assumed to affect the flow. Ridges of overall length of less than 500 m are also disregarded. This assumption is arbitrary, and needs to be explored by further CFD studies for ridges at different angles. More

complicated effects on the flow and deposition would be expected for ridges that make a shallow angle to the wind direction.

Having eliminated those ridges that do not meet the above criteria, the script then determines the ridge slope. A multi-step approach is needed to approximate this value. Firstly the average slope of the ridge within a 5-cell window is calculated. Then the average effective ridge height (ridge peak elevation less map-averaged elevation) is calculated. From this, a rough estimate of the ridge base length is calculated. The slope over this area is then determined using the slope calculated for each point using the appropriate window size (between 3 and 19 cells), calculated at the beginning of the script. This value is then used to calculate the extent of the affected area by choosing values from those presented in Table 7.4. Two areas are delimited, one upwind and one downwind, both parallel to the ridge. This area is then added to a cumulative map of deposition-affected areas. As for the peak script, areas of increase are increased by a value of 1.0 on the cumulative map. No areas of decrease are distinguished for the ridge script because of the small extent of these areas.

An example of the application of the script to the same region of the Scottish highlands is presented in Figures 7.10 (c) and (d). Affected areas for two wind directions are shown. There is clearly overlap between the areas affected by each section of ridge.

Combine script

Having calculated the affected areas for peaks and ridges, a combined map is required. A short script is used to combine the two outputs. In addition to adding the results together, they are also classified into bands according to the number of overlapping affected regions. The banding scheme used is presented in Table 7.5.

To divide each value into one of these bands, a number of steps are followed. Firstly, the sum of the peak and ridge map is put into a temporary raster map. Secondly, by calculating the remainder of the value held in each cell when divided by 1.0, the numbers after the decimal place are placed into a second temporary raster map. The summed map and the map containing only the fractional part, are then interrogated. Where there is both an increase in deposition (summed map value > 1.0) and a decrease in deposition ($0.0000 < \text{fractional map value} < 0.0999$) these areas are assigned a flag value of 0.1. All other areas are equal to the sum of the peak and ridge maps. An alternative approach would be to include some weighting for mixed regions. However, without further experiments of CFD studies it is not clear what the effect on deposition would be.

Where there is no deposition the resultant map contains values of 0. Where there is one or more area of decreased deposition, the value will lie between 0.0001 and 0.0999 for between 1 and 999 overlying areas. Where there is a mixture of areas of increased and decreased deposition the value is equal to 0.1. Where there are one or more areas of increased deposition, the value will lie between 1 and 999, for between 1 and 999 overlying areas. This data is then recoded into the banding system in Table 7.5. Labels are also applied using the 'reclass' command.

An example of the result from the application of this script is given in Figure 7.11 (c) and (d) for the same area and two different wind directions. The banding system used, allows an immediate assessment of the likelihood of deposition being affected by the landscape. Such a system has been used in preference to a quantitative system, because of the uncertainties involved in applying such an automated system. It provides sufficient information to identify whether an area should be sampled, and how representative a sample from such an area will be.

Summary of GIS scripts

The three scripts described above have been applied to a larger area, equal to six 20x20km tiles, over the Lake District, Cumbria, UK. Again, the data were Landform Panorama data © Crown Copyright Ordnance Survey supplied by the EDINA Digimap/JISC service. The scripts were applied to the combined maps rather than to each tile individually. The results are shown in Figure 7.12. From a qualitative inspection of the map of affected deposition, it can be seen that the area broadly agrees with the area of raised elevation. The ridges lying at approximately 90° to the wind direction have a strong influence on the affected area map.

The time taken to run these scripts is relatively short. The actual run time will depend on the nature of the landscape and the number of peak and ridge features. For a desktop personal computer at the time of writing, this is estimated to be less than 5 minutes, for moderately complex landscape region of area 2400 km². This makes the system available for use in timescales not achievable by complex CFD or complex meteorological models, where run times can be in the order of several hours or days.

As an important caveat, it should be stressed that the scripts above contain a number of simplifications and in their present form do not represent a rigorous application of the results. Further experiments and CFD studies are required before such a system can be fully implemented. However, the scripts above demonstrate the principle by which the CFD results for individual features could be applied to a real landscape.

7.5. Dispersion modelling

A fully developed version of the ‘proof-of-principle’ system described above would be used to identify areas where deposition is likely to be influenced by the topography. Before it could be applied successfully, it would be necessary to know the broad area affected by contamination. Meteorological dispersion models can be used to predict the spread of airborne contamination and the average deposition rate. Using details of the release conditions and the meteorology, the movement of the contaminant plume can be predicted. By choosing a threshold concentration, the results from the dispersion model can be used to delimit the area within which the effect of topography should be considered. A contour defining this threshold could easily be produced from the output from a dispersion model and incorporated into the GIS. For the purposes of the type being considered in this study, the UK Meteorological Office’s NAME model is the model likely to be used.

7.6. Case study

Although the system described above is a simplified ‘proof-of-principle’ example, containing many broad assumptions, it is worthwhile comparing the results from it with real deposition

data. There are relatively few data sets that can be used to provide a comparison for dry deposition over a wide area. To be suitable the deposited material needs to be as a result of a short period of deposition, so that variations in meteorology are small, and to not be influenced by other deposition processes. One case that fits these criteria reasonably well is the deposition of radioactive material released from the accident at Windscale, Cumbria, UK, on 10-11 October 1957. The material was released as a result of a reactor accident and was released from a 120 m stack at No.1 Pile at Windscale (Crabtree, 1959).

Iodine-131 (^{131}I half-life 8.02 days), and caesium-137 (^{137}Cs half-life 30.2 years) were released during the accident (Chamberlain, 1959) (half-life data obtained from Unterweger *et al* (1992)). The physical characteristics of the released radionuclide material are not well known, but Chamberlain (1959) suggests that they may have been adsorbed to particles of other material released, such as graphite. Chamberlain also suggests that the ^{137}Cs will have been more likely to associate with the particulate phase than ^{131}I . There is no information on particle size distribution of the material released. It can safely be assumed that the material was polydisperse, and that the very large and very small particles would be deposited relatively quickly, leaving the micrometer sized particles to disperse further afield.

An aerial sampling survey of deposited radionuclides, in the area surrounding the Windscale site, was carried out by Dr David Sanderson of the Scottish Universities Research and Reactor Centre (SURRC), as reported by Argyraki *et al.* (1999). This data set provided information on ^{134}Cs and ^{137}Cs present in the soil. The longer-lived isotope, ^{137}Cs , is due to contamination from the Windscale accident and the more recent Chernobyl disaster. The shorter lived ^{134}Cs is due exclusively to the Chernobyl accident. Because the original $^{134}\text{Cs}/^{137}\text{Cs}$ ratio is known, its value can be used to subtract the ^{137}Cs deposition from Chernobyl, yielding the concentration due to Windscale. The data set was produced with a reasonable spatial

resolution, and can be used to compare predicted deposition patterns. A map of the net deposition of ^{137}Cs is shown in Figure 7.13.

Unfortunately, from the point of view of providing a simple test case, the meteorological conditions changed during the period of release of the material from Windscale. Crabtree described the weather conditions which prevailed during the release (Crabtree, 1959). During the early period of the release from 16:00 on the 10th October, the wind was lightly blowing from the SW. After 01:00 – 02:00 on the 11th October the wind direction changed to blowing more strongly from the NW. The strongest period of release was believed to be from 16:00 on the 10th October until 11:00 the next day.

Using this information, two runs of the automated GIS system were performed, assuming wind direction angles of 225° and 315° for the early and late periods respectively. The results of these runs are presented in Figures 7.14 (a) and (b). A comparison of these results with those for the net ^{137}Cs deposition showed some agreement but the predicted areas were patchy. The script used to identify the effect from ridges, disregarded ridges of length less than 500 m. The maps shown in Figures 7.14 (a) and (b) suggested that this may have been too restrictive. This criterion was therefore relaxed to a minimum length of 200 m, and the process repeated. The results are presented in Figures 7.15 (a) and (b). These maps clearly show better agreement between the predicted and actual affected areas. Comparison of these two figures with the map of net ^{137}Cs deposition showed good agreement. The region to the southeast of the release point is in very good agreement and the area to the east shows reasonable agreement.

Note that the passage of the plume of material from the release has not been included on these figures, because the exact meteorological conditions are not known. It should be borne in

mind that the total area produced by the GIS is likely to be larger than the area covered by the plume. For a real application the risk maps presented in Figures 7.15 (a) and (b) would be masked by an outline of the dispersed plume. Although there were two main wind directions during the release, there will also have been intermediate angles as the wind altered between these. This changing direction will have caused a different effect from the topography.

Another confounding factor is the more complex flow that occurred during the evening of the release. At this point the surface winds were N or NE, probably caused by katabatic flow from the nearby topography, whilst those at the height of the release were from the SW. The released material is therefore likely to have been blown inland before being blown back towards the coast at lower altitude (Crabtree, 1959). The pattern of dispersion during this period is unlikely to be affected by the complex topography in the same way, because the pattern of katabatic flow is more likely to have controlled the spread of the contaminant. A further consideration, because of the period of time between the deposition and the survey, is the resuspension and redeposition of material, which may have altered the pattern of original deposition.

Figures 7.16 and 7.17 show the maps of predicted deposition risk and the map of ^{137}Cs deposition, with the predicted maps presented on transparent material for ease of comparison between the two data sets. There is good general agreement in the areas affected by deposition and the predicted areas of likely increased deposition. The areas of predicted deposition extend beyond the limits of the survey of deposited material and suggest that further deposition would have occurred further inland. A full comparison is difficult because of the lack of fine resolution in the survey data.

Chamberlain (1959) described the pattern of ground deposition of ^{131}I and ^{137}Cs after the accident. Amongst the data presented was a plot of deposition along the plume centreline SE of Windscale. This showed high deposition close to the source, decreasing with distance, and a secondary maximum at approximately 20 km from the source. This data has been replotted in Figure 7.18, together with the elevation of the landscape along the same line.

The high deposition close to the source may be due to the settling out of large particles, and possibly the presence of moisture causing smaller particles to increase in size and deposit more rapidly. The samples, taken at a distance of 15 km and greater, show a clear correlation with elevation. Although there is quite coarse spatial resolution, the secondary maximum of deposition coincides well with the peak in elevation. The landscape in this peak region effectively presents a ridge to the oncoming plume. The results show a similar pattern as predicted by both the wind tunnel and CFD results for a ridge, in particular the maximum at the peak and reduction in the near wake.

In this particular case, the vertical distribution is not uniform close to the source, with the source starting from a height of approximately 122 m. However, at a distance of more than 15 km, the vertical distribution will have become much more uniform. As described above, it is not known whether the released material was all found in the gas or particle phase and the size distribution of any particles present. The possible presence of limited rainfall is mentioned by Chamberlain (1959), and it is possible that this may also have affected the results to some extent. Moisture from the cooling towers at Calder may also have had some effect, but this is more likely to be the case for the deposition close to the source.

The Windscale test case provides a useful data set against which to compare the developed system. However, because of the age of incident, there are some areas of limited information,

which make a direct comparison difficult. The other well known, and much more catastrophic, case of the accident at Chernobyl is not readily comparable, because the majority of the deposition resulted from rainfall through the dispersing plume. To provide a true test of the importance of the effect of complex topography on dry deposition, a well-controlled field study would be required.

One of the problems with field studies of aerosol behaviour is the generation of sufficient quantities of aerosol to enable the detection of deposition over a short period. A potential solution to this problem would be to use a naturally occurring aerosol from a well-defined source. A suitable candidate is sea-salt aerosol, which is naturally generated from a coastline. A carefully chosen site with complex topography would be required, and the experiment would need to be conducted in the presence of onshore winds, although these are frequently found at coastal sites during the daytime. One potential problem would be the change in aerosol size and perhaps composition with travel inland. This could be overcome to some extent by conducting the experiment some distance downwind and/or carefully monitoring size distribution and concentration. An alternative way to test the approach would be to examine the deposition surrounding a point source of particles close to complex topography. By comparing the topography and statistical information about the meteorological conditions with the cumulative deposition, validation might be possible. However, using this method might make a conclusive assessment more difficult.

7.7. Conclusions

The work described in this chapter is presented as an example of how some of the results, produced from the CFD studies in previous chapters, could be incorporated into an expert

system, to guide sampling strategy. The developed system is not presented as a working system, rather as a 'proof of principle'. To produce this demonstration system a number of assumptions have been made and as a result, it must be stressed that the system is not intended for use in real applications. At present the system has only incorporated results for deposition to a narrow range of landscape shapes, in neutral boundary layer conditions and has only explored briefly the interaction of landscape features in two dimensions. In addition, no consideration has been given to different surface roughness lengths. To produce a robust and reliable system would require considerable further development, improvement and validation.

The approach used has been to simplify the results from the CFD into a series of rules that can be applied to real landscape features. GIS software has been used to handle digital elevation data and existing algorithms (Wood, 1996) have been used to extract landscape features from this data. These features have been used as the starting point for a GIS analysis and the identification of areas likely to be affected by increased or decreased deposition.

The GRASS GIS system has been used because of its flexibility and rich feature set. Three automation scripts have been developed that take the identified features, together with wind direction, and outline potentially affected areas. The influences of three-dimensional peaks and two-dimensional ridges have been included, and a number of simplifying assumptions have been used. The areas affected by single and multiple features are then classified to produce a map of areas where the dry deposition is likely to be affected.

Examples of the application of the developed system have been demonstrated. The results have also been compared for a case study of radionuclide deposition following the Windscale accident in 1957. Good general agreement was seen for the main areas indicated as expecting

to have increased deposition. The spatial resolution of the deposition data was not sufficient to allow detailed comparison, although one transect provided such a comparison, and showed good agreement.

The derivation of the rules from the CFD results highlighted areas in which further modelling work would be valuable. For example, the limiting slope at which deposition is affected for two-dimensional ridges and three-dimensional hills would be useful. Also, the effect of ridge angle to oncoming flow on deposition pattern could be investigated. A more thorough investigation of the effect of elongated hills and short ridges would be useful and could be added to the automated system. An additional set of features that could be incorporated into the GIS system might be a land use dataset. This could identify areas supplying the food chain that are at risk, and suitable roughness lengths for the surface, e.g. for forestry, orchards, and built-up areas. The additional roughness would be expected to enhance deposition relative to smoother surfaces.

In conclusion, the results from the CFD studies for isolated shapes could be applied to a real landscape using a GIS. The example system produced has many limitations and is not suitable for use in real emergency situations as it stands. A number of assumptions were required in this case and further CFD work would be valuable to remove the need for these. The case study suggests that the feature and rule based approach could provide useful information to guide sampling strategy, following such an accident. Additional development and case study data would be required to optimise and validate the system further.

The approach used is quite distinct from an integrated modelling approach. The decoupling of the landscape features has limitations, in particular the treatment of adjacent features.

However, the approach used has significant advantages in terms of speed of use and the inclusion of fine landscape detail that could not be include in a combined model.

8. CONCLUSIONS

8.1. Introduction

There is a need to predict areas of increased risk of dry deposition of atmospheric particles, particularly in the immediate aftermath of an accidental release of radioactive material. Traditional methods of predicting dry deposition do not provide sufficient spatial resolution, and do not account for local effects caused by topography. This leads to a risk of missing the capture of contamination hotspots, as supported by experience from emergency exercises (Argyrazi *et al.*, 1999). There is a limited amount of experimental work that has investigated the influence of local topography, and that which is available has focussed on large particle deposition, for example (Goossens, 1988b; Goossens, 1996; Goossens and Offer, 1990; Offer and Goossens, 1995). To fully account for these local effects on small particle deposition, an understanding of the atmospheric properties in the vicinity of such topography is needed. A review of the literature surrounding computational fluid dynamics (CFD) suggested that CFD, as a technique, is capable of predicting atmospheric flows around complex topography, and can also be used to track particle motion and deposition. The time and complexity involved in CFD modelling precludes its use in an emergency situation. However, it can be used in advance to derive rules for deposition that can be applied in such situations.

An approach to CFD modelling of atmospheric flows was developed and tested using wind tunnel and field data, for the flow past a 6m cube. The CFD approach used for this test case performed well in predicting velocities close to the obstacle and in its wake. A similar approach was therefore used for the further study of flow over hills and for the modelling of particle deposition. Following the validation of the CFD technique with wind tunnel

experiments, further parametric CFD studies were carried out. The results from these were used to develop an example GIS based system for real topography. Each of these steps is summarised below.

8.2. Experimental deposition measurements

To confirm that complex topography does affect dry deposition, a series of experimental studies was carried out. The first series of experiments used scale model landscape features in wind tunnel flows. The results were compared with CFD studies to validate the modelling approach used for dry deposition prediction. To investigate more specifically, the relationship between dry deposition and turbulence, a second set of experiments was conducted, using grid generated turbulence and small collection elements.

8.2.1 Scale landscapes

Field studies of particle deposition are logistically difficult and very expensive to carry out. With careful experimental design it is possible to produce realistic scale models of the atmospheric flow over landscape features. Wind tunnel experiments were accordingly used to investigate the effects of simple landscape features on deposition. These experiments were followed by CFD modelling of the same cases. More details are provided in the next two sections.

Wind tunnel

Wind tunnel experiments on the deposition of small particles onto a set of two-dimensional and three-dimensional landscape features were carried out. Experiments to a flat surface were

carried out as a reference, and the ratio of deposition to the landscape and to the flat case was calculated. All experiments were carried out in a neutral boundary layer.

The presence of the landscape had a significant effect on deposition, with rates in some places reaching a maximum increase of 2.1 times the flat deposition. Areas of reduced deposition were also seen, mainly in the wake and on the lee side of the hills, with a minimum value of 0.07 in one case. A common pattern of deposition variation was seen for the cases studied. Deposition tended to increase on the windward face of the hills, reduce on the leeward face and near wake, and recover back to the flat case value further downwind. The three-dimensional case showed a more complex pattern, with regions of increased deposition to either side of the centreline in the wake. The location of the source was important for the pattern of deposition, particularly in the wake.

CFD

Using a similar technique to that developed for modelling a 6m cube in an atmospheric boundary layer, the flows over the landscape shapes studied in the wind tunnel were modelled. Particle trajectories and deposition were predicted using a stochastic technique and the ratio of deposition to the flat case was calculated.

The CFD results for the flow showed good agreement with the experimentally measured flow properties in the wind tunnel, with fractional bias as low as -0.0087 , and provided good estimates of reattachment length. The agreement between the CFD values for deposition was also very good for the two-dimensional ridges, with fractional bias in the relative deposition as low as $+0.11$. For the three-dimensional case the agreement was qualitatively good, but showed some areas of discrepancy, particularly in the wake.

Only a small selection of geometries was studied with wind tunnel experiments. Further work investigating more realistic hill shapes would be of value.

8.2.2 Uniform turbulence

The results from the wind tunnel and CFD studies of deposition around landscape shapes suggested that turbulence in the flow was an important variable, influencing the rate of deposition. To try to understand how the particle deposition depends on turbulence, a set of experiments was conducted, together with a CFD study.

Wind tunnel

A small cross-section wind tunnel (0.2x0.2m) was used for a series of deposition experiments to two collecting surfaces: a cylinder and a vertical plane parallel to the flow. Turbulence was generated using a square grid. Distance from the grid was used to control turbulence intensities. Velocities and turbulence levels were measured using a hot-wire anemometer and custom designed data acquisition software.

Turbulence levels downwind from the grid were similar to those predicted by theory (Comte-Bellot and Corrsin, 1966). The collecting surfaces were exposed to aerosol particles in flows containing different levels of turbulence intensity. A general increase in deposition was seen with increasing turbulence, although the relationship between deposition velocity and turbulence intensity was not a linear one.

CFD

The CFD study showed good agreement with the experiment, in terms of predicting the trend of increasing deposition velocity with increasing turbulence intensity. However, the magnitude of the deposition velocity was significantly over-predicted by a factor of approximately 20 for the cylinder case and approximately 50 for the plane. This is believed to be a result of either the isotropic turbulence model used or a lack of modelling of the smallest scales. The CFD results also provided important insights into the process and ideas for improvements to the experimental design. For example, the deposition was predicted to vary strongly with location, particularly for the cylinder case, with an expected peak on the windward face, but also secondary maxima further around the cylinder. The relationship with turbulence intensity was also predicted to be stronger for a cylinder of smaller diameter. This indicates a complex relationship between the free-stream turbulence and the boundary layer around the cylinder. It also suggests that repeating the experiment with an adapted geometry would give clearer support to the relationship between free-stream turbulence and deposition rate. A wider range of turbulence intensities would be useful in future work.

8.3. CFD

Having established a technique for the modelling of atmospheric flows and predicting the relative dry deposition rates of particles over complex topography, the method was applied to a wide range of landscape shapes. A wide selection of two-dimensional landscape shapes was modelled and a smaller number of three-dimensional shapes. The sensitivity to a number of other parameters was also studied, as described below.

The CFD results showed a range of interesting features and the most significant are described below. Model parameters that were most important to the predictions were mesh density and choice of turbulence model. However, even though the coarsest mesh density missed details of the deposition predicted by finer models, the broad features were the same. There was a significant difference in relative deposition between the k-epsilon and Reynolds stress models, with the RSM model over-predicting compared with experiment.

Sensitivity to wind speed, particle diameter and density were also studied. Whilst absolute deposition velocity depended linearly on wind speed over the range studied, there was no variation of relative deposition with wind speed. Particle diameter caused a variation in the pattern of deposition for unit density particles larger than 10 μ m. Deposition velocity for smaller particle sizes varied slightly from the trend reported in experimental studies for smoother surfaces (Sehmel and Hodgson, 1980). The values were however of the same order as experimental measurements for rougher surfaces. The lack of variation with smaller particle diameter is believed to be due to the lack of explicit modelling of the smallest scales near the surface. Because the landscape features considered are much larger than these neglected scales and because the real surfaces are rougher, this necessary omission will not alter the predicted relative deposition. Particle density did not have a significant impact on relative deposition for typical densities found in atmospheric particles.

The presence of landscape shapes showed a significant impact on deposition rates, compared to the flat case, as expected from earlier experimental and CFD studies. The general pattern was an increase in deposition to the windward face of hills and ridges (with averages over the upwind side of a factor of 1.2 - 1.9 increasing with slope), and a decrease on the leeward face and in the near wake, and a further increase downwind (with average factors of 1.4 - 2.0 also increasing with slope). The larger the gradient of the hill or ridge, the more pronounced was

the effect on relative deposition. The curvature of the slope was also found to be related to deposition rate, although comparison between a flat-sided and sinusoidal ridge showed only local differences in deposition. Valley geometries studied showed a reduction in deposition to the upwind valley side and the valley bottom and an increase to the downwind valley side (a maximum factor of 2.5 – 3.3 for the cases studied). The three-dimensional cases showed similar patterns to the two-dimensional case for the surface of the hill. For the steeper geometries there were regions of increased deposition in the wake, to either side of the centreline.

The CFD results compared well with the limited field data available for larger particle sizes and with the wind tunnel data. The main differences were observed for the three-dimensional cases. Whilst the study has considered a broad range of cases and conditions there is scope for further modelling and experimental work. A wider range of three-dimensional CFD cases could be investigated and the inclusion of non-neutral flow conditions would be useful. Further studies of multiple features would also be valuable, both in two and three dimensions. A field trial based around particles of the desired size range would be valuable, possibly using a short duration coastal aerosol or a longer exposure from a point source and statistical meteorology data.

8.4. Application

The results from the CFD work described above, were used to develop a feature-and-rule based system, to predict areas of potentially increased or decreased dry deposition. A demonstration system was constructed with a geographical information system (GIS) to show how this approach might be used.

The demonstration system took digital elevation data and wind direction as input. The first step was the identification of landscape features with existing algorithms. These were then used to apply rules derived from the CFD, to identify the areas surrounding these features at risk of increased or decreased deposition relative to a flat case. A set of scripts was developed to automate this process and allow it to be performed as part of a larger system.

The system was applied to a set of digital elevation data and compared with a test data set. The case used was the deposition of radionuclides, following the Windscale accident in Cumbria, 1957. The predicted areas of increased and decreased deposition showed good broad agreement, although only a small amount of detailed comparison was possible because of the low resolution of the field data.

The developed system showed promise and suggested that such a reductionist, feature-and-rule approach may be valuable, particularly where there is not time to carry out a detailed modelling study. A number of areas of further CFD work were identified as requirements to develop the approach further. More case studies would also be required to optimise and validate the approach.

8.5. Conclusions

This project was born from a requirement to rapidly assess and predict the potential variation in particle dry deposition, caused by the change in atmospheric flow over landscape features. In particular, the effects that landscape features can have on the speed, direction and the turbulent properties of the flow over them. For example, raised landscape features can cause increased wind speeds at their peak, reduced speeds or recirculating flows in the near wake and increased turbulence in the further wake. Wind tunnel studies confirm that such features

do alter the dry deposition rate when compared to a flat landscape. Information in the literature also confirms this for larger particle sizes (Goossens, 1988b).

CFD modelling is becoming increasingly commonly used, and more widely validated for atmospheric flows. A stochastic, inertial particle tracking model, combined with a CFD model for flow, has been used to predict the deposition of particles in such flows and the influence of landscape features on patterns of deposition. Comparison of CFD model results for relative deposition to wind tunnel data, show that CFD appears to capture all the important features and provides good quantitative agreement in the majority of the cases.

Further wind tunnel and CFD studies showed that deposition was related to turbulence and concentration in the bulk flow, as well as surface properties. Comparison between experimental and CFD results also showed that CFD was capable of predicting relative amounts of particle deposition. Wind tunnel comparisons indicated that CFD over-predicts the absolute deposition velocity compared to experiment. It is thought that this is due to the isotropic nature of the turbulence models used, which overestimate the vertical turbulence in boundary layer flows. Lack of modelling of the smallest scales close to the surface may also contribute to this overestimation, by not explicitly modelling the slow transfer very close to the surface. These limitations do not appear to be important where deposition is controlled by bulk, rather than surface flow.

The CFD technique used has been applied to a wide range of two- and three-dimensional landscape features, and has highlighted a number of features of increased and decreased deposition. These relationships to landscape shape have been used within an automated GIS-based expert system to demonstrate the prediction of areas likely to be exposed to increased or

decreased deposition. The system has been applied to a case study and has shown good broad agreement.

In summary, CFD coupled with stochastic particle tracking has been shown to be useful in predicting trends in particle dry deposition. Although initially time consuming, the results from such studies can be extracted into a set of rules that can then be applied rapidly, to a real landscape, to help guide emergency sampling strategy.